AN ABSTRACT OF THE THESIS OF

Hannah M. Rolston for the degree of Master of Science in Environmental Engineering presented on July 24, 2017.

Title: Experimental Demonstration and Modeling of Aerobic Cometabolism of 1,4-Dioxane by Isobutane-Utilizing Microorganisms in Aquifer Microcosms

Abstract approved:

_____

Lewis Semprini

1,4-dioxane, a probable human carcinogen at low (< 1ppb) concentrations, has emerged as a groundwater contaminant due to its historical use as a stabilizer for the chlorinated solvent 1,1,1-trichloroethane. Aerobic cometabolism, the use of a primary substrate to induce the production of microbial enzymes that fortuitously degrade other compounds, is a promising *in situ* treatment strategy for 1,4-dioxane because it has the potential to mineralize trace 1,4-dioxane concentrations to carbon dioxide. The effectiveness of biostimulation with isobutane (2-methylpropane) as a primary substrate and bioaugmentation with *Rhodococcus rhodochrous* strain ATCC 21198 was assessed in microcosms constructed with aquifer solids from Fort Carson, Colorado, a site with 1,4-dioxane and trichloroethene (TCE) co-contamination. Isobutane effectively stimulated native 1,4-dioxane-degrading microorganisms in the aquifer solids after a lag of approximately one week. Microcosms bioaugmented with 21198 showed immediate consumption of isobutane and cometabolism of 1,4-dioxane after isobutane was consumed below 0.15 mg/L, indicating primary substrate inhibition. At a concentration of 200 µg/L, TCE did not inhibit 1,4-dioxane degradation, however TCE was not readily cometabolized. 1,4-dioxane-cometabolizing microbial populations remained active in bioaugmented and biostimulated microcosms with repeated additions of isobutane over approximately 300 days, though transformation rates slowed without inorganic nutrient amendment. Modeling of simultaneous isobutane utilization, 1,4-dioxane degradation, and biomass growth according to Michaelis-Menten and Monod kinetics accurately simulated data from microcosms not experiencing inorganic

nutrient limitation. Optimization of kinetic parameters yielded the following values: $K_{max,1IB}$=2.58 mg/mg/day, $K_{s,IB}$=0.1 mg/L, $K_{max,14D}$=0.87 mg/mg/day, $K_{s,14D}$=4.35 mg/L, K_I=0.13 mg/L, b=0.03 1/day, and Y=0.885 mg/mg.

Experimental Demonstration and Modeling of Aerobic Cometabolism of 1,4-dioxane by Isobutane-Utilizing Microorganisms in Aquifer Microcosms

by
Hannah M. Rolston

A THESIS

submitted to

Oregon State University

in partial fulfillment of
the requirements for the
degree of

Master of Science

Presented July 24, 2017
Commencement June 2018

Master of Science thesis of Hannah M. Rolston presented on July 24, 2017.

APPROVED:

Major Professor, representing Environmental Engineering

Head of the Department of Chemical, Biological & Environmental Engineering

---

Dean of the Graduate School

I understand that my thesis will become part of the permanent collection of Oregon State University libraries. My signature below authorizes release of my thesis to any reader upon request.

Hannah M. Rolston, Author

ACKNOWLEDGEMENTS

I would like to thank my advisor, Dr. Lewis Semprini, for his guidance and patience. Lew fosters a supportive, exciting, and fun research environment, and I am grateful to be a part of it. I will be eternally grateful to Dr. Mohammad Azizian for his support in the lab. Without Mohammad's analytical expertise, none of the instruments would function and this thesis would not accomplished.

I would also like to thank my committee members: Dr. Mark Dolan, Dr. Tyler Radniecki, and Dr. Jack Istok. I appreciate your commitment as researchers, educators, and mentors.

I feel so lucky to have worked with other members of the Semprini lab group: Kyle Vickstrom, Jill Schlrau, Paige Molzahn, Suvadee Thankiatkul, Emma Ehret, Marina Cameron, and the newest members, Mitchell Rasmussen, Riley Murnane, and Krysta Krippaehne. I could not have asked for a more fun, inspiring, and supportive group of coworkers. I also owe a large debt of gratitude to the numerous undergraduate student researchers who have assisted with this project: Eileen Lukens, Stephanie Rich, Stephenie Wright, Willow Walker, Allison Burns, and Spencer Helterline.

A huge thank you to the other CBEE graduate students and the Graduate Student Association. I am so grateful to work and learn among coworkers who are also great friends.

This research was funded by the Department of Defense Strategic Environmental Research and Development Program, grant ER-2303. I am grateful for the guidance of Michael Hyman at North Carolina State University as lead investigator on the grant. I would also like to thank the various entities that have provided financial support specifically for me as a graduate student: the OSU Graduate School for the Provost Fellowship, the National Defense Science and Engineering Graduate (NDSEG) Fellowship Program, and Wells Fargo for their scholarship facilitated by the Achievement Rewards for College Scientists (ARCS) program.

Finally, I would like to thank my family, particularly my parents, Mary and Layne Rolston, and my sister, Emily Rolston. Words cannot express how grateful I am for a lifetime of love, motivation, and fun.

TABLE OF CONTENTS

TABLE OF CONTENTS (Continued)

LIST OF FIGURES

Figure Page

LIST OF FIGURES (Continued)

LIST OF FIGURES (Continued)

LIST OF FIGURES (Continued)

LIST OF TABLES

Tables Page

LIST OF APPENDIX FIGURES

LIST OF APPENDIX TABLES

LIST OF ABBREVIATIONS

14D	1,4-dioxane
1,1,1-TCA	1,1,1-trichloroethane
1,1-DCE	1,1-dichloroethene
1,1-DCA	1,1-dichloroethane
cis-DCE	cis-dichloroethene
CO_2	Carbon dioxide
COC	Contaminant of concern
CVOC	Chlorinated volatile organic compound
E	Nash-Sutcliffe Efficiency
ECD	Electron capture detector
EPA	Environmental Protection Agency
ERH	Electrical resistance heating
FID	Flame ionization detector
GC	Gas chromatograph
GC-MS	Gas chromatograph mass spectrometer
H_{cc}	Dimensionless Henry's constant
IB	Isobutane
ISCO	In situ chemical oxidation
MCL	Maximum contaminant level
MNA	Monitored natural attenuation
N	Nitrogen
NH_4	Ammonium
N_2O	Nitrous oxide
NO_3^-	Nitrate
OD	Optical density
P	Phosphorous
PO_4	Phosphate
PVDF	Polyvinylidene difluoride
RCRA	Resource Conservation and Recovery Act
RDX	Hexahydro-1,3,5-trinitro-1,3,5-triazine
TCE	trichloroethene (trichloroethylene)
THF	Tetrahyrofuran
TSS	Total suspended solids
TRI	Toxic Release Inventory
UCMR3	Third Unregulated Contaminant Monitoring Rule
VC	Vinyl chloride
WWTP	Waste water treatment plant
X	Biomass
XSVE	Extreme soil vapor extraction

LIST OF MODELING NOMENCLATURE

b	Endogenous decay coefficient (1/day)
C_g	Gas concentration (mg/L)
C_l	Liquid concentration (mg/L)
E	Nash-Sutcliffe Efficiency
Exp_{avg}	Average of experimental values
Exp_i	Experimental values
H_{cc}	Dimensionless Henry's constant
K_{FO}	First order rate constant (L/mg biomss/day)
K_I	Inhibition constant (mg/L)
K_{max}	Maximum rate of substrate utilization (mg substrate/mg biomass/day)
K_s	Half saturation constant (mg/L)
M	Total mass (mg)
Mdl_i	Model values
M_o	Initial mass (mg)
S_C	Cometabolic substrate
S_G	Primary substrate
SSE	Sum of squared errors
t	Time (days)
V_g	Gas volume (L)
V_l	Liquid volume (L)
X	Biomass concentration (mg/L)
X_o	Initial biomass concentration (mg/L)
Y	Microbial yield (mg biomass/mg substrate)

I. INTRODUCTION and OBJECTIVES

Prior to the enactment of the Resource Conservation and Recovery Act (RCRA) in 1980, waste solvents were often disposed of in unlined or clay landfills leading to widespread groundwater contamination[1]. Evidence has recently emerged that 1,4-dioxane, a cyclic ether, is a common groundwater contaminant (often as a co-contaminant at chlorinated solvent-impacted sites) due to its historical use as a stabilizer for the chlorinated solvent 1,1,1-trichloroethane (1,1,1-TCA)[2–4].

The properties of 1,4-dioxane provide unique challenges for groundwater remediation. A common remedial strategy for chlorinated solvent contamination is pumping followed by *ex situ* treatment via air stripping or sorption onto granular activated carbon. However, 1,4-dioxane, which typically accompanies chlorinated solvent contamination, has low volatility at ambient temperatures and is less sorptive than chlorinated volatile organic compounds (CVOCs), which renders these common CVOC remediation strategies ineffective[1,4,5]. Ex situ remediation of 1,4-dioxane has been achieved through sorption to synthetic media, advanced oxidation processes, and in bioreactors, however these methods typically have high capital, operational, and maintenance costs[5–7].

While 1,4-dioxane is relatively recalcitrant to biodegradation because of its heterocyclic ether structure[8], the literature now contains numerous examples of 1,4-dioxane biodegradation though both direct metabolism and cometabolism, suggesting bioremediation may be a feasible *in situ* treatment strategy. The majority of strains capable of utilizing 1,4-dioxane as a sole carbon and energy source are actinomycetes, primarily in the *Rhodococcus* and *Pseudonocardia* genera[9,10]. Cometabolism of 1,4-dioxane has been achieved using numerous primary substrates for growth and/or induction of cometabolic enzymes, the most common of which is tetrahydrofuran (THF)[11–16]. Propane[15,17], 1-butanol[18,19], toluene[13], and yeast extract[14,15,20] have also successfully induced cometabolic 1,4-dioxane degradation by various cultures.

The objectives of this study were to:

1. Use aquifer microcosms to assess the efficacy of isobutane (2-methylpropane) as a primary substrate to stimulate 1,4-dioxane cometabolism among members of a mixed subsurface microbial community;
2. Assess the ability of the model microorganism *Rhodococcus rhodochrou*s strain 21198 to degrade 1,4-dioxane when grown on isobutane and bioaugmented in aquifer microcosms;
3. Determine whether cometabolism can be sustained through repeated additions of 1,4-dioxane and assess potential differences in degradation capacity between bioaugmented and biostimulated microcosms;
4. Assess whether the presence of trichloroethene (TCE) inhibits the degradation of 1,4-dioxane;
5. Model simultaneous isobutane utilization, 1,4-dioxane degradation, and biomass growth in the microcosms according to Michaelis-Menten and Monod kinetics; and
6. Incorporate statistical analysis into a numerical model in order to estimate values of key kinetic parameters.

II. LITERATURE REVIEW

A. 1,4-Dioxane: General Background

1. Production and Use

1,4-dioxane, $C_4H_8O_2$, is a cyclic ether, as shown in Figure 1. It is most commonly produced by heating ethylene glycol and reacting it with concentrated sulfuric acid. 1,4-dioxane was first produced for commercial sale in 1929, with large-scale production in the US by 1951. 1,4-dioxane has many uses, including but not limited to textile processing, pharmaceutical purification, and organic synthesis. It is a component of many paints, varnishes, detergents, adhesives, cosmetics, fumigants, and polishing agents, occuring either intentionally or as an impurity[1,21].

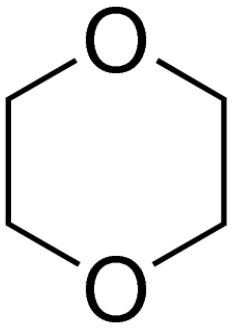

Figure 1. 1,4-dioxane, $C_4H_8O_2$

The use of 1,4-dioxane most pertinent to this thesis was as a stabilizer for the chlorinated solvent 1,1,1-TCA, also known as methyl chloroform. Chlorinated solvents have been a key component of manufacturing since the 1940s, though their use has fallen by over 90% since the 1970s due to environmental regulations. 1,1,1-TCA was most commonly used in cold cleaning, vapor degreasing, and ultra-sonic cleaning baths. It became widely used as a less-toxic replacement for carbon tetrachloride in the 1950s and trichloroethylene (TCE) in the mid-1960s. Of the four major chlorinated solvents (dichloromethane, perchloroethylene, TCE, and 1,1,1-TCA), 1,1,1-TCA is the least stable. The reactivity of 1,1,1-TCA with aluminum was a major problem for vapor degreasing, so 1,4-dioxane was used in concentrations up to 8% by weight to compete with 1,1,1-TCA for electron deficient sites on aluminum chloride.

(1,4-dioxane is a Lewis base because the oxygen atoms have electrons available to be shared.) As 1,1,1-TCA stabilization was the primary demand for 1,4-dioxane, 1,1,1-TCA production drove 1,4-dioxane production. Ninety percent of the 30.8 million pounds of 1,4-dioxane produced worldwide in 1985 (25 million pounds in the US) was used to stabilize 1,1,1-TCA. The 1989 Montreal Protocol on ozone-depleting substances reduced 1,1,1-TCA production, and by 1994 1,4-dioxane production in the US had correspondingly dropped below 10 million pounds[1].

2. Toxicity and Regulation

1,4-dioxane is considered a "likely" human carcinogen by the U.S. Environmental Protection Agency (EPA) Integrated Risk Information System. Animal studies have shown it has the potential to cause liver and kidney damage as a result of ingestion, inhalation, and dermal exposure at high doses[21]. A study of 165 employees exposed to 1,4-dioxane at low levels and short exposures did not find a significantly higher number of cancer deaths than expected[22].

A federal maximum contaminant level (MCL) for 1,4-dioxane in drinking water has not been set, however the EPA published a 10^{-6} lifetime cancer risk level of 0.35 µg/L. 1,4-dioxane was included in the EPA's Third Unregulated Contaminant Monitoring Rule (UCMR3) in 2012, which mandates data collection for potential drinking water contaminants that do not have health-based standards set by the Safe Drinking Water Act (i.e. MCLs). The minimum reporting level was 0.07 µg/L[23]. Thirty-two states had established 1,4-dioxane action levels in 2016, with concentrations ranging from 0.25 µg/L in New Hampshire to 200 µg/L in Iowa[24]. Chlorinated solvents relevant in this thesis and their MCLs are as follows: 1,1,1-TCA, 200 µg/L; 1,1-dichloroethane (1,1-DCA), no MCL established; 1,1-dichloroethene (1,1-DCE), 7 µg/L; TCE, 5 µg/L; cis-dichloroethene (cis-DCE), 7 µg/L; and vinyl chloride (VC), 2 µg/L[25].

3. *Environmental Fate and Occurrence*

The physical and chemical properties of 1,4-dioxane determine its fate in the environment. Several of these properties are listed in Table 1 for comparison with 1,1,1-TCA and TCE. 1,4-dioxane is stable due to its symmetrical shape, and is unreactive with moderate strength acids, oxides, and oxidizing agents[1]. One of the most notable properties of 1,4-dioxane is its miscibility. As a single molecule 1,4-dioxane is not polar; however, it dimerizes via intermolecular hydrogen bonds, thereby exposing two oxygen atoms to interact with water molecules, and thus is completely miscible in water[1,26].

Table 1. Physical and chemical properties of 1,4-dioxane, 1,1,1-trichloroethane, and trichloroethylene[1]

Property	1,4-dioxane	1,1,1-TCA	TCE
Molecular weight (g/mol)	88.1	133.42	131.39
Density (g/cm^3)	1.028	1.32	1.46
Vapor Pressure at 25^{o}C (mm Hg)	38.09	100	60
Solubility (mg/L)	miscible	1334	1280
Log Koc	1.23	2.18	2.1
Boiling point (^{o}C)	101	74.1	87

1,4-dioxane has relatively low vapor pressure, making it unlikely to volatilize. According to an Estimation Programs Interface Suite model, it would take 34 days for 99% volatilization of 1,4-dioxane from a model river, compared with 8.4 hours for TCE and 1,1,1-TCA. 1,4-dioxane's organic carbon-water partitioning coefficient (log Koc) is also low, meaning is has less tendency to sorb to and be retarded by organic carbon in soil and less potential for bioaccumulation than chlorinated solvents [1,21]. Direct photolysis of 1,4-dioxane will not occur because it is photolyzed at wavelengths of 165-191 nm, which are shorter than light that penetrates Earth's atmosphere. Photo-oxidation by hydroxyl radicals or atomic chlorine results in an atmospheric residency of 22.4 hours, assuming an annual average tropospheric hydroxyl radical concentration of 10^6 mol/cm^3. This reaction produces ethylene glycol diformate, a toxic compound with atmospheric residency of 24 days. Photo-oxidation of 1,4-dioxane can also occur in water, resulting in half-life estimates ranging from 67 days to 9.1 years [1].

The widespread and continued use of 1,4-dioxane has led to the occurrence of 1,4-dioxane in many sectors of the environment, including in the food supply, wastewater, drinking water, and groundwater. 1,4-dioxane's relatively high boiling point led to increased concentrations in waste solvents due to principle solvent losses during vapor degreasing processes[21]. The maximum estimated concentration of 1,4-dioxane in 1,1,1-TCA waste is 15 to 20 percent[5]. Data from the EPA's Toxic Release Inventory (TRI) shows that 15 million pounds of 1,4-dioxane have been released to the environment between 1988 and 2004. Twenty-eight million pounds were transferred to waste treatment facilities during the same period. Peak releases occurred in 1993, with a six-fold reduction by 2004[1]. TRI was established as part of the Emergency Planning and Community Right to Know Act in 1986 and data first collected in 1988, meaning the peak production and use (and likely release to the environment) for 1,1,1-TCA and 1,4-dioxane were not captured by the database.

After 1,4-dioxane was detected in tap water ranging from 0.2 to 1.5 mg/L in Kanagawa, Japan during the mid-1990s, a study was conducted to determine if 1,4-dioxane was also present in the food supply. 1,4-dioxane was present at 2 to 15 μg/kg across 12 food groups representing the average diet in Kanto region (which includes Kanagawa). The total daily intake calculated from these results was 0.440 μg, which was determined not to be a carcinogenic risk[27]. 1,4-dioxane is also found as an impurity in polysorbates (emulsifiers used in ice cream and other frozen desserts) and in glycerides and polyglycides of hydrogenated vegetable oils (used in dietary supplements). However, the maximum exposure to 1,4-dioxane from these sources is three to four orders of magnitude below the EPA's Integrated Risk Information System daily oral slope factor for carcinogenic risk of 0.011 mg/kg[1].

1,4-dioxane is commonly found in wastewater treatment effluent. In a survey of 40 municipal wastewater treatment plants (WWTP) across the United States, 38 effluents had 1,4-dioxane concentrations above 0.3 μg/L (the study's detection limit) with a median concentration of 1.11 ± 0.6 μg/L. The study's Monte Carlo analysis of dilution factors and 1,4-dioxane concentrations concluded that there was likely not a risk to downstream drinking water intakes[28]. A study of four municipal WWTPs in Germany found influent 1,4-

dioxane concentrations ranging from 262 to 834 ng/L, and no removal of 1,4-dioxane during treatment. An increase up to 62.3 µg/L was observed at one WWTP, likely due to impurities in the methanol used for denitrification. The study also found that increased 1,4-dioxane concentrations positively correlated with distance from river origin along the Oder, Rhine, and Main Rivers, illustrating the influence of anthropogenic activity along the rivers. In addition, two drinking water treatment facilities using bank filtered water from the Rhine River were found to reduce influent 1,4-dioxane concentrations by a maximum of 27% via conventional ozone, oxidation, carbon filtration, and chlorine disinfection, which did not meet the precautionary limit of 100 ng/L set by the German Federal Environmental Agency[29]. As a result of the screening mandated by UCMR3, 1,4-dioxane was detected in 4,905 public water systems in the US between 2013 and 2016. Concentrations greater than or equal to 0.07 µg/L were detected in almost 22% of public water systems in the United States[23].

4. Groundwater Remediation

Groundwater is the most important environmental sector of 1,4-dioxane contamination for the work presented in this thesis. Prior to the enactment of RCRA in 1980, waste solvents (potentially containing 1,4-dioxane) were often dumped on the ground or disposed of in unlined or clay-lined landfills[1], and therefore became widespread groundwater contaminants. Given the conditions in which 1,4-dioxane was released, it is unsurprising that 1,4-dioxane contamination in groundwater is commonly associated with chlorinated solvent contamination. A data mining study of California's GeoTracker database found that 1,4-dioxane was detected at 194 of the 605 sites that were analyzed, with 95% of the sites accompanied by one or more chlorinated solvents [2]. A survey across 49 United States Air Force installations found that 1,4-dioxane was present in 18% of the nearly 6000 wells surveyed, with 94% co-occurance with 1,1,1-TCA and/or TCE[3]. While there is no conclusive evidence that 1,4-dioxane was used to stabilize TCE, co-occurance of the two compounds is common due to the sequential use of TCE and 1,1,1-TCA. (1,1,1-TCA largely

replaced TCE in the mid-1960's [1].) There may be TCE but not 1,1,1-TCA co-contamination with 1,4-dioxane because the abiotic half-life of 1,1,1-TCA is only about two years, much shorter than that of TCE[1]. At legacy contamination sites, it is possible that 1,4-dioxane would accompany not only the parent chlorinated solvents, but their transformation products as well (1,1-DCE and 1,1-DCA from 1,1,1-TCA, and cis-DCE and VC as products of the anaerobic reductive dehalogenation of TCE).

Due to 1,4-dioxane's miscibility and low sorption potential, it is commonly predicted that 1,4-dioxane plumes will lead those of their chlorinated solvent co-contaminants[1,21]. While there are examples—including the site referenced in this study—to support this prediction, 62% of sites with dual contamination identified in the California GeoTracker survey had longer chlorinated solvent plumes than 1,4-dioxane plumes[2]. This is likely due to the higher concentrations of chlorinated solvents than 1,4-dioxane in source zones, and the use, improper disposal, and subsequent groundwater contamination by chlorinated solvents two decades prior to the widespread use of 1,4-dioxane as a stabilizer for 1,1,1-TCA[5].

The properties of 1,4-dioxane provide unique challenges for groundwater remediation. A common remedial strategy for chlorinated solvent contamination (that, as learned in recent decades, 1,4-dioxane often accompanies) is pumping followed by ex situ treatment via air stripping or sorption onto granular activated carbon. However, 1,4-dioxane has low volatility at ambient temperatures and less sorptive potential relative to chlorinated volatile organic compounds (CVOCs) (see Table 1 for comparison), rendering these common CVOC remediation strategies ineffective[1,4,5]. 1,4-dioxane is also resistant to zero valent iron reduction and biodegradation by anaerobic dehalogenating microorganisms, common in situ remedial strategies for CVOCs[5]. Analytical methods for 1,4-dioxane were not available prior to the 1990s[1], and there is still not uniform regulatory requirements to test for 1,4-dioxane at contaminated sites. For many sites with chlorinated solvent contamination, a record of decision was reached without consideration of 1,4-dioxane. While the selected remedial methods may have been effectively remediating CVOCs for decades of operation, they were likely not removing 1,4-dioxane. 1,4-dioxane may be discovered later, which causes sites to

be reevaluated or even reopened in order to reassess plume boundaries, risks to human health, and the chosen treatment technology[1].

While commonly applied remediation strategies for chlorinated solvents are generally ineffective for 1,4-dioxane treatment, several *ex situ* and *in situ* remediation methods for 1,4-dioxane have been developed. Because 1,4-dioxane is miscible and does not sorb to aquifer material, it is readily pumped out of the subsurface for *ex situ* treatment[5]. *Ex situ* methods include sorption onto the synthetic media Ambersorb™, advanced oxidation processes (including Fenton's Reagent, hydrogen peroxide and UV or ozone), and *ex situ* biological treatment in bioreactors[5–7]. These methods typically have high capital, operational, and maintenance costs[6]. Pumping and *ex situ* treatment for 1,4-dioxane may also be a lengthy remedial strategy due to storage in and back diffusion from low permeability layers in the subsurface[5,30].

In situ remediation methods include in situ chemical oxidation (ISCO), electrical resistance heating (ERH)[31], enhanced soil vapor extraction(XSVE)[32], phytoremediation[33], bioremediation, and monitored natural attenuation(MNA) [5–7]. While in situ 1,4-dioxane treatment strategies typically require less infrastructure and a smaller environmental footprint than *ex situ* strategies[7], ISCO, ERH, and XSVE typically have moderate to high capital, operation, and maintenance costs[6]. A detailed description of bioremediation, the focus of this study, is below.

B. Bioremediation of 1,4-Dioxane

1. Biodegradation Background

Mandelbaum et al (1997) define bioremediation as "the engineered application of microbiological processes to clean up contaminated soil and groundwater"[34]. Microbial degradation of contaminants of concern (COCs) can occur via direct metabolism or cometabolism. In direct metabolism, microbes utilize the COC as a sole carbon and energy source for growth and cellular processes. By contrast, cometabolism is the fortuitous transformation of COCs by enzymes induced via a primary growth substrate. The primary

substrate supplies the cell with carbon and energy, while the COC transformation does not benefit the cell. Cometabolism is a potentially important process for bioremediation because it allows for the transformation of trace concentrations that would not support a microbial community dependent on the COC for direct metabolism[35].

Bioremediation can occur through bioaugmentation and/or biostimulation. Bioaugmentation is the addition of microorganisms to an environment to achieve the intended transformations. Biostimulation is the addition of a primary substrate, oxygen, and/or nutrients to stimulate microorganisms native to the subsurface with the ability to transform the COCs. Bioaugmentation may also include the addition of nutrients and a primary substrate in addition to a model microorganism.

The literature contains numerous studies on both direct metabolism and cometabolism of 1,4-dioxane. 1,4-dioxane is relatively recalcitrant to biodegradation because of its heterocyclic ether structure[8], however there are many examples of successful biotransformation, both by mixed and pure cultures. The most commonly referenced direct metabolizer of 1,4-dioxane is *Pseudonocardia dioxanivorans* CB1190, an actinomycete originally isolated from an industrial sludge contaminated with 1,4-dioxane[36,37]. Like CB1190, the majority of strains capable of utilizing 1,4-dioxane as a sole carbon and energy source are actinomycetes, primarily in the Rhodococcus and Pseudonocardia genera[9,10], though direct metabolizers have also been identified in the *Mycobacterium*[38] and *Afpia* genera[10].

Cometabolism of 1,4-dioxane has been achieved using numerous primary substrates for growth and/or induction of cometabolic enzymes, the most common of which is tetrahydrofuran (THF)[11–16]. Propane[15,17], 1-butanol[18,19], toluene[13], and yeast extract[14,15,20] have also successfully induced cometabolic 1,4-dioxane degradation by various cultures. Several cultures are able to degrade 1,4-dioxane with enzyme stimulation from multiple primary substrates, though not at equal rates[14,15,18,20]. Some strains, including CB1190, are capable of both direct metabolism of 1,4-dioxane and cometabolism with THF as a primary substrate[39,40], because 1,4-dioxane and THF are structural analogues[16].

Most biodegradation of 1,4-dioxane has been studied in aerobic conditions. While some field data has suggested that 1,4-dioxane undergoes anaerobic biodegradation, no degradation was observed in anaerobic laboratory microcosms constructed from aquifer solids[41,42]. However, anaerobic degradation of 1,4-dioxane by Iron(III)-reducing microorgansisms was observed in municipal wastewater treatment sludge, indicating that iron-reducing conditions in the subsurface may support direct metabolism of 1,4-dioxane in the subsurface[43].

At the time of writing, only one field scale demonstration of 1,4-dioxane cometabolism was found in the literature: a study of propane biosparging and bioaugmentation with *Rhodococcus ruber* ENV425. While biostimulation with propane and oxygen did not stimulate 1,4-dioxane degradation in a control well, bioaugmentation with *Rhodococcus ruber* ENV425 effectively reduced 1,4-dioxane concentrations from 1090 µg/L to less than 2 µg/L[17]. Stable isotope probing suggested mineralization to carbon dioxide[44].

Though typically considered a recalcitrant compound, evidence of natural attenuation of 1,4-dioxane has recently emerged. Laboratory studies found natural attenuation occurred in aquifer material from three California sites over a period of 20 weeks[45] and in arctic groundwater from Alaska over a period of six months[8]. Bacteria capable of 1,4-dioxane degradation were enriched from soil sampled at a drainage area around a 1,4-dioxane manufacturer in Japan, however other samples from wastewater treatment sludge, an uncontaminated garden, and the Yamato River did not demonstrate 1,4-dioxane degradation capabilities[46]. Biomarkers for molecular analysis to predict direct and cometabolic 1,4-dioxane degradation have been developed, which can be used as part of a multiple lines of evidence approach to evaluate MNA potential for a given site[47–49]. Data mining of California GeoTracker and US Air Force databases revealed 1,4-dioxane attenuation positively correlated with increased levels of dissolved oxygen and negatively correlated with increased metals and CVOC concentrations, and suggested that natural attenuation could potentially be used to manage 1,4-dioxane at some but not all sites[50].

2. Extent and Mechanisms of Biotransformation of 1,4-Dioxane

Biotransformation of hazardous compounds is useful for remediation when the transformation products are less hazardous than the parent compound. In aerobic settings, the ideal result is complete mineralization to carbon dioxide (CO_2)[1]. Aerobic 1,4-dioxane transformation has resulted in a range of products, including CO_2 to various extents. A direct metabolism study of 1,4-dioxane degradation by an isolated fungus found that ethylene glycol was the terminal end product[51]. Direct metabolism by CB1190 resulted in approximately 60% recovery as CO_2 after 48 hours, with 5% incorporated into biomass[52]. Direct metabolism by *Rhodanobacter* AYS5 resulted in 85% recovery as CO_2[14].

Cometabolic studies with THF as primary substrate found no degradation beyond 2-hydroxyethoxyacetic acid (2HEAA) after 402 hours with no conversion to biomass by *Pseudonocardia* strain ENV478[15], 78% mineralization to CO_2 and 2% incorporated into biomass by a mixed culture after an unknown time[16], and approximately 40% mineralization to CO_2 (no conversion to biomass) after 48 hours by *Pseudonocardia tetrahydrofuranoxydans* K1[52]. Cometabolism of 1,4-dioxane by *Mycobacterium vaccae* JOB5 grown on propane and *Pseudomonas mendocina* KR1 grown on toluene resulted in approximately 40% and 45% recovery as CO_2 after 48 hours, respectively, and no assimilation into biomass[52]. A natural attenuation study saw a maximum of 44% 1,4-dioxane recovery as CO_2 after a 28-week incubation period[45]. All of the transformation products studies referenced above are laboratory studies that used uniformly labeled 1,4-[^{14}C]dioxane and liquid scintillation analysis. A field study tracing cometabolism of uniformly labeled 1,4-[^{13}C]dioxane with propane as a primary substrate found both biomineralization and accumulation in biomass, though recovery as a mass balance was not quantified[44]. This range of results indicates that mineralization of 1,4-dioxane to CO_2 is possible and even likely, though the extent of biomineralization appears to depend on microbial cultures and cometabolic substrate.

Researchers have studied the transformation pathway of 1,4-dioxane in both bacterial and mammalian cells. Mahendra et al proposed a complete mineralization pathway

for 1,4-dioxane in 2007[52], which extended previous efforts from studies where complete mineralization was not observed[15]. Additional/alternate transformation products were recently proposed by Chen et al[11].

Multiple lines of evidence suggest 1,4-dioxane transformation is likely catalyzed by monooxygenase enzymes. 1,4-dioxane degradation is typically blocked by the presence of acetylene, a known monooxygenase blocker[53], and *E. coli* mutants were capable of 1,4-dioxane degradation containing cloned toluene monooxygenases[13]. In addition, the annotated genome sequence of CB1190 found eight gene clusters encoding multicomponent monooxygenase enzymes [54]. Analysis of soluble di-iron monooxygenase genes in THF and 1,4-dioxane degrading members of the *Pseudonocardia* and *Rhodococcus* genera found that "propane monoxygenase-like" enzymes can also contribute to 1,4-dioxane degradation[9]. Cells can express different monoxygenase enzymes based on their primary substrate or inducer, which impact the 1,4-dioxane degradation rates and capacity[18]. However, 1,4-dioxane degradation by *Xanthobacter flavus* DT8, also a direct metabolizer, was not affected by acetylene at five percent by volume in headspace, which indicated cytochrome P450 may not always be responsible for catalyzing 1,4-dioxane degradation[11].

A study of the THF monooxygenase gene cluster indicated that, while this enzyme catalyzed 1,4-dioxane degradation, it was not responsible for the degradation of the product 2HEAA[40]. The abundance of aldehyde dehydrogenase genes (aldH) also correlates with 1,4-dioxane degradation, which suggests it may be responsible for transformation of daughter products[48,55].

The literature contains a range of findings about 1,4-dioxane transformation product toxicity. Propane and 1-butanol induced cells showed a 16% and 42% reduction in viability after 1,4-dioxane transformation by *Mycobacterium vaccae* JOB5[18]. Mahendra and Alvarez-Cohen (2006) also found that cometabolic 1,4-dioxane transformation resulted in product toxicity for multiple cultures[13], however product toxicity from 1,4-dioxane transformation with THF as primary substrate did not appear to impact the consortium studied by Zenker et al (2000) [16].

3. Inhibition of Biotransformation

1,4-dioxane contamination in groundwater is often accompanied by chlorinated solvent contamination, which may reduce 1,4-dioxane biotransformation rates and capacities. Kinetic inhibition can be competitive, noncompetitive, and uncompetitive[56]. Competitive inhibition between growth and cometabolic substrates is common because the enzyme synthesized by the primary substrate is specifically intended for the transformation of the primary substrate. The enzyme's lack of specificity allows for the fortuitous transformation of other compounds (cometabolism), but they are likely in competition with the primary substrate for active sites on the same enzyme[16,57]. Inhibition in 1,4-dioxane cometabolism is expected because previous work has shown competitive inhibition between the growth and cometabolic substrate is likely when dioxygenase and monoxygenase enzymes are involved[58]. Substrate inhibition of 1,4-dioxane cometabolism has been observed with THF used as a primary substrate[11,12]. However, average rates of 1,4-dioxane degradation can ultimately be increased by the use of a primary substrate[11,20].

Inhibition among chlorinated solvent mixtures is well documented in the literature[35,59,60]. The seminal study on inhibition of 1,4-dioxane degradation by co-occurring chlorinated solvents investigated the influence of 1,1,1-TCA and 1,1-DCE on aerobic bioremediation of 1,4-dioxane by three cultures: 1) direct metabolism by CB1190, and cometabolism by 2) *Pseudonomas mendocina* KR1 with toluene as primary substrate, and 3) *E. coli* expressing the toluene monoxygenase of KR1. 1,1,1-TCA and 1,1-DCE concentrations of 0.1-10 mg/L and .0096-.96 mg/L, respectively, were each found to inhibit 1,4-dioxane degradation by all strains. Inhibition of CB1190 was not competitive and reversible. The cometabolizing cultures also degraded the chlorinated solvents, though inhibition was competitive and irreversible. A mixture of both 1,1,1-TCA and 1,1-DCE was not presented[61]. Another study found that the presence of TCE at 5 mg/L reduced the cometabolic 1,4-dioxane degradation capacity of two bacterial strains, JOB5 and RHA1, when induced by

both propane and 1-butanol. Greater product toxicity was evident after the transformation of the 1,4-dioxane and TCE mixture than 1,4-dioxane alone[18].

A study of CB1190 found that direct metabolism of 1,4-dioxane was also inhibited by transition metals (cadmium, copper, and nickel) and organic ligands (tannin and cysteine)[62]. BTEX mixtures were also found to inhibit 1,4-dioxane degradation by a direct metabolizer[63]. Because 1,4-dioxane is so often present in contaminant mixtures, particularly chlorinated solvent mixtures, inhibition interactions should be further explored.

C. Microcosms

Microcosms are "miniaturized ecosystems" [64] which facilitate site-specific bioremediation experiments in small-scale, highly controlled conditions[65]. Microcosms can be used to determine if a culture for bioaugmentation can be introduced into an environment with geochemical conditions similar to a given field site and achieve the intended transformation as well as growth[60]. While microcosm studies are commonly performed in laboratory settings, in situ microcosms have gained popularity since their inception in the 1990s for their ability to better represent the biogeochemical conditions of a site.[34] Batch microcosm tests may not be enough to predict successful field application of bioaugmentation because cell morphologies and growth characteristics may impede transport of bioaugmented cultures in the subsurface, especially if they form clumps, filaments, and readily attach to surfaces[17]. For example, ENV478 (likely a *Pseudonocardia* species) formed dense clumps when grown on THF[15].

Microcosms studies are commonly used to assess 1,4-dioxane degradation in groundwater and aquifer solids from various sites. However, at the time of writing, there was only one example relating microcosm studies to a field demonstration in the literature. Microcosms constructed from aquifer material from Vandenberg Air Force Base, CA showed that propane biostimulation was a potentially effective remediation strategy for 1,4-dioxane in shallow regions of the aquifer. Propane-utilizing microbes could not be enriched from deep aquifer sediments, but bioaugmentation with *Rhodococcus ruber* ENV425 resulted in

1,4-dioxane transformation with the addition of nitrous oxide as an inorganic nutrient. Field tests confirmed the effectiveness of ENV425 as a bioaugmentation culture, but biostimulation with propane and oxygen was ineffective[17].

D. Rhodococcus Rhodochrous

The model microorganism used in this study was *Rhodococcus rhodochrous* strain American Type Culture Collection (ATCC) 21198, hereafter "21198." Formerly known as *Nocardia paraffinica*, 21198 was isolated from soil[66]. It is a Biosafety Level 1 bacterium, meaning it is not known to consistently cause disease in healthy adult humans[66,67].

R. rhodochrous is a gram positive bacterium of the Actinobacteria phylum and Nocardiaceae family[68]. Bacteria in the *Rhodococcus* genus are aerobic, non-sporulating, prolific in the environment, and their metabolic diversity allows for numerous applications in the chemical, energy, pharmaceutical, and environmental industries[69]. Numerous physiological characteristics allow rhodococci to access and degrade a wide variety of organic compounds. Long chains of mycolic (fatty) acids in the cell wall allow rhodococci to access hydrophobic substrates[70]. Rhocococci are also able to alter their membrane fatty acid composition based on available substrates, which changes the fluidity of the cell envelope and likely contributes to their ability to resist numerous toxic compounds[71]. Rhodococci can also survive in starvation conditions[70,72].

R. rhodochrous, including strain ATCC 21198, have been shown to degrade a variety of environmental contaminants through both direct and cometabolic processes. These contaminants include a variety of aromatic and chlorinated aliphatic hydrocarbons[73,74], BTEX compounds (benzene, toluene, ethylbenzene, and xylene)[74], crude oil[75], the plasticizer bis-2-ethylhexyl adipate[76], the explosive hexahydro-1,3,5-trinitro-1,3,5-triazine (RDX)[77], and cyanide[78]. This is not an exhaustive list.

At the time of writing, there were no published studies of 1,4-dioxane degradation by 21198 or any *R. rhodochrous* strain. However, there are numerous examples of 1,4-dioxane degradation by other species in the *Rhodococcus* genus. Cometabolic degradation of 1,4-

dioxane occurs in *Rhodococcus* strains grown on a variety of primary substrates: *Rhodococcus* RR1 grown on toluene[13], *Rhodococcus jostii* RHA1 grown separately on both propane and 1-butanol[18], and *Rhodococcus* sp. strain 219 (later identified as *Rhodococcus ruber*[79]) and *Rhodococcus aetherivorans* JCM 14343 grown on tetrahydrofuran[9,39]. Direct metabolism of 1,4-dioxane was achieved by *Rhodococcus ruber*[39] and *Rhodococcus aetherivorans* JCM 14343[9].

E. Modeling Cometabolism

Modeling is a potentially useful tool for understanding and predicting cometabolism, and ultimately designing bioremediation systems[60,80]. Potentially relevant factors in an aerobic cometabolic degradation scenario that could be incorporated into a model include: oxygen availability, the presence or absence of primary (growth) substrate, the concentration of the cometabolic substrate of interest (COC), the presence of co-contaminants, reducing energy availability, product toxicity, nutrient availability, and the microorganisms themselves [58–60,80,81]. The number of factors included influence the complexity of the model. The foundation of cometabolic models is typically differential equations of varying complexity describing rates of primary substrate utilization, dS_G/dt; cometabolic substrate (the contaminant(s) of interest), dS_C/dt; and biomass growth, dX/dt [82].

The simplest cometabolic models employ zero or first order kinetics, though cometabolic models more commonly combine Michaelis-Menten and Monod kinetics[59]. The Michaelis-Menten model describes the rate of substrate utilization in an enzyme-mediated reaction, K, according to Equation 1,

$$\mathrm{K} = -\frac{K_{max} * \mathrm{S}}{K_S + \mathrm{S}} \qquad (1)$$

where K_{max} is the maximum substrate degradation rate and K_S is the half-saturation constant. K_S is the substrate concentration where K is half of K_{max}, which quantifies enzyme affinity for substrate. The Monod model describes cell growth rate, μ, according to Equation 2,

$$\mu = -\frac{\mu_{max} * S}{K_S + S} \quad (2)$$

where μ_{max} is the maximum growth rate of cells and K_S is the same half saturation constant as in the Michaelis-Menten model, though in the Monod model it is the substrate concentration when μ is half of μ_{max}. Michaelis-Menten and Monod models are combined via a yield coefficient, Y, which gives the quantity of biomass produced per quantity of substrate consumed. This results in equations for biomass growth and substrate transformation as shown in Equations 3 and 4, respectively,

$$\frac{dX}{dt} = Y\frac{K_{max,G} * S_G * X}{K_{s,G} + S_G} - bX \quad (3)$$

$$\frac{dS}{dt} = -\frac{K_{max} * S * X}{K_s + S} \quad (4)$$

where X is biomass and b is the first order endogenous decay coefficient. Equation 4 can describe both primary and cometabolic substrate transformation when used with their respective parameter values.

Increasing the complexity of model involves additional parameters. A common parameter included in many cometabolic models is transformation capacity, T_c, which is the maximum quantity of a cometabolic substrate transformed per unit of cells[59 5883]. Compounds with higher transformation product toxicity will have lower transformation capacities. Parameters can also be added to account for competition between the primary and cometabolic substrate and/or mixtures of cometabolic substrates. Competitive

inhibition between the growth and cometabolic substrate is likely when dioxygenase and monoxygenase enzymes are responsible for transformation [58].

Numerous cometabolic models varying in size and complexity have been presented in the literature. While many models utilize the Michaelis-Menten and Monod kinetic parameters described above, agreement has not been reached about the most useful model for cometabolism in general. A study by Liu et al, 2015, evaluated five cometabolism models for suitable model size and complexity and the models' ability to fit experimental data and identify parameters. Each model used the Michaelis-Menten model (Equation 4) to determine primary substrate utilization, with cometabolic substrate transformation and biomass growth determined from (listed in order of increasing complexity) first order, standard Michaelis-Menten, co-limiting (reductant), competitive inhibition, and combined (reductant and competitive inhibition) models. The comparison indicated that no single model fit simulated data well across a range of batch experimental conditions[82]. Precise calculation of Michaelis-Menten and Monod kinetic and inhibition parameters can be obtained through extensive rate tests in a laboratory setting [57], however this may not be possible for microcosm and field studies[84]. Simplified first or zero order models may be more relevant in these settings[84,85]. Numerous field-scale factors including subsurface heterogeneities, contaminant sorption, and the transport of microorganisms and nutrients in the subsurface have the potential to dilute the importance of microscale reaction kinetics[80]. However, the development of models with kinetic parameters determined from laboratory work have been used to successfully simulate trends observed in field studies, and therefore have the potential to inform the design of *in situ* bioremediation schemes (Semprini et al., 2007; Semprini and McCarty, 1991).

Studies of chlorinated solvent and/or 1,4-dioxane cometabolism typically quantify degradation using standard Michaelis-Menten kinetic parameters, K_s, K_{max}, Y, and b. Zenker et al (2002) modeled cometabolic transformation of 1,4-dioxane by a mixed culture in the obligate presence of THF. Their model included microbial growth on THF, loss of 1,4-dioxane

degradation capability in absence of THF, and substrate inhibition[81]. Prior work[16] showed no product toxicity from 1,4-dioxane transformation, which was supported by high T_c values.

III. METHODS

A. Chemicals

All chemicals used were analytical grade: Isobutane, 99.99%, Gas Innovations; 1,4-dioxane, 99%, Baker; deuterated 1,4-dioxane, >99%, Sigma-Adrich; TCE, 99.9%, Macron Fine Chemicals.

B. Analytical Methods

Isobutane and TCE were analyzed via 100 µL gas headspace samples extracted by Hamilton 1700 Series gas-tight syringes. Isobutane was analyzed on a Hewlett Packard Gas Chromatograph, Series 6890, equipped with a Flame Ionization Detector (GC-FID) and capillary column (Agilent 30 m x 0.53 mm). Helium was the carrier gas at 15 mL/minute and the oven temperature was a constant 150°C. TCE was analyzed on a Series 6890 Hewlett Packard Gas Chromatograph equipped with an Electron Capture Detector (GC-ECD) and capillary column (Agilent 30 mx 0.32 mm). Helium was the carrier gas at 8.0 mL/minute and the oven temperature was a constant 200°C.

1,4-dioxane was analyzed from liquid samples via Gas Chromatography-Mass Spectrometry (GC-MS) preceded by a heated purge and trap concentrator[86]. The purge and trap is a Tekmar Dohrmann 3100 Sample Concentrator with an AQUA Tek 70 Liquid Autosampler. The GC-MS is a Hewlett Packard 6890 series GC equipped with a capillary column (Restk 30 mx 0.2 mm Rtx-VMS) and a model 5973 Mass Selective Detector. The GC-MS was run in single ion mode in order to detect low concentrations of standard 1,4-dioxane (m/z 88) and deuterated 1,4-dioxane (m/z 96) run as an internal standard[87]. The 1,4-dioxane detection limit is approximately 0.1 µg/L. Approximately 25 mL of liquid was required for each 1,4-dioxane sample. Due to the relatively large sample volume and the sensitivity of the instrument, samples were typically diluted 250-125 times. Prior to analysis, samples were filtered and stored at 4°C. Samples less than 1 mL were filtered with 0.2 µm polyvinylidene fluoride (PVDF) syringe tip filters (Phenomenex AF6-5205-12), and samples greater than 1 mL were sampled with 0.2 µm cellulose acetate syringe tip filters (VWR 28145-477).

All reactors were stored on shaker tables (approximately 150 rpm) to support the assumption that chemicals were in equilibrium between the gas and liquid compartments. Henry's Constant was used to determine the total mass of each chemical in the reactor according to Equations 5 and 6,

$$H_{cc} = \frac{C_g}{C_l} \quad (5)$$

$$M_T = C_l * V_l + C_g * V_g \quad (6)$$

where H_{cc} is the dimensionless Henry's constant, C_g is the concentration in the gas phase, V_g is the gas volume of the reactor, C_l is the concentration in the liquid phase, and V_l is the liquid volume in the reactor. Henry's constant values used for chemicals in this study are listed in Table 2[88].

Table 2. Henry's Constants used in the study[88]

Chemical	Henry's Constant, H_{cc} (dimensionless)
Isobutane	49.2
1,4-dioxane	0.000198
Trichloroethene	0.42

Biomass was quantified as cell dry weight by total suspended solids (TSS) analysis. Bacterial solutions were vacuum filtered through 0.45 µm mixed cellulose ester membrane filters (Advantec A045A047A). Filters were dried at 100°C for one hour. Optical density (OD) readings taken at 600 nm on an Orion Aquamate 8000 UV-Vis Spectrophotometer (Thermo Scientific) were correlated with TSS measurements to determine bacterial concentrations in solution.

C. 21198 Growth reactors and Pure Culture

Rhodococcus rhodochrous strain 21198 was obtained from Michael Hyman at North Carolina State University, and is also available from the American Type Culture Collection.

Pure culture 21198 was grown in batch in 720 ml Wheaton or Kimble glass bottles with plastic caps containing butyl septa. Each growth reactor contained 300 mL sterile, phosphate-buffered mineral salts media (concentrations of constituent anion and cations listed in Table 3 and recipe in Appendix A)[89], leaving 420 mL air headspace. Growth reactors were fed 30 mL isobutane, an excess given that only 21 mL (0.86 mmol) could be oxidized with the available oxygen in the air headspace according to Equation 7.

$$C_4H_{10} + 6.5O_2 \rightarrow 4CO_2 + 5H_2O \quad (7)$$

Growth reactors were inoculated with a cluster of colonies taken from a mineral salts media growth plate (recipe in Appendix B) incubated at 30°C with 2-3% v/v isobutane/air. After approximately 20 mL isobutane had been consumed in the growth reactor (typically 3-4 days), growth reactors were opened to exchange the headspace (resupply oxygen) and another 30 mL isobutane was provided. The culture would be in late exponential growth phase with high activity for experimental use the following day. All manipulations of the culture were performed in a laminar flow hood to maintain culture purity. Heterotrophic growth plates (recipe in Appendix B) were streaked when the growth reactors were opened on the third or fourth day after inoculation to verify the culture purity prior to the following day's experiment. Cells were typically harvested via centrifugation, washed and resuspended to a desired concentration in 50 mM monosodium phosphate (pH 7).

D. Microcosms

Microcosms were constructed with aquifer solids obtained from well cores from Fort Carson, Colorado, a site with 1,4-dioxane and TCE contamination. Maps of the 1,4-dioxane and TCE plumes at Fort Carson are shown in Figure 2 and Figure 3, respectively. At this site, the 1,4-dioxane plume extends far beyond the TCE plume. Sufficient information was not provided to correlate the core samples with a well on the site map. The solids appeared to be a fine-grained clay silt, though an analysis of particle size, organic matter, and nutrient composition was not performed. Aquifer solids were stored in 1L wide mouth glass Ball jars at 4°C.

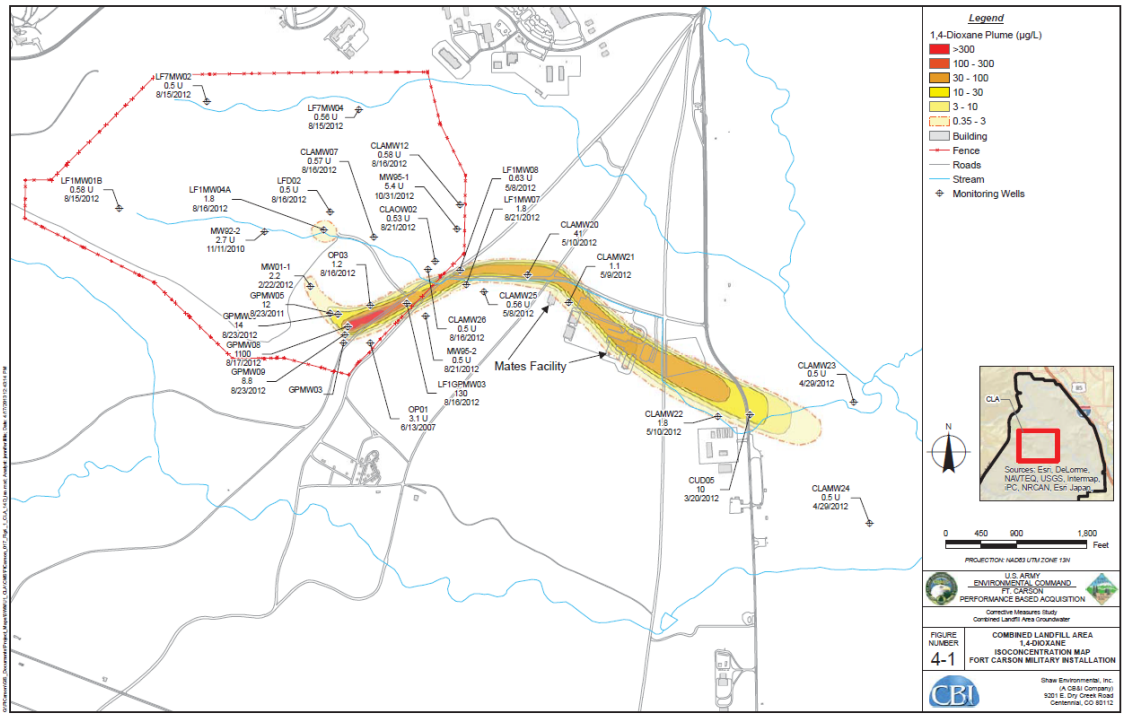

Figure 2. 1,4-Dioxane plume at Fort Carson, Colorado. Map prepared by Shaw Environmental, Inc in 2013 and obtained by Jack Istok (OSU) for this study

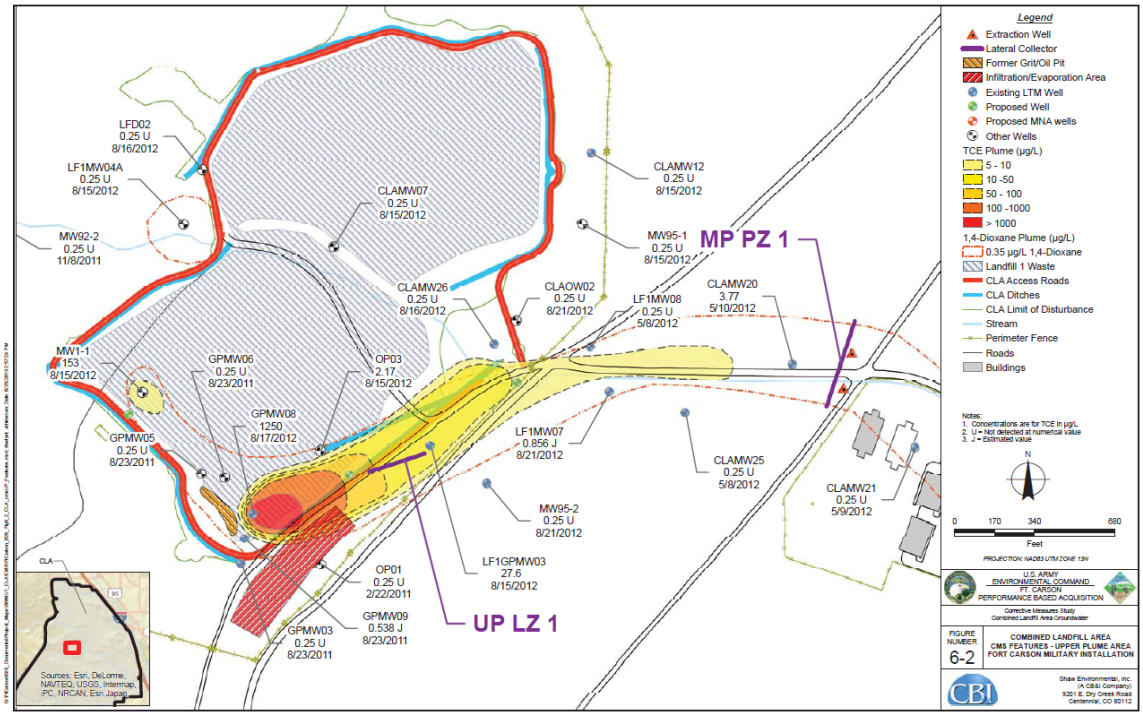

Figure 3. Trichloroethene plume at Fort Carson, Colorado. Map prepared by Shaw Environmental, Inc in 2013 and obtained by Jack Istok (OSU) for this study.

Artificial groundwater was constructed to replicate the constituents described in a 1984 USGS report on groundwater quality at the Fort Carson golf course[90]. The constituent concentrations in the groundwater report and in the artificial groundwater are listed in Table 3. The recipe for the artificial groundwater is given in Appendix C. The aquifer solids were combined with the artificial groundwater for a concentration of 52 g aquifer solids/L groundwater. For each set of microcosms, the required mass of aquifer solids was taken from the refrigerated sample, mixed with the artificial groundwater, and portioned into individual microcosms as a slurry to ensure consistency within the set. This practice did expose the aquifer solids to additional oxygen prior to use in the construction of later sets of microcosms.

Table 3. Concentration of cations and anions in Fort Carson groundwater, in artificial groundwater used in microcosms, and in microcosms after inoculation with 21198 suspended in spent growth media or nutrient amendment.

	Concentration (mg/L)					
Cations	USGS Study of Fort Carson Groundwater	Artificial Groundwater (Native microcosm without nutrient amendment)	Long-term Bioaugmented Microcosms	Short-term microcosms: "Bioaug Uw"*	Short-term microcosms: "Bioaug W+N" and "Native+N"*	Pure culture reactors (1x growth media)
Ca	189	190	190	190	190	0.33
Mg	105	101	101	101	101	8.96
K	3.09	3.15	4.06	7.01	3.53	348
Na	371	354	354	356	354	163
Fe	0.081	0.084	0.085	0.086	0.084	0.20
Mn	0.19	0.18	0.18	0.185	0.182	0.28
Cr	0.0026	0.0025	0.0025	0.0025	0.0025	0.0
NH_4	0.21	0.67	2.52	8.45	1.45	700
Cd	0.00328	0.00307	0.00307	0.00307	0.00307	0.0
Zn	NA	0.0	0.00263	0.01112	0.00111	1.00
Cu	NA	0.0	0.00020	0.00085	0.00009	0.08
Co	NA	0.0	0.00023	0.00096	0.00010	0.09
Mo	NA	0.0	0.00031	0.00133	0.00013	0.12
Anions						
Cl	91	93	96	108	94	1354
SO_4	1217	1241	1241	1242	1241	74.6
F	0.81	0.79	0.79	0.79	0.79	0.0
NO_3	3.6	2.3	2.3	2.3	2.3	0.0
NO_2	0.58	0.67	0.67	0.67	0.67	0.0
P	0.036	0.045	1.35	5.55	0.60	495
CO_3		286	286	286	286	0.0

* defined in Table 5

Microcosms were either biostimulated with isobutane (hereafter referred to as "native" microcosms) or bioaugmented with pure culture 21198 *and* biostimulated with isobutane (hereafter referred to as "bioaugmented" microcosms). Acetylene, a known monooxygenase inhibitor[13,53], was used at 5% or 10% headspace volume for controls. Aquifer microcosms were constructed in either 155 or 310 mL glass Wheaton bottles with

plastic caps and butyl septa. For each total volume, 40% was air headspace and 60% was groundwater slurry. Microcosms were stored at 20^{o}C and shaken at approximately 150 rpm to maintain equilibrium partitioning between the gas and liquid compartments. Microcosms were used for both long and short-term studies to assess the influence of several variables, including bioaugmentation with 21198, chlorinated solvent co-contamination, and inorganic nutrient concentration.

Microcosms for the long-term experiment were created in 155 mL bottles (95 mL groundwater slurry). Two conditions were tested in triplicate for both native and bioaugmented environments: 1) isobutane and 1,4-dioxane; and 2) isobutane, 1,4-dioxane, and TCE. The conditions and associated names used in figure legends are summarized in Table 4. This set of microcosms received seven additions of all chemicals applicable to each condition, approximately one month apart. Bioaugmentation with 0.05 mg 21198 suspended in 250 µL spent growth media occurred only in the first addition. The total mass of isobutane, 1,4-dioxane, and TCE added in each addition were 0.95 mg (0.4 mL), 0.048 mg, and 0.025 mg, respectively. The starting concentrations of 1,4-dioxane (500 µg /L) and TCE (200 µg/L) were chosen because they are intermediate concentrations out of the source zones of the Fort Carson plumes. These starting concentrations allow assessment of transformation starting at relatively low concentrations, which is a key motivation for the use of cometabolism for remediation. The microcosms were opened to the atmosphere for approximately 15 minutes prior to the addition of more chemicals to ensure an excess of oxygen in the headspace, but any remaining chemicals were not actively sparged from the reactors at this time. Acetylene was added at 5% v/v headspace for both native and bioaugmented controls (3 mL per addition). After five additions of chemicals, 200 µl spent growth media was added to two of the three native microcosms (without TCE) to assess the influence of additional inorganic nutrients in the 21198 inoculum in the bioaugmented. The initial concentration of anions and cations in the microcosms are listed in Table 3. (The native microcosms are represented by the artificial groundwater solution as no additional nutrients were added.)

Table 4. Microcosm conditions tested and names referenced in figure legends for long-term experiments

Name	Microcosm Description: environment, initial biomass (if applicable), and mass of isobutane, 1,4-dioxane, and TCE (if applicable) added in each addition (approximately one month apart)	n
Bioaug	In groundwater slurry: 0.05 mg 21198 suspended in 250 µL spent growth media, 0.95 mg isobutane, 0.048 mg 1,4-dioxane	3
Bioaug + TCE	In groundwater slurry: 0.05 mg 21198 suspended in 250 µL spent growth media, 0.95 mg isobutane, 0.048 mg 1,4-dioxane, 0.025 mg TCE	3
Native	In groundwater slurry: 0.95 mg isobutane, 0.048 mg 1,4-dioxane	3
Native + TCE	In groundwater slurry: 0.95 mg isobutane, 0.048 mg 1,4-dioxane, 0.025 mg TCE	3
Acetylene Controls	Acetylene controls were constructed for each microcosm condition listed above. Acetylene was added at 5% of headspace volume.	3

Microcosms for the short-term experiment were constructed in 310 mL bottles (180 mL groundwater slurry) to assess the impact of inorganic nutrients and bioaugmentation on the cometabolism of isobutane and 1,4-dioxane according to the following conditions: 1) bioaugmentation with 0.5 mg 21198 suspended in 2 mL spent growth media; 2) bioaugmentation with 0.5 mg 21198 washed in sodium phosphate buffer and 200 µL fresh growth media added as inorganic nutrients; 3) 200 µL growth media as inorganic nutrients for native microcosms; 4) native microcosms without nutrient amendment; and 5) pure culture reactors inoculated with 0.5 mg 21198 in 1x growth media. The conditions and associated names in figure legends for the short-term microcosm experiments are summarized in Table 5. These microcosms received four additions of 1.9 mg (0.8 mL) isobutane and 0.09 mg 1,4-dioxane approximately two to three days apart (as soon as the previous addition of chemicals had been transformed). Where applicable, bioaugmentation with 21198 and nutrient amendment with growth media occurred only in the first addition. The initial concentration of anions and cations in the microcosms are listed in Table 3. (Just as in the long-term experiments, the native microcosms without growth media are represented by the artificial groundwater solution.) Microcosms were opened to the

atmosphere between additions using previously described procedures. Acetylene was added at 10% v/v headspace for all controls.

Table 5. Microcosm conditions tested and names referenced in figure legends for short-term experiments

Name	Microcosm Description: environment, initial biomass (if applicable), nutrients (if applicable), and mass of isobutane and 1,4-dioxane added in each addition (approximately two days apart)	n
Bioaug Uw	In groundwater slurry: 0.5 mg 21198 suspended in 2 mL spent growth media, 1.9 mg isobutane, 0.09 mg 1,4-dioxane	2
Bioaug W+N	In groundwater slurry: 0.5 mg 21198 washed in phosphate buffer, 200 µl growth media for inorganic nutrients, 1.9 mg isobutane, 0.09 mg 1,4-dioxane	3
Native+N	In groundwater slurry: 200 µl growth media for inorganic nutrients, 1.9 mg isobutane, 0.09 mg 1,4-dioxane	3
Native no N	In groundwater slurry: 1.9 mg isobutane, 0.09 mg 1,4-dioxane	2
Pure Culture	In growth media: 0.5 mg 21198, 1.9 mg isobutane, 0.09 mg 1,4-dioxane	2
Acetylene Controls	Acetylene controls were constructed for each microcosm condition described above. Acetylene was added at 10% of headspace volume.	2

Zero order rates of isobutane utilization and 1,4-dioxane degradation were calculated from linear regression of the initial linear region of the curves indicating the fastest rate of transformation of each addition using the command “fitlm” in MATLAB. Rates were calculated for each microcosm and averaged across the duplicate or triplicate. Welch’s t-tests (a more conservative method than the Student’s t-test due to the assumption of unequal variances) were used to compare mean rate differences at a significance level of p=0.05.

E. Model Development

1. Model equations and parameter development

Simultaneous utilization of isobutane, degradation of 1,4-dioxane, and growth of biomass were modeled according Michaelis-Menten and Monod kinetics. Equations for growth substrate utilization, S_G (isobutane), cometabolic substrate degradation, S_C (1,4-

dioxane), and biomass growth, X, in batch reactors are shown in Equations 8, 9, and 10[82]. Cometabolic substrate degradation is often impacted by competitive inhibition[58]. As shown in the denominator of Equation 9, the model used for 1,4-dioxane degradation includes competitive inhibition by the presence of isobutane[60].

$$\frac{dS_G}{dt} = \frac{-K_{max,G} * S_G * X}{K_{s,G} + S_G} \quad (8)$$

$$\frac{dS_C}{dt} = \frac{-K_{max,C} * S_C * X}{K_{s,c} + S_C + \frac{K_{s,c} * S_G}{K_I}} \quad (9)$$

$$\frac{dX}{dt} = Y * \frac{dS_G}{dt} - bX = \frac{Y * K_{max,G} * S_G * X}{K_{s,G} + S_G} - bX \quad (10)$$

Transformation capacity and oxygen concentration were not included in the model equations for these experiments. Concentrations of 1,4-dioxane were low (500 µg/L and lower), so transformation capacity was assumed to have a negligible influence on degradation. The reactors were regularly opened to the atmosphere, thereby providing an excess of oxygen.

The dimensionless Henry's constant was used to determine the concentrations of each constituent in the liquid and gas compartments of the microcosms according to Equation 5. Biological reactions occur in the liquid compartment, so the kinetic parameters K_{max} and K_s correspond to rates according to liquid phase concentrations. In order to model the transformation of the total mass, dM/dt, of both isobutane and 1,4-dioxane, S_G and S_C on the right side of Equations 8 and 9 should be the concentrations in the liquid compartments, which was determined from total mass using Equation 6. The updated equations used to model the transformation of the total masses (mg) of isobutane, M_{IB}, and

of 1,4-dioxane, M_{14D}, are shown in Equations 11 and 12, respectively. Biomass, X, was modeled as a liquid concentration (mg TSS/L) according to Equation 13.

$$\frac{dM_{IB}}{dt} = \frac{-K_{max,IB} * X * V_l * \frac{M_{IB}}{V_l + V_g * H_{cc,IB}}}{K_{s,IB} + \frac{M_{IB}}{V_l + V_g * H_{cc,IB}}} \quad (11)$$

$$\frac{dM_{14D}}{dt} = \frac{-K_{max,14D} * X * V_l * \frac{M_{14D}}{V_l + V_g * H_{cc,14D}}}{K_{s,14D} + \frac{M_{14D}}{V_l + V_g * H_{cc,14D}} + \frac{K_{s,14D} * \frac{M_{IB}}{V_l + V_g * H_{cc,IB}}}{K_I}} \quad (12)$$

$$\frac{dX}{dt} = \frac{-K_{max,IB} * X * Y * \frac{M_{IB}}{V_l + V_g * H_{cc,IB}}}{K_{s,IB} + \frac{M_{IB}}{V_l + V_g * H_{cc,IB}}} - bX \quad (13)$$

The three equations were solved simultaneously in MATLAB using the command "ode45," a numerical method for initial value problems that uses an adaptive time step evaluator and fourth- and fifth-order Runge Kutta algorithms to minimize error[91]. The model was reinitiated and run for each addition of the experiment. Initial values for each run were the first quantities of isobutane and 1,4-dioxane measured for each addition. The initial value for biomass concentration for the first addition was a measured value from TSS analysis, however in model runs for subsequent additions the initial biomass value was the final model output for biomass from the previous addition. This method was used because biomass concentrations were not known in the microcosms after the initial bioaugmentation inoculum (when applicable), and data points for biomass concentrations in pure culture reactors obtained from OD analysis did not correlate to the beginning of each addition.

Initial estimates of the values of K_{max} and K_s for both isobutane and 1,4-dioxane were made through the development of Monod Curves. Rapid, pure culture tests were performed to assess the initial, zero order rate (mg/mg 21198/day) across a range of initial isobutane and 1,4-dioxane concentrations. Rate tests were performed in 27 mL glass bottles closed

with aluminum crimp tops and butyl septa. The parameters K_{max} and K_s were determined by nonlinear regression of the zero-order rate vs the initial liquid concentration using Equation 1 and the command "nlinfit" in MATLAB.

Further estimates of parameter values were made from optimization to pure culture and microcosm data by a simple iterative search method[91]. A range of values and a step size for the individual parameter(s) being optimized were specified to generate a vector of test values for each parameter. The model was run with every value for an individual parameter or every combination of values in the case of multiple parameters. The optimum parameter value or combination of parameter values was determined as that which minimized the sum of the squared errors, SSE, between model and data values for the same time point according to Equation 14

$$\text{SSE} = \sum_{i=1}^{n}(Exp_i - Mdl_i)^2 \qquad (14)$$

in which Exp_i are experimental values, Mdl_i are model values.

The goodness of fit of the model to the experimental data was quantified using the Nash-Sutcliffe efficiency, E, determined according to Equation 15

$$E = 1 - \frac{\sum_{i=1}^{n}(Exp_i - Mdl_i)^2}{\sum_{i=1}^{n}(Exp_i - Exp_{avg})^2} \qquad (15)$$

where Exp_{avg} is the mean of a given set of n experimental values. A perfect fit would have an E value of one, and an E value less than zero indicates that the mean of the data set is a better fit than the model. Because the calculation of E squares the difference between model and experimental values, it is more influenced by larger values in a data set[92].

2. *Model Verification and Sensitivity Analysis*

Analytical solutions described by Smith et al (1998) were used to verify model performance[93]. An integrated solution for primary substrate utilization is given by Equation 16.

$$t = \frac{1}{K_{max,G}}\left\{\left(\frac{K_{s,G}}{X_0 + Y * S_{G,0}} + \frac{1}{Y}\right) ln\left[\left(X_0 + Y(S_{G,0} - S_G\right)\right] + \left(\frac{K_{s,G}}{X_0 + Y * S_{G,0}}\right) \ln\left[\frac{S_{G,0}}{X_0 * S_G}\right] - \frac{1}{Y}\ln(X_0)\right\} \quad (16)$$

The concentration of substrate, S_G, is an implicit variable in the equation for time, t. In order to compare the model output with the analytical solution, model values for isobutane were input into Equation 16 and the corresponding times were compared with the input time values for the model simulation. Equation 16 incorporates cell growth but not decay and does not account for partitioning of the substrate between gas and liquid phases. Therefore, in order to use Equation 16, the model (Equations 11-13) was run with b set at zero and the total mass of isobutane was made into a liquid concentration by setting V_g to zero and dividing the total mass by V_l. As shown in Figure 4, the model and analytical solution produced the same results.

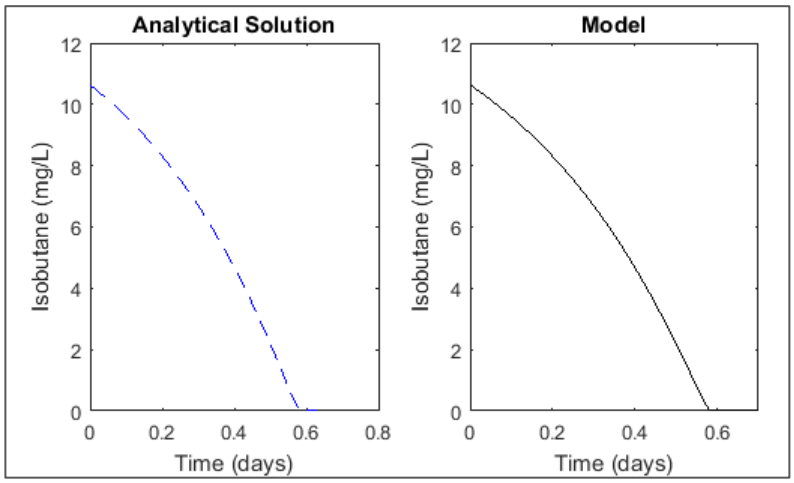

Figure 4. Comparison of analytical solution and model output for isobutane utilization assuming a single-phase liquid system (V_g=0) and no endogenous decay (b=0).

Verification of the partitioning of isobutane between the gas and liquid phases was performed by assessing the total biomass generated through substrate consumption. The anticipated biomass in the system is given by Equation 17.

$$X = X_0 + Y(M_0 - M) \tag{17}$$

The total isobutane transformed in the pure culture experiment was 7.62 mg (the sum of the initial measured isobutane values across four additions). With an initial biomass of 0.5 mg and yield of 0.885 mg 21198/mg substrate, the anticipated biomass according to Equation 17 was 7.24 mg. This was also the final biomass value from the model output when run with b set to zero.

An integrated solution for cometabolic substrate utilization is given by Equation 18 [93]. As shown in the equation, this solution includes gas-liquid partitioning to model the transformation of the total mass of the cometabolic substrate. The equation is for resting cells and does not include endogenous decay, so Y and b were set to zero to generate 1,4-dioxane model values as input for the analytical solution. The analytical solution also does not include primary substrate inhibition, so the third term in the denominator of Equation 12 was removed when the model was run to generate comparative values.

$$t = \frac{1}{K_{max,C}}\left\{\left(\frac{K_{s,C}\left(V_l + H_{CC} * V_g\right)}{V_l\left(\frac{M_o}{T_c * V_l} - X_0\right)}\right) ln\left[\frac{M * X_o}{M_o\left(X_o - \frac{1}{T_c * V_l}(M_o - M)\right)}\right] + T_c * ln\left[\frac{X_o}{X_o - \frac{1}{T_c * V_l}(M_o - M)}\right]\right\} \tag{18}$$

Equation 18 also includes transformation capacity, T_C, which was not used in model development due to the low quantities of 1,4-dioxane transformed in the microcosms.

Therefore, in order to verify model performance, Equation 18 was simplified to Equation 19 by assuming an infinitely large transformation capacity. However, Equation 18 was also used to assess the validity of the assumption that transformation capacity was negligible in these systems by using a transformation capacity of 2 mg 1,4-dioxane/mg 21198 as determined previously.

$$t = \frac{1}{K_{max,C}}\left\{\left(\frac{K_{s,C}\left(V_l + H_{CC} * V_g\right)}{-V_l * X_0}\right) ln\left[\frac{M}{M_o}\right]\right\} \qquad (19)$$

The model and the analytical solution from Equation 19 produced the same result, which verified the code. The analytical solution including the transformation capacity term, Equation 18, also produced the same output with T_c=2 mg 1,4-dioxane/mg 21198. This confirmed that the small quantities of 1,4-dioxane transformed did not exert an influential toxicity on the cells (also seen in other cometabolism studies[16]) and validated the decision not to include the transformation capacity in model development.

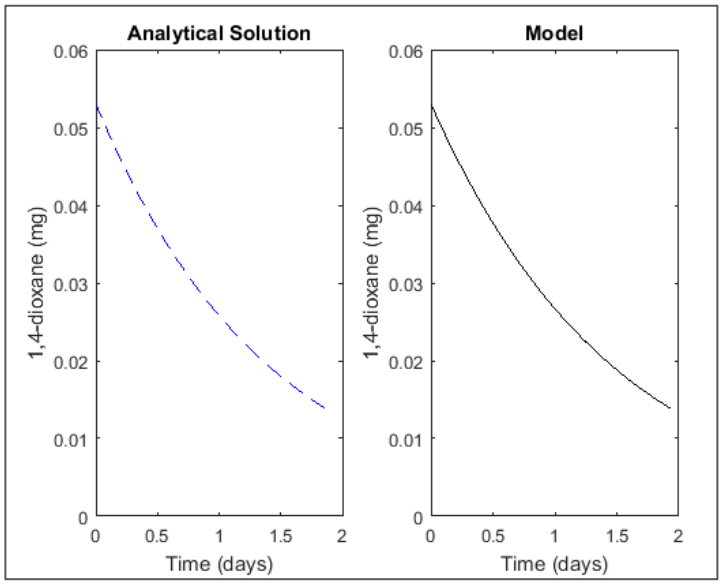

Figure 5. Comparison of analytical solution and model output for 1,4-dioxane degradation assuming resting cell conditions (Y=0), no endogenous decay (b=0), and no primary substrate inhibition. Results for the analytical solution were the same when obtained with a transformation capacity equal to infinity and 2 mg 1,4-dioxane/mg 21198.

The sensitivity of each parameter in the model equations (Equations 11, 12, and 13) was tested individually after final parameter adjustment. The model was run with a single parameter increased or decreased by 30% of its value. The model's sensitivity to the parameter change was assessed by calculating the percent difference in the value of the Nash-Sutcliffe efficiency, E.

IV. RESULTS

A. Overview

Aquifer microcosms were constructed to assess biodegradation of 1,4-dioxane when biostimulated with isobutane, bioaugmented with 21198, in the presence of TCE, and with a range of available nutrients. Long-term microcosms received seven additions of chemicals approximately one month apart, and short-term microcosms received four additions of chemicals two to three days apart. Descriptions of each set of microcosms are located in Table 4 (long-term microcosms) and Table 5 (short-term microcosms). Comparisons between microcosm conditions were primarily based on the analysis of initial, zero order degradation rates. Isobutane utilization, 1,4-dioxane degradation, and biomass growth were simultaneously modeled according to Michaelis-Menten and Monod kinetics.

B. Long-term Microcosm Experiments

1. Comparison of bioaugmented and native microcosms

Biostimulation of Fort Carson aquifer microcosms with isobutane effectively stimulated microorganisms native to aquifer sediments. As shown in the upper plot of Figure 6, isobutane was consumed in native microcosms approximately one week after initial biostimulation. Biostimulation rates can depend on a variety of factors, including primary substrate and microcosm construction. For comparison, the biostimulation lag in these microcosm experiments is significantly shorter than a three to ten month lag period for soil microcosms biostimulated with THF described by Zenker et al (2000)[16]. Figure 6 also shows the consumption of isobutane coincided with transformation of 1,4-dioxane.

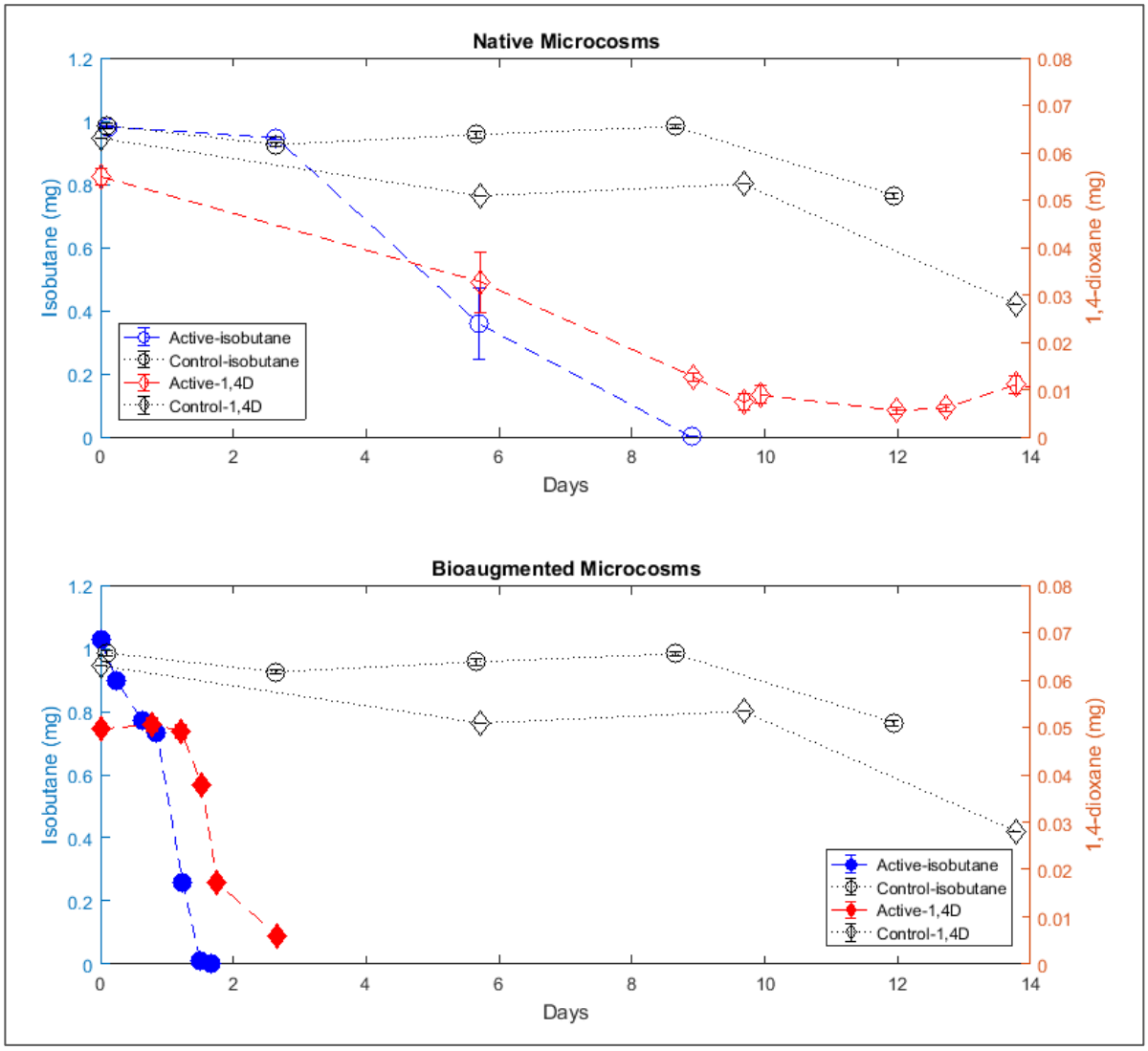

Figure 6. Transformation of isobutane and 1,4-dioxane in native and bioaugmented microcosms and acetylene controls. Error bars (hidden by marker fill when small) show one standard error.

The lower plot in Figure 6 also shows that in microcosms bioaugmented with 21198, isobutane was transformed immediately. 1,4-dioxane was not rapidly transformed until isobutane in the microcosm was consumed below approximately 0.5 mg (0.15 mg/L in liquid). This indicates substrate inhibition, a common phenomenon in cometabolic processes involving monooxygenase enzymes due to a lack of enzyme specificity[58]. Primary substrate inhibition has also been observed in cometabolic transformations of 1,4-dioxane with THF as a primary substrate[15,16]. Isobutane and 1,4-dioxane were not transformed in acetylene

controls, which further supports the hypothesis that a monooxygenase enzyme catalyzed the reaction[13,53].

A comparison of isobutane and 1,4-dioxane transformation between averaged triplicates of native and bioaugmented microcosms over five additions spanning approximately 180 days is shown in Figure 7. Transformation of isobutane (blue, left axis) and 1,4-dioxane (red, right axis) is shown in a separate subplot for each addition, which occurred approximately one month apart. Transformation of the initial addition, shown previously in Figure 6, is the first column of subplots in Figure 7. Note different time scales in subplots for native and bioaugmented microcosms were needed to show the full transformation of each addition. Time between additions was removed for better data visualization. The experiment on the continuous timescale is shown in Appendix D.

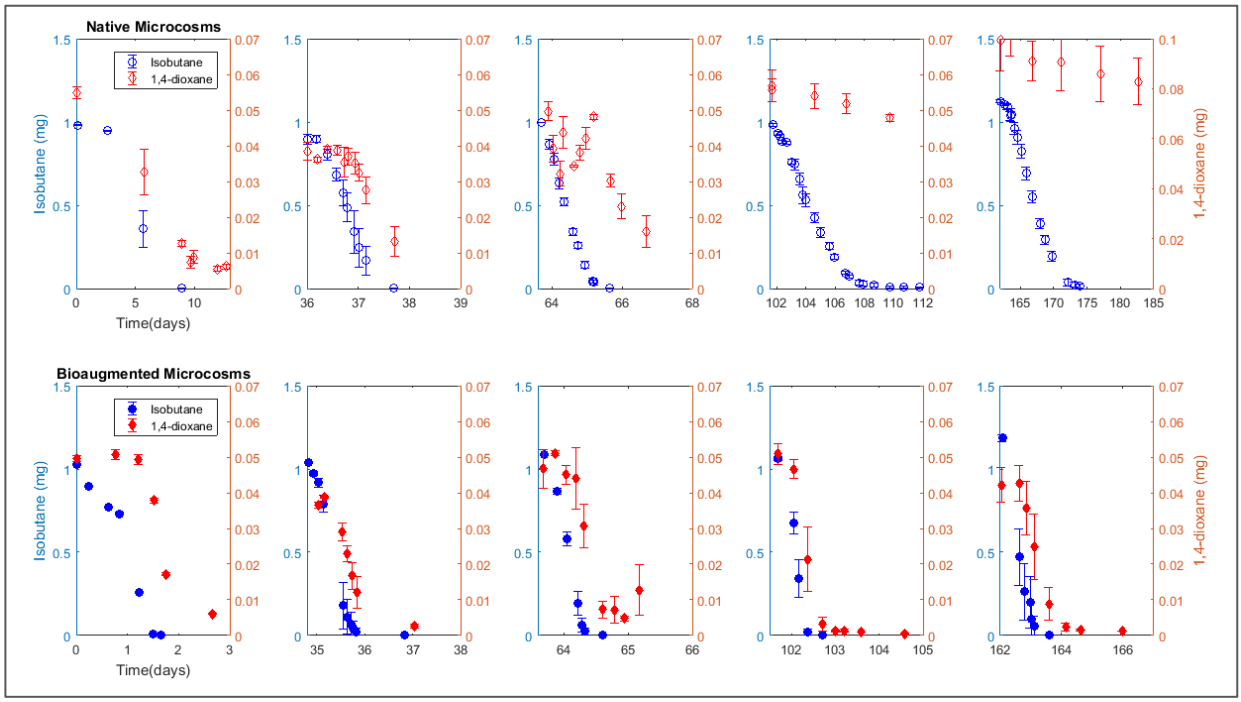

Figure 7. Transformation of five additions of isobutane (blue) and 1,4-dioxane (red) in native (upper plot) and bioaugmented (lower plot) microcosms. Error bars represent one standard error.

Figure 7 shows that after the initial biostimulation lag in the first addition, the time required for isobutane and 1,4-dioxane transformation in the second addition was very similar in the native and bioaugmented microcosms, and the total time to complete the

transformation was less in both environments. This suggested an increase in active biomass, as expected from isobutane (primary growth substrate) consumption. In the third addition, the total time for isobutane and 1,4-dioxane transformation further decreased as expected in the bioaugmented microcosms, however it increased in the native microcosms, resulting in a difference in the performance between native and bioaugmented environments. In the fourth addition, isobutane transformation in the native microcosms took approximately four times as long as it had in the third addition and almost no 1,4-dioxane transformation occurred. In the fifth addition, the time for total isobutane transformation further increased and 1,4-dioxane transformation remained stalled. By contrast, in the bioaugmented microcosms, the time for isobutane and 1,4-dioxane transformation further decreased between the second and third additions, remained approximately constant between the third and fourth additions, and slowed slightly between the fourth and fifth additions. This led to widened differences in activity and degradation capacity between the native and bioaugmented microcosms in the fourth and fifth additions.

Figure 7 also illustrates that inhibition of 1,4-dioxane degradation by the presence of isobutane occurred in each addition throughout the experiment. The lag in 1,4-dioxane transformation due to isobutane inhibition appeared to increase as isobutane transformation slowed in later additions. However, the stall of 1,4-dioxane transformation in native microcosms during the fourth and fifth additions appears to be a result of more than just isobutane inhibition. This suggests that when isobutane transformation slows below a certain rate, little 1,4-dioxane cometabolism would occur.

Zero order degradation rates were estimated from the initial linear region of each isobutane and 1,4-dioxane degradation curve. Isobutane and 1,4-dioxane transformation rates averaged across each triplicate are shown in the top and middle subplots, respectively, in Figure 8. Degradation curves and the linear regions selected to determine rates for each individual reactor are shown in Appendix E. Rates were calculated from regions exhibiting linear rates of degradation, and therefore do not represent lag periods due to biostimulation or primary substrate inhibition. Differences in rates between native and bioaugmented

microcosms and between each addition can be seen through a visual examination of Figure 8, and Welch's t-tests were used to compare mean rate differences at a significance level of p=0.05. The bottom subplot in Figure 8 shows a linear regression of average 1,4-dioxane vs isobutane rates, performed separately for native and bioaugmented microcosms.

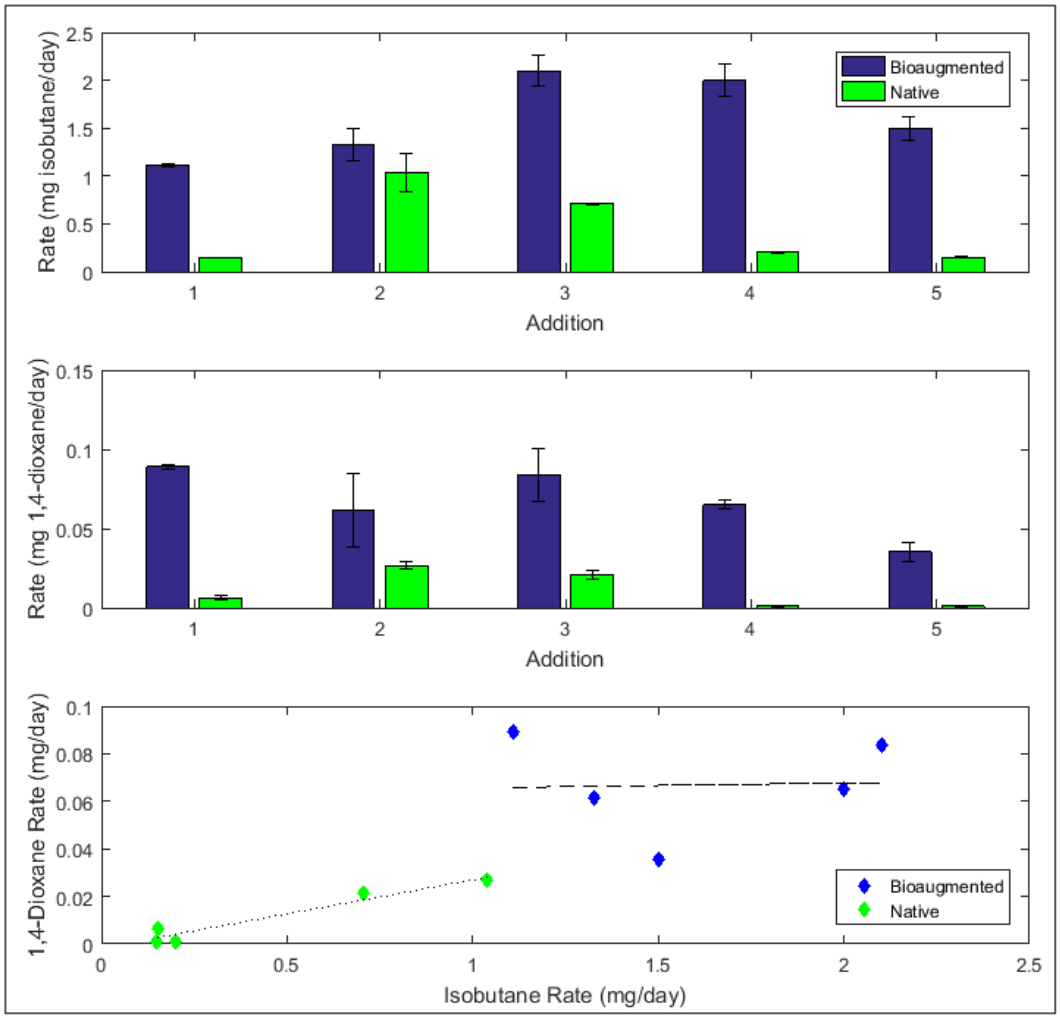

Figure 8. Initial, zero order isobutane utilization rates, 1,4-dioxane degradation rates, and linear regression of 1,4-dioxane vs isobutane rates, over five additions in long-term bioaugmented and native microcosms. Error bars show one standard error.

The rate analysis closely mirrors the conclusions drawn from assessment of the total time required to complete each transformation. As expected from assessment of the transformation curves in Figure 7, rates in native and bioaugmented microcosms were similar in the second addition. Statistically significant differences in isobutane

transformation rates in native and bioaugmented microcosms were found in the first, third, fourth, and fifth additions. 1,4-dioxane transformation rates were significantly different between native and bioaugmented microcosms in the first, fourth, and fifth additions. Figure 8 also shows that little 1,4-dioxane transformation occurred when the isobutane transformation rate fell below 0.5 mg/day, indicating that little cometabolism of 1,4-dioxane occurred with slow turnover of the monooxygenase enzyme.

As shown in the bottom subplot in Figure 8, the regression analysis appears to indicate correlation between 1,4-dioxane and isobutane transformation rates in native microcosms. The linear regression for the native microcosms resulted in a line with a slope of 0.0286 mg 1,4-dioxane/mg isobutane, intercept of -0.0016 mg 1,4-dioxane/day, and correlation coefficient, R^2, of 0.94. The negative intercept agrees with trends observed through analysis of the degradation curves: at low rates of isobutane utilization, corresponding 1,4-dioxane cometabolism did not occur. The linear regression of the rates in the bioaugmented microcosms resulted in a slope of 0.0021 mg 1,4-dioxane/mg isobutane and , R^2, of 0.0017, and therefore do not suggest correlation between 1,4-dioxane and isobutane rates. The intercept of 0.064 mg 1,4-dioxane/day for approximately horizontal line suggests a constant rate of 1,4-dioxane degradation regardless of the isobutane utilization rate, though there is considerable scatter in the data. The horizontal line could also indicate a maximum rate of 1,4-dioxane transformation, however concentrations in each addition were low and therefore not in the K_{max} range (additional comments in the discussion of model development).

The slowing of 1,4-dioxane degradation in later additions in both native and bioaugmented microcosms (to different degrees) was not due to a lack of carbon or energy from the growth substrate because isobutane was still consumed (though also more slowly). Microcosms were opened to the atmosphere between each addition so a lack of oxygen was also not the cause of the rate decreases. Groundwater slurry, however, was not exchanged or replenished between additions, so a shortage of inorganic nutrients was potentially the source of the rate decrease in later additions. A difference in inorganic nutrient

concentrations was also the potential cause of the large differences in transformation rates between the native and bioaugmented microcosms after the second addition. Specifically, higher concentrations of inorganic nutrients may have allowed the bioaugmented microcosms to maintain higher transformation rates until slowing in the fifth addition.

When bioaugmentation occurred, 0.05 mg 21198 was added directly from the growth reactor so the inoculum was suspended in 250 µl of spent growth media. While the nutrient concentrations in the media shown in Table 3 were likely reduced through 21198 biomass generation in the growth reactor, the addition of this spent growth media resulted in potentially up to an additional 175 µg ammonium (NH_4) and 124 µg phosphorous (as well as other micronutrients) in the bioaugmented microcosms. This results in NH_4 and phosphorous concentrations approximately 3.8 and 30 times, respectively, greater in the bioaugmented microcosms than in the native microcosms. The only source of inorganic nutrients in the native microcosms was the artificial groundwater solution. A comparison of the potential composition of the bioaugmented microcosms after inoculating with 21198 in spent growth media and the artificial groundwater solution is shown in Table 3. Note that the growth media includes trace amounts of micronutrients not included in the Fort Carson groundwater summary[90] (and therefore not considered in the formulation of the artificial groundwater solution).

The influence of inorganic nutrient availability on the slowing of transformation rates was confirmed when 200 µL spent growth media (140 µg NH_4 and 99 µg phosphorous) was added to two of the three native microcosms and resulted in an increase in isobutane and 1,4-dioxane transformation rates in a sixth and seventh addition of isobutane and 1,4-dioxane, as shown in Figure 9. The sixth and seventh additions occurred 273 and 303 days, respectively, after the first addition. After nutrient amendment, rates in the sixth addition increased to approximately match rates from the second or third additions. In the seventh addition rates slowed again, indicating that the 200 µL growth media did not provide nutrient excess. Figure 9 also shows that rates in bioaugmented microcosms—that slowed in the fourth and fifth additions—slowed further in the sixth and seventh additions. This

suggested the additional inorganic nutrients provided during the 21198 inoculation in the bioaugmented microcosms were also eventually exhausted. Endogenous decay of biomass over the relatively large time scale of the experiment would also influence transformation rates. However, the influence of inorganic nutrients is demonstrated by the greater rates in nutrient-amended native microcosms than in the bioaugmented microcosms in the sixth and seventh additions.

Linear regression the 1,4-dioxane and isobutane rates for the sixth and seventh additions show similar slopes for bioaugmented and nutrient-amended native microcosms, 0.043 and 0.047 mg 1,4-dioxane/mg isobutane. As rates in bioaugmented microcosms slowed (potentially due to nutrient limitation), the slope for the linear regression of the final two additions was on the same order of magnitude as that of the native microcosms throughout the experiment. This suggests that with similar inorganic nutrient limitation, rates in from biostimulation with isobutane and bioaugmentation with 21198 are potentially equal.

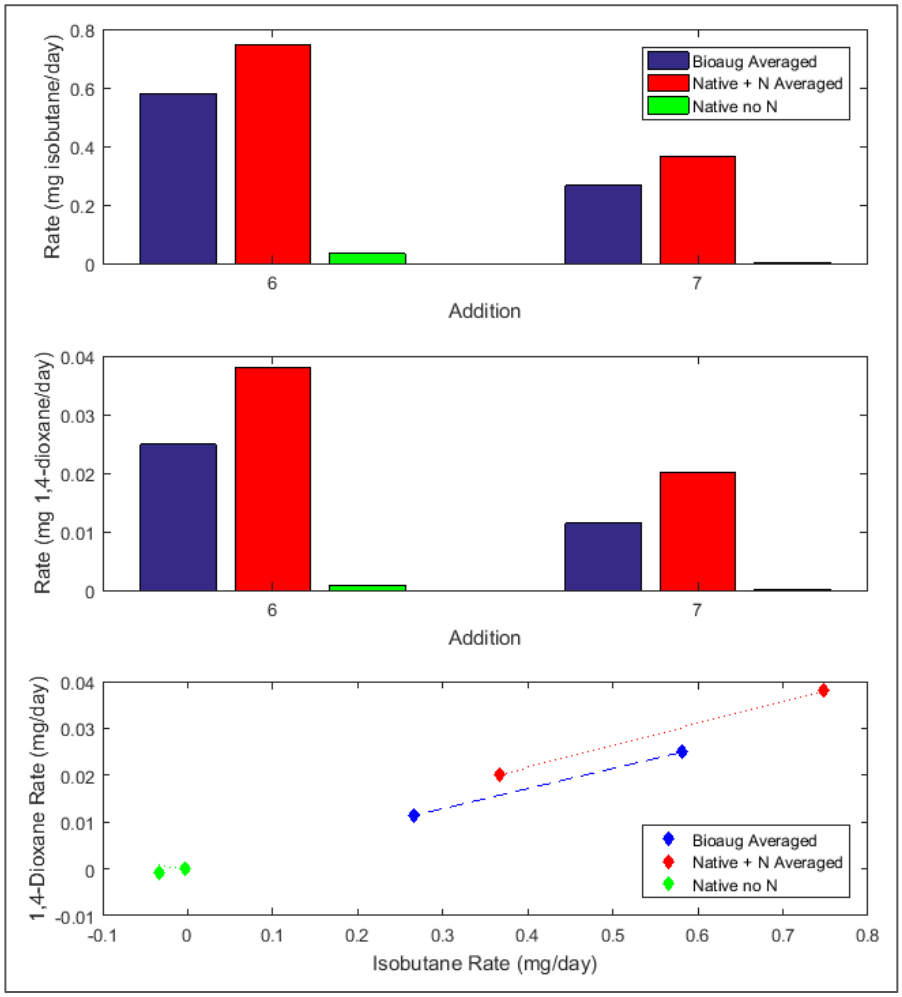

Figure 9. Initial, zero order isobutane utilization rates, 1,4-dioxane transformation rates, and linear regression of 1,4-dioxane vs isobutane rates in bioaugmented (averaged triplicate) and native microcosms with (averaged duplicate) and without (single microcosm) nutrient amendment in additions 6 and 7 of the long-term microcosm experiment.

Further laboratory testing to determine which specific inorganic nutrient(s) in the growth media were limiting was not performed. However, review of the literature highlights the importance of nitrogen and phosphorous as macronutrients for cell function. Nitrogen, typically 13% of bacterial cell dry weight[94], was provided to the microcosms as NH_4. Nitrogen is a commonly studied limiting factor in bioremediation studies and has been added as a nutrient amendment in the form of NH_4 [95,96], nitrate (NO_3^-)[96,97], nitrous oxide (N_2O)[17,98], yeast[14], cabbage leaf extract[99], and molasses[99]. Phosphorous, typically 2.5% of bacterial dry cell weight[94], is commonly added as phosphate (PO_4) for nutrient amendment[95,98,99]. Studies have shown that nitrogen and phosphorous can be limiting in bioremediation[98,100,101].

Given the stated importance of nitrogen and phosphorous in microbial systems, a theoretical analysis of each nutrient (as N and P) in the microcosms was performed to compare the ratio of nitrogen and phosphorous to total biomass, X. Experimental data for nitrogen and phosphorous was not collected during the microcosm experiments and was therefore not available for the analysis. The values were assumed from the initial concentrations of each constituent in the growth media and artificial groundwater solution, as shown in Table 3. Biomass was also not quantified experimentally. Rather, it was theoretically determined from the microbial yield, Y, from substrate consumption after each addition. Determination of the value of Y, 0.885 mg 21198/mg isobutane, is described in the modeling discussion below. For example, the consumption of 0.95 mg isobutane in each addition theoretically generated 0.84 mg biomass. The addition of N and P into the system from releases by decaying microorganisms was not considered in the analysis. Values of N/X less than 0.13 and P/X less than 0.025 were considered nutrient limited based on their typical composition of biomass given in the Brock Biology of Microorganisms textbook[94].

The theoretical ratios are shown in Figure 10; the N/X ratio in the left subplot and the P/X ratio in the right subplot. As shown in the figure, the theoretical N/X ratio dropped below 13% in the native microcosms after biomass generation from the second addition of isobutane, and after biomass generation from three isobutane additions in the bioaugmented microcosms. This suggests all microcosms were theoretically nitrogen limited early in the experiment, however experimental rates did not slow until later additions. The figure also shows native microcosms that received nutrient augmentation in the sixth addition were still theoretically nitrogen limited. However, their theoretical N/X ratios were approximately equal to the bioaugmented microcosms, which may explain the similarity of transformation rates in bioaugmented and nutrient-amended native microcosms in the sixth and seventh additions.

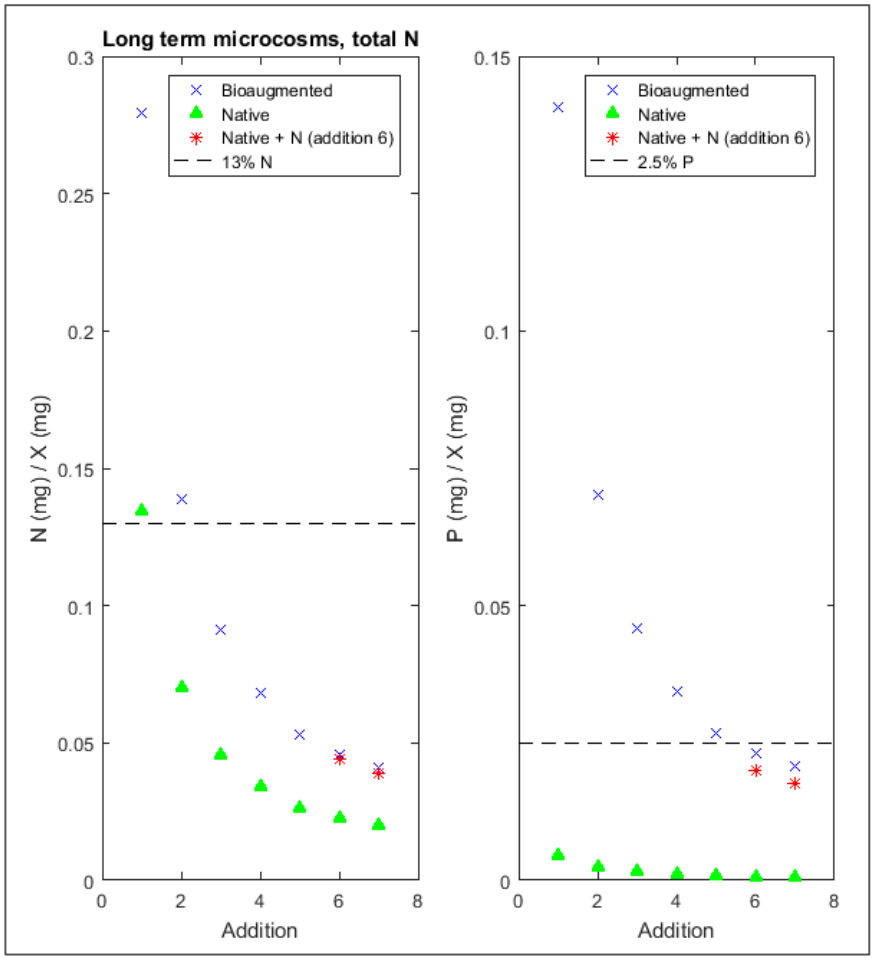

Figure 10. Theoretical ratios of nitrogen (left) and phosphorous (right) to biomass after consumption of each isobutane addition in long-term bioaugmented and native microcsosms. Nutrient augmentation for two of the three native microcosms occurred in the sixth addition.

The plot of the P/X ratio indicates that the native microcosms were theoretically phosphorous limited for the entirety of the experiment, which, like the N/X analysis, does not correlate to the pattern of increasing and decreasing rates observed experimentally. However, the bioaugmented microcosms theoretically approached phosphorous limitation after biomass generation from the sixth addition of isobutane, which more closely resembles the timing of the observed rate decreases. Like the N/X ratio, bioaugmented and nutrient-amended native microcosms had similar P/X ratios in the sixth and seventh additions. Given the almost entirely theoretical nature of this analysis, nitrogen or phosphorous limitation cannot be proven or disproven. However, it was interesting to see similar rates in

bioaugmented and nutrient-amended native microcosms corresponded to theoretically similar N/X and P/X ratios for the sixth and seventh additions.

The role of micronutrients such as vitamins and trace metals also have demonstrated importance in bioremediation. A study of 1,4-dioxane cometabolism with propane as a primary substrate found that molybdenum, was a critical nutrient for degradation[100]. Molybdenum was present as a trace nutrient in this study's mineral salts (growth) media but not in the artificial groundwater solution. Iron is another potentially important micronutrient because the oxidation of isobutane and 1,4-dioxane appears to catalyzed by a monooxygenase enzyme[9,13], which often requires iron as a cofactor[102,103]. However, the 21198 inoculation resulted in only 0.6% more iron in the bioaugmented microcosms than in the native microcosms. Swindoll et al found that amendment with combinations of inorganic nutrients generally resulted in greater biodegradation than single nutrients[95]. This could be particularly relevant to the microcosms in this study because of the potential competition for inorganic nutrients among diverse microbes metabolizing 1,4-dioxane transformation products[101].

2. Assessment of TCE Inhibition

TCE was added to additional sets of long-term native and bioaugmented microcosms to assess the potential for inhibition of 1,4-dioxane degradation by chlorinated solvent co-contaminants. In microcosms testing this condition, 0.025 mg TCE was added with 1,4-dioxane and isobutane for each of the first five additions, creating an initial liquid concentration of approximately 200 µg/L. This concentration is representative of the first contour outside of the source zone of the TCE plume at Fort Carson (see Figure 3) and well below the solubility limit of 1100 mg/L. As shown in Figure 11, TCE was transformed incompletely throughout the experiment, with negligible transformation in the native microcosms when cells were likely nutrient limited. Residual TCE was not sparged between additions, so the mass of TCE in each microcosm at the beginning of each addition increased slightly throughout the experiment. Figure 11 also shows decreases in TCE total mass at the

beginning of each addition occurred in both the acetylene controls and active microcosms, which could potentially be due to sorption to the aquifer solids.

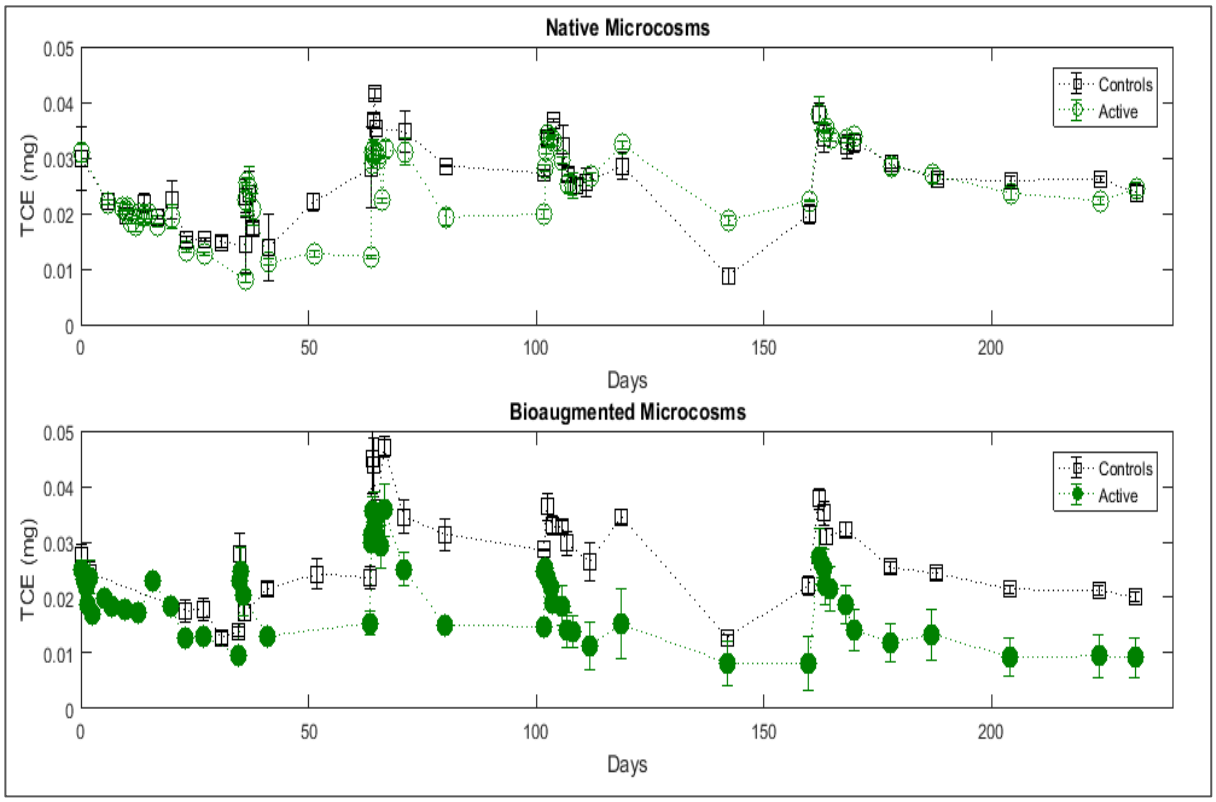

Figure 11. Five additions of trichloroethylene in bioaugmented (filled markers) and native (unfilled markers) microcosms, active reactors (green circles) and acetylene controls (black squares). Error bars represent one standard error.

As shown in Figure 12, rates of isobutane and 1,4-dioxane transformation were not impacted by the presence of TCE at the concentration tested. (Data for zero order rate calculations in microcosms containing TCE are shown in Appendix E.) A Welch's t-test confirmed that there was not a difference in average rates between microcosms (neither bioaugmented nor native) with and without TCE at a significance of p=0.05. The linear regression coefficients summarized in Table 6 also show little difference with the presence of TCE, nor did the presence of TCE change the biostimulation lag period in the native microcosms.

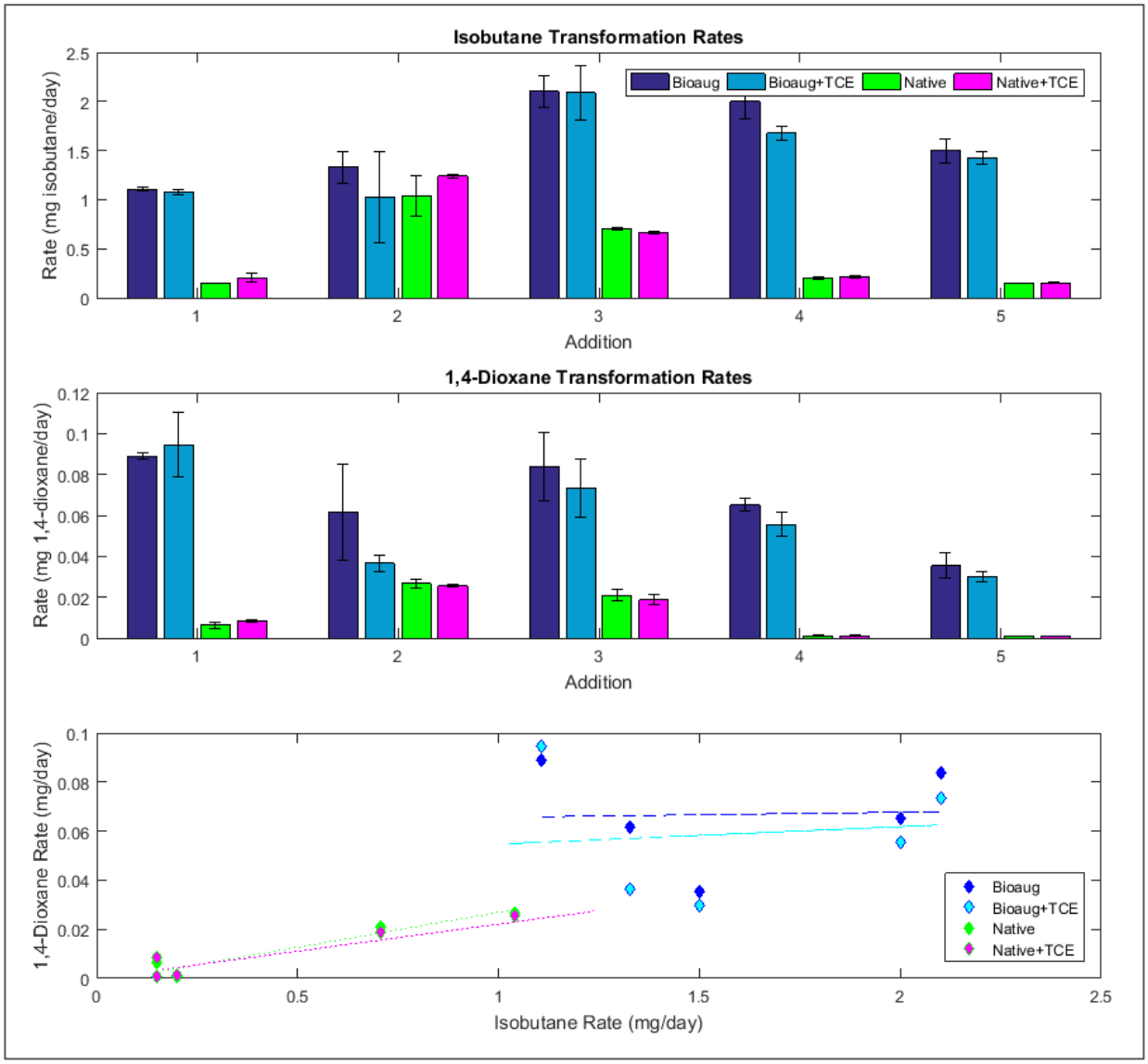

Figure 12. Initial, zero order isobutane utilization rates, 1,4-dioxane degradation rates, and linear regression of 1,4-dioxane vs isobutane rates, over five additions in long-term bioaugmented and native microcosms with and without TCE. Error bars show one standard error.

Table 6. Coefficients for linear regression of zero order 1,4-dioxane vs isobutane transformation rates in long-term native and bioaugmented microcosms with and without TCE.

	Long-term Microcosms			
	Bioaug	Bioaug + TCE	Native	Native + TCE
n	5	5	5	5
slope	0.0021	0.0071	0.0286	0.0221
intercept	0.0636	0.0476	-0.0016	0.0000
R^2	0.0017	0.0138	0.9414	0.8859

Other research has shown TCE does inhibit biotransformation of 1,4-dioxane, however this occurred at TCE concentrations of 5 mg/L in a study of cometabolism by *Mycobacterium vaccae* JOB5 and *Rhodococcus jostii* RHA1[18] and 50 mg/L in a direct metabolism study with CB1190[55]. Other studies showed lesser chlorinated transformation products, 1,1-DCE and cis-DCE, were found to be more significant inhibitors at low concentrations[55,61]. In this study, the limited transformation of TCE likely indicated that toxicity from TCE transformation did not impact the microcosms. Based on the plume configuration at Fort Carson, there would likely be little area in which TCE concentrations are high enough to inhibit 1,4-dioxane cometabolism.

C. Short-term Microcosm Experiments

Short-term microcosm experiments were conducted under multiple inorganic nutrient conditions and offer better assessment of the impact of inorganic nutrients on potential differences between bioaugmentation with 21198 and biostimulation alone in native microcosms. Growth media was added as an inorganic nutrient amendment to both native and bioaugmented microcosms, with 21198 washed from its growth media in a phosphate buffer prior to bioaugmentation (“Bioaug W+N” and “Native+N”). Native and bioaugmented microcosms mimicking the nutrient conditions of the long-term experiment were also repeated (“Bioaug Uw” and “Native no N”), and pure culture reactors with the same starting inoculum of 21198 as bioaugmented in microcosms were constructed in growth media instead of groundwater slurry to simulate ideal conditions. Microcosm

conditions tested in the short-term experiments are summarized in Table 5 and initial concentrations of cations and anions in all sets of microcosms are shown in Table 3 in the methods section. All microcosms were tested over four additions of isobutane and 1,4-dioxane.

"Bioaug Uw" and "Native no N" exhibited similar results as the long-term microcosms. Bioaugmented microcosms immediately transformed both isobutane and 1,4-dioxane, whereas the native microcosms exhibited a biostimulation lag period of approximately one week. "Bioaug Uw" microcosms maintained rapid rates of isobutane and 1,4-dioxane transformation, whereas rates in "Native no N" microcosms slowed in later additions and no 1,4-dioxane degradation occurred by the fourth addition. Isobutane and 1,4-dioxane transformation in these microcosms is shown in Appendix F.

A comparison of isobutane and 1,4-dioxane transformation in native and bioaugmented microcosms with equal nutrient conditions ("Bioaug W+N" and "Native+N") is shown in Figure 13. Transformation by "Bioaug W+N" and "Native+N" in each of the four additions is shown in an individual subplot, isobutane in the left column and 1,4-dioxane in the right column. The time for each addition starts at zero in order to directly compare the performance of "Bioaug W+N" and "Native+N" in each addition. (The second through fourth additions did not actually happen at the same time for "Bioaug W+N" and "Native+N" because of the initial biostimulation lag.) Transformation on a continuous time scale for the experiment in these microcosms and the pure culture reactors is shown in Appendix F. As illustrated by the figure, the time required for complete transformation of isobutane and 1,4-dioxane in the native and bioaugmented microcosms is approximately equal by the third addition. Both sets show similar slowing in the fourth addition, potentially due to equal nutrient limitation.

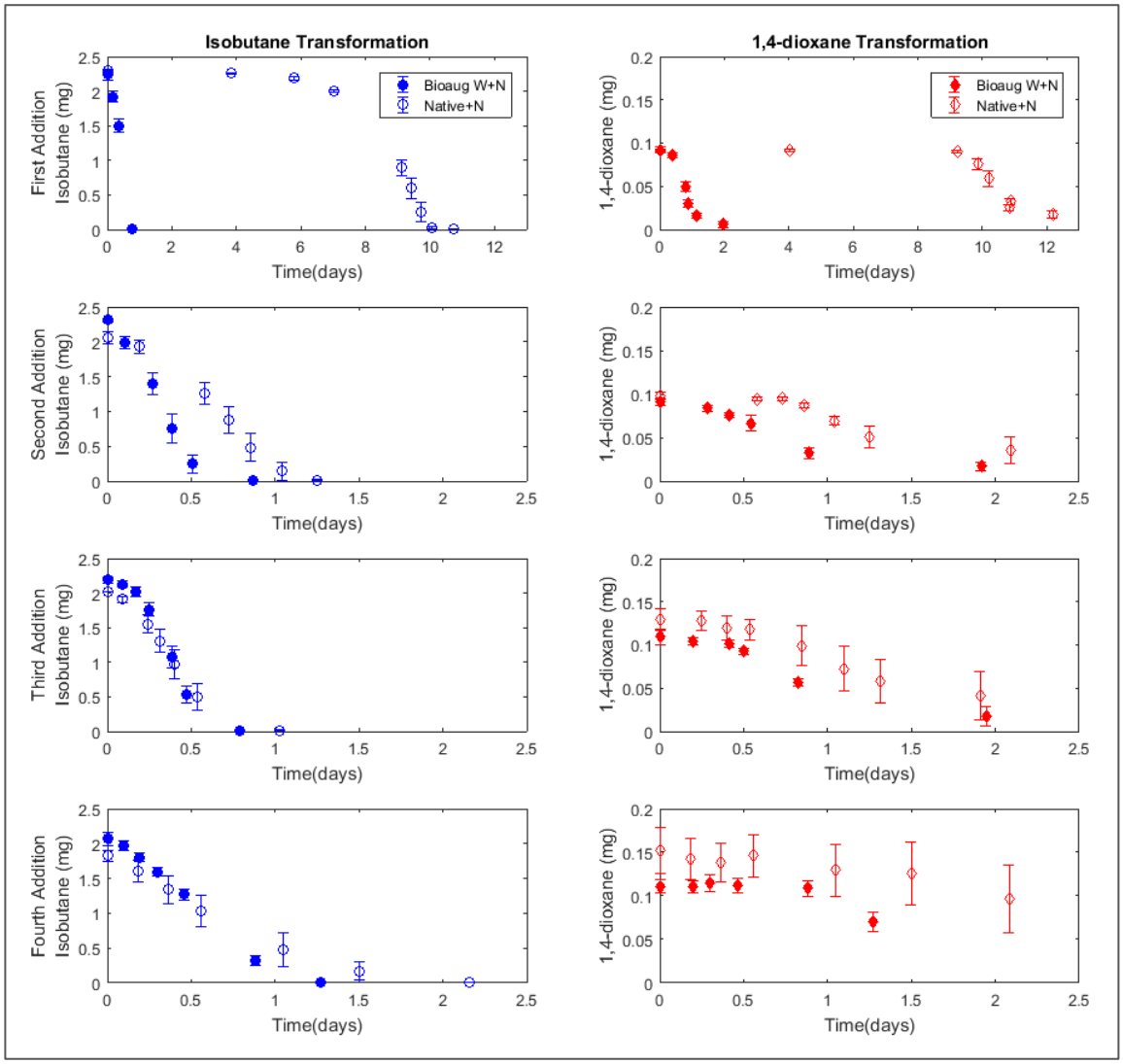

Figure 13. Isobutane and 1,4-dioxane transformation over four additions in short-term native and bioaugmented microcosms that received equal inorganic nutrient amendment ("Native +N" and "Bioaug W+N"). Error bars represent one standard error.

Zero-order isobutane and 1,4-dioxane transformation rates for all short-term microcosms and the pure culture reactors are shown in Figure 14. (Transformation curves from which the linear rate for each microcosm was calculated are shown in Appendix G.) As expected, rates in all microcosms increased in the second addition, indicating biomass growth from isobutane consumption. Rates in microcosms with inorganic nutrient amendment were stable through the third addition, whereas rates decreased in the native microcosms without growth media ("Native no N"). Similar to the long-term experiment,

rates in the “Native no N” microcosms again showed that when the isobutane rate was below 0.5 mg/day, little 1,4-dioxane cometabolism occurred. The 1,4-dioxane transformation rate was highest in the pure culture reactors in additions 2-4, indicating that the most sustained 1,4-dioxane transformation would be achieved in conditions of nutrient excess.

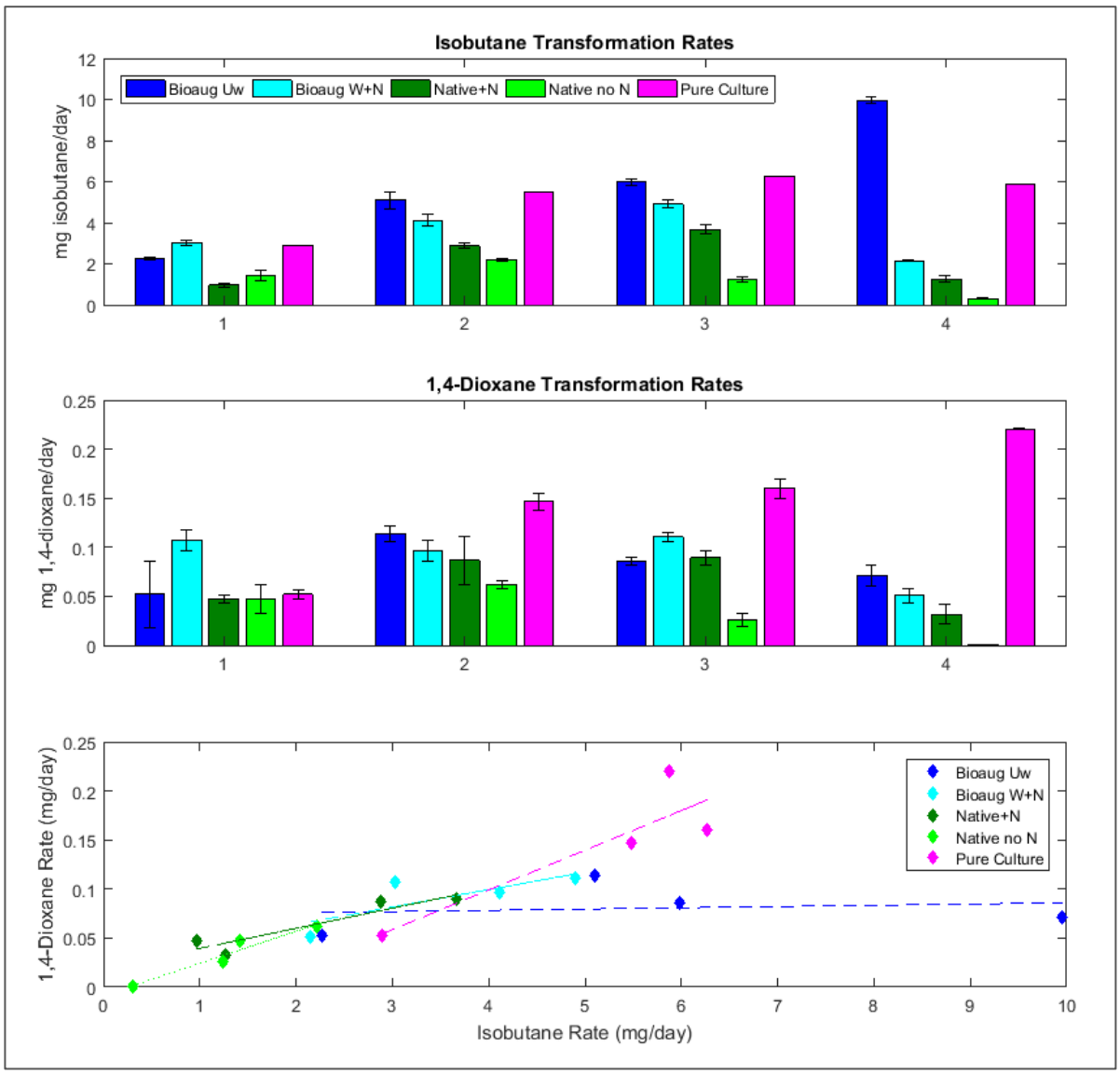

Figure 14. Initial, zero order isobutane utilization rates, 1,4-dioxane degradation rates, and linear regression of 1,4-dioxane vs isobutane rates, over four additions in short-term bioaugmented and native microcosms with varying nutrient conditions and pure culture reactors. Error bars show one standard error.

Rates for short and long-term bioaugmented microcosms should not be directly compared because different quantities of 21198 were used for the bioaugmentation inoculum. However, comparison of the linear regression coefficients listed in Table 8 suggested similar behavior in long and short-term microcosms. Isobutane and 1,4-dioxane rates in microcosms bioaugmented with 21198 suspended in growth media (likely not experiencing nutrient limitation) did not correlate in either the long or short-term experiments, but both had flat slopes with approximately equal intercepts. Linear regression of rates from bioaugmented microcosms with limited nutrients ("Bioaug W+N") and all sets of native microcosms (short and long-term; all likely experiencing nutrient limitation) resulted in slopes of the same order of magnitude, approximately 0.02-0.03 mg 1,4-dioxane/mg isobutane. The most similar slopes and intercepts matched similar nutrient conditions: long and short-term native microcosms without additional nutrients had slopes of 0.03 mg 1,4-dioxane/mg isobutane and negative intercepts, and the short-term native and bioaugmented microcosms with similar nutrient conditions ("Bioaug W+N and "Native+N") had slopes of 0.02 mg 1,4-dioxane/mg isobutane and positive intercepts. These trends seem to suggest steeper slopes correspond to greater nutrient limitation. This might suggest a maximum ratio of 1,4-dioxane to isobutane transformation rates when inorganic nutrients are not limiting. This would make sense if the 1,4-dioxane degradation rate was near K_{max}, however this is unlikely because initial 1,4-dioxane concentrations in each addition were low. In addition, the slope for the regression in the pure culture reactors, the least nutrient stressed environment, was the steepest at 0.04 mg 1,4-dioxane/mg isobutane and had the most negative intercept. If the data point for the rates from the first addition in the pure culture reactors is removed as an outlier, the trend shown in the regression would resemble the non-nutrient limited bioaugmented microcosms.

Table 7. Coefficients for linear regression of zero order 1,4-dioxane vs isobutane transformation rates in short and long-term native and bioaugmented microcosms.

	Long-term Microcosms				Short-term Microcosms				
	Bioaug	Bioaug + TCE	Native	Native + TCE	Bioaug Uw	Bioaug W+N	Native +N	Native no N	Pure culture reactors
n	5	5	5	5	4	4	4	4	4
slope	0.0021	0.0071	0.0286	0.0221	0.0013	0.0178	0.0205	0.0328	0.0405
intercept	0.0636	0.0476	-0.0016	0.0000	0.0628	0.0282	0.019	-0.0086	-0.0628
R^2	0.0017	0.0138	0.9414	0.8859	0.0246	0.5981	0.8578	0.9348	0.7824

The theoretical assessment of the ratios of nitrogen and phosphorous performed for the long-term microcosms was also performed for the short-term microcosms, as shown in Figure 15. The assessment suggests that the “Native no N” microcosms were theoretically nitrogen limited for the duration of the experiment, microcosms with equal nutrient conditions (“Bioaug W+N” and “Native+N”) were nitrogen limited after biomass generation in the second addition, and the native microcosms without additional nutrients were nitrogen limited after the first addition. Just as in the long term experiment, the development of theoretical nitrogen limitation does not follow the pattern of observed rate decreases. The theoretical phosphorous limitation suggested by the analysis is a better match with rate decreases, with rates in the “Bioaug W+N” and “Native+N” microcosms decreasing in the fourth addition after the P/X ratio dropped below 2.5% from biomass generation in the third addition.

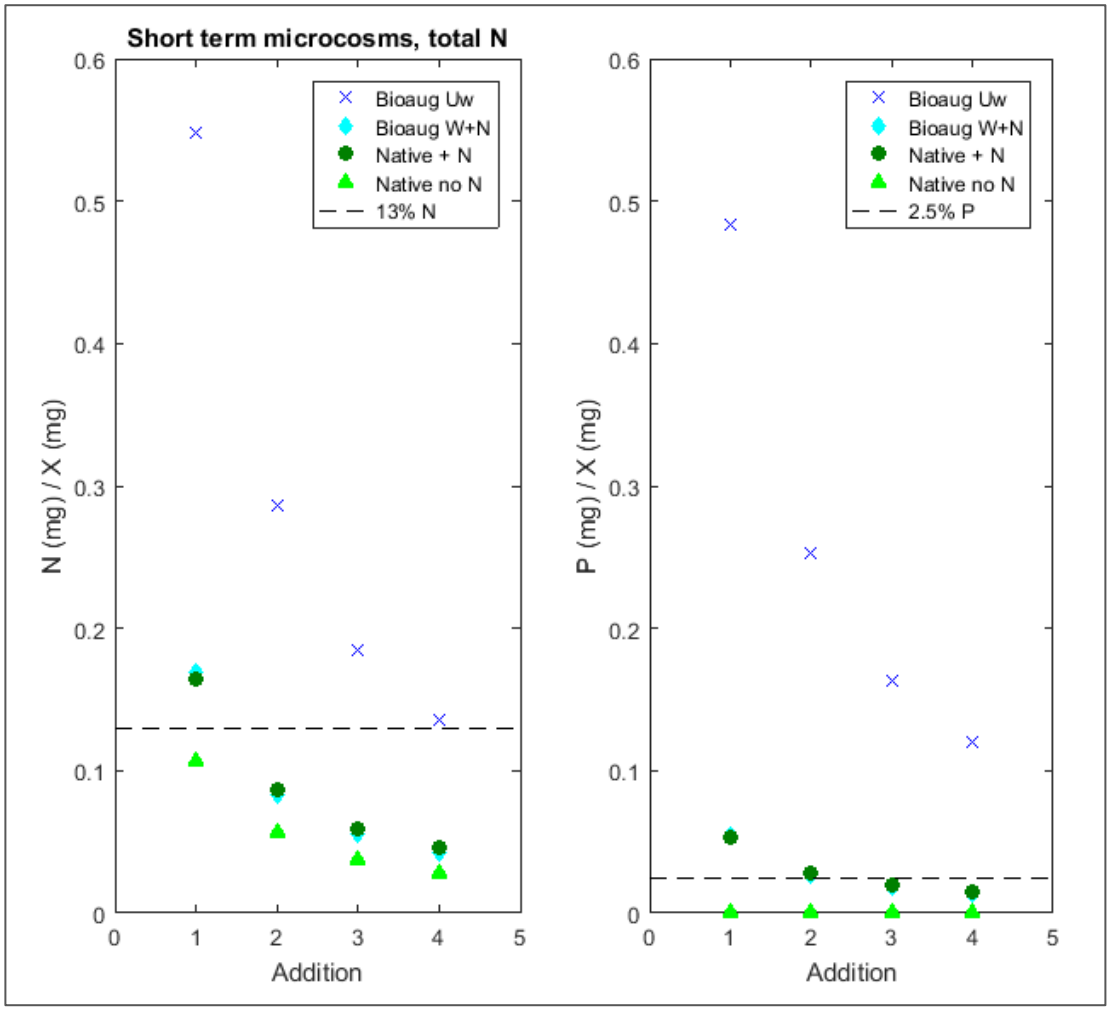

Figure 15. Theoretical ratios of nitrogen (left) and phosphorous (right) to biomass after consumption of each isobutane addition in short-term microcosms. Pure culture reactors not shown because their N/X and N/P ratios are so high that the axes are distorted and microcosm values obstructed.

The impact of bioaugmentation with 21198 is best assessed by comparing the native and bioaugmented microcosms with washed 21198 and additional nutrients ("Bioaug W+N" and "Native+N") because it removes the influence of inorganic nutrient availability. A Welch's t-test with p=0.05 was used to compare mean rates of isobutane and 1,4-dioxane transformation between native and bioaugmented microcosms in each addition. The test indicated that there were statistically significant different mean rates of isobutane transformation in the first, second, and third additions, but only in the first addition for 1,4-dioxane transformation. This indicates that, over time and with sufficient inorganic

nutrients, the results of bioaugmentation with 21198 may not be different from biostimulation alone. However, as demonstrated in the Vandenberg Air Force Base field study[17], significant differences between laboratory conditions and actual site subsurface conditions may indicate bioaugmentation with a known 1,4-dioxane degrader would more reliably achieve 1,4-dioxane degradation.

Repeated degradation of 1,4-dioxane in both long and short-term microcosm experiments indicates that isobutane has the potential to be an effective primary substrate to achieve 1,4-dioxane cometabolism in the field. However, evidence of inhibition suggests isobutane would need to be delivered in pulsed intervals, a method demonstrated in previous cometabolism field studies[104]. Immediate transformation of 1,4-dioxane in all bioaugmented microcosms suggests 21198 would also potentially be an effective microorganism in field settings with an adequate supply of inorganic nutrients. The *Rhodococcus* species is known to be able to survive long periods of starvation [70,72], which is likely demonstrated in these experiments by the reactivation of biomass after months between isobutane additions.

D. Modeling

1. Parameter Determination

Simultaneous utilization of isobutane, degradation of 1,4-dioxane, and biomass growth were modeled according to Monod and Michaelis-Menten kinetics shown in Equations 11, 12, and 13. Initial estimates of parameters were obtained as follows: The maximum rate of substrate utilization, K_{max}, and the half saturation constant, K_s, were initially determined through the development of Monod curves from pure culture studies for both isobutane and 1,4-dioxane transformation by 21198[105], which are shown in Figure 16 and Figure 17, respectively. This resulted in K_{max} values of 2.58 mg isobutane/mg TSS/day and 0.87 mg 1,4-dioxane/mg TSS/day, and K_s values of 0.83 mg isobutane/L and 31.0 mg 1,4-dioxane/L. The inhibition constant, K_I, for inhibition of 1,4-dioxane transformation by the presence of isobutane shown in Equation 12 was determined to be 3 mg isobutane/L via

additional rapid, pure culture 1,4-dioxane rate tests across a range of isobutane concentrations, a value that was significantly higher than the concentration of 0.15 mg isobutane/L observed in the microcosm studies. The biomass yield for 21198 from primary substrate consumption, Y, was estimated from a pure culture growth test to be 0.8 mg TSS/mg isobutane. A value of 0.1 1/day for the endogenous decay coefficient, b, was chosen from a reactive transport model for cometabolism by butane-utilizing microbes[60]. The gas and liquid volumes were 0.13 L and 0.18 L, respectively, for the short-term microcosms, and 0.06 L and 0.095 L, respectively, for the long-term microcosms.

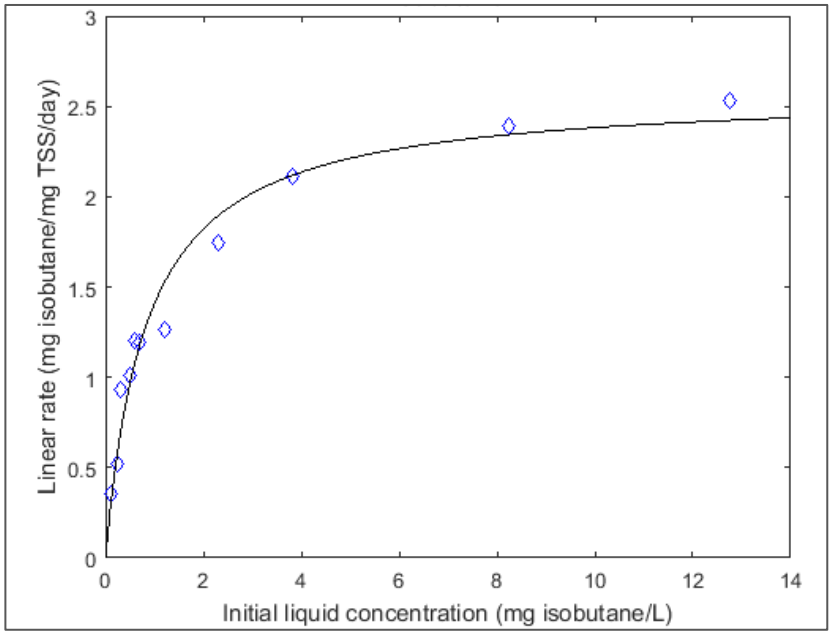

Figure 16. Monod curve for isobutane transformation by pure culture Rhodococcus rhodochrous *strain 21198*[105].

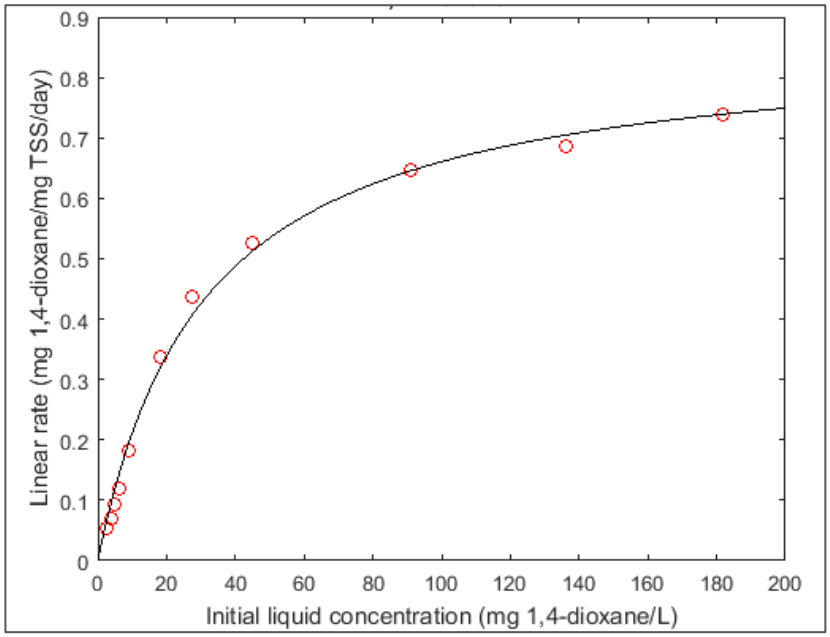

Figure 17. Monod curve for 1,4-dioxane transformation by resting pure culture Rhodococcus rhodochrous *strain 21198*[105].

When these initial parameter estimates were used to run the model for isobutane utilization and 1,4-dioxane degradation in the microcosms, the model provided a very poor fit to the data. The model run with data from the short-term bioaugmented microcosms in which 21198 was suspended in growth media when inoculated ("Bioaug Uw"), is shown in Figure 18. This would theoretically be the easiest microcosm experiment to model because it was not nutrient limited and occurred over a short period of time. The Nash-Sutcliffe efficiencies, E, as determined by Equation 15 for the isobutane and 1,4-dioxane data were -1.05 and -0.128, respectively. Both values are less than zero, indicating that the mean of the data series is a better predictor than the model[92].

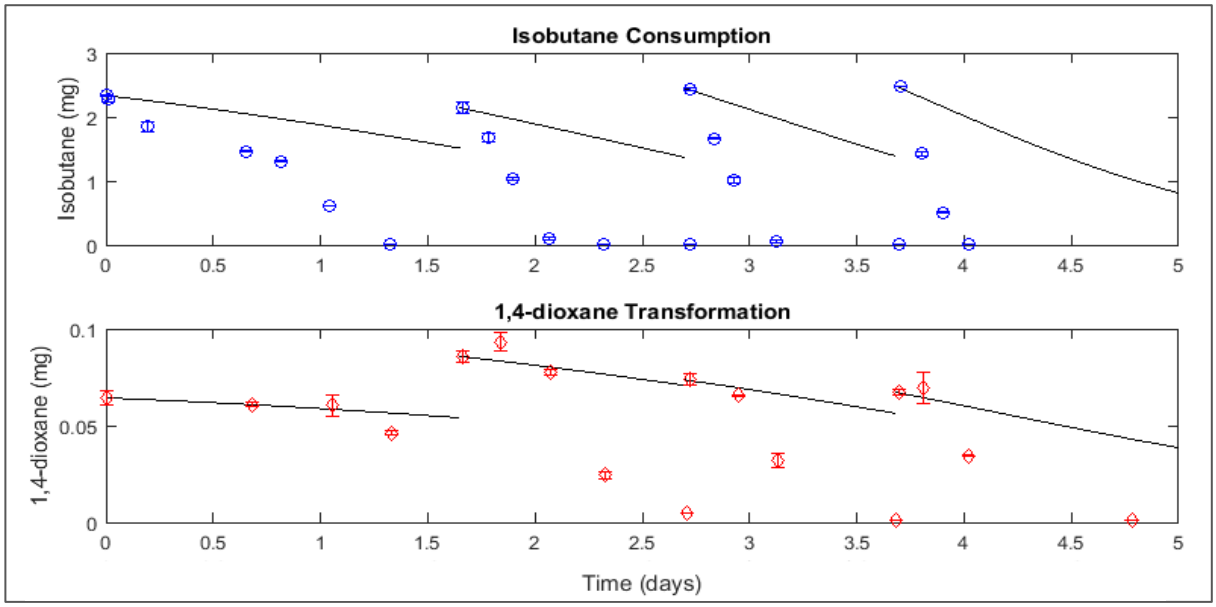

Figure 18. Model simulation using K_{max} and K_s values determined from Monod curves (K_{max}=2.58 mg/mg/day and K_s=0.83 mg/L for isobutane and K_{max}=0.87 mg/mg/day and K_s=31 mg/L for 1,4-dioxane), Y=0.8 mg/mg determined from a growth experiment, b=0.1 chosen from literature values, and X_o=2.78 mg/L (measured) for isobutane and 1,4-dioxane data from short-term bioaugmented microcosms ("Bioaug Uw").

In order to test whether the poor fit was a result of the microcosm environment, the model was run for the pure culture experiment performed in growth media instead of groundwater slurry (though otherwise identical to the bioaugmented microcosm experiment). As shown in the Figure 19, biomass growth was also tracked over the course of the experiment. Biomass was analyzed through optical density measurements, which was not possible in the microcosm experiments because of the aquifer solids. The model was run for the pure culture data with the same initial parameter estimates listed above. As illustrated in Figure 19, the model again provided a poor fit to the experimental data, with E values for isobutane, 1,4-dioxane, and biomass of -1.073, -0.741, and 0.120, respectively. The poor fit of the model to this data indicated that the groundwater and aquifer solids characterizing the microcosm environment were not the source of the model's inability to replicate the data.

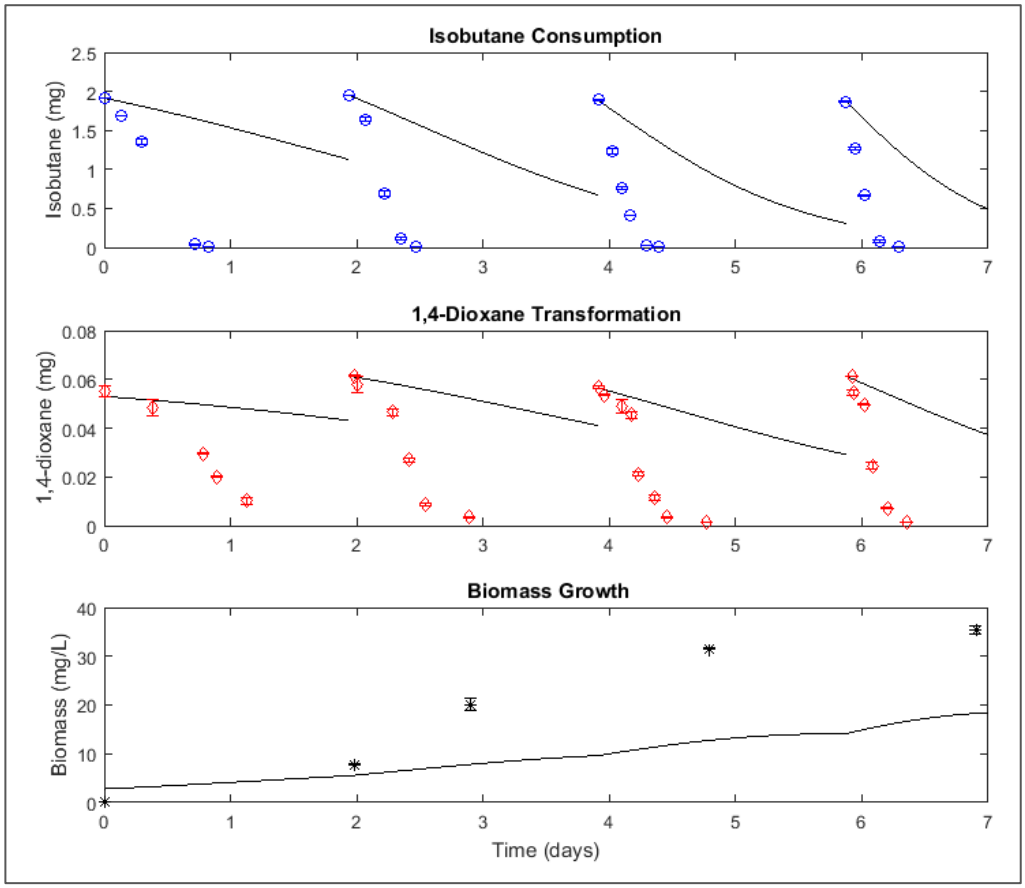

Figure 19. Model simulation using K_{max} and K_s values determined from Monod curves (K_{max} =2.58 mg/mg/day and K_s =0.83 mg/L for isobutane and K_{max}=0.87 mg/mg/day and K_s =31 mg/L for 1,4-dioxane), Y=0.8 mg/mg determined from a growth experiment, and b=0.1 chosen from literature values for isobutane and 1,4-dioxane data from short-term Pure Culture experiment.

The next step was to determine whether Equations 11, 12, and 13 could be used to model the pure culture replicate of the bioaugmented microcosms by adjusting the parameter values. The pure culture experiment was chosen as the data set for fitting parameters because of the possibility of fitting biomass data and the likelihood that these reactors were not nutrient limited. Determining best-fit parameters was a multi-step process. The full description of this process follows in the next several pages, and is summarized in Figure 20. The parameter values and corresponding figures for each simulation are listed in Table 8. The Nash-Sutcliffe efficiencies, E, for the goodness of fit of each simulation to the isobutane, biomass, and 1,4-dioxane data sets are listed in Table 9.

Simulation 1, shown in Figure 19, was run with the original estimates of the parameter values from the Monod curves, as listed in the first line of Table 8.

1. *Initial Parameter Values*

- K_{max}, K_s, and K_I for isobutane and 1,4-dioxane determined from Monod curves
  - RESULTS: isobutane: K_{max}=2.58 mg/mg/day, K_s=0.83 mg/L; 1,4-dioxane: K_{max}=2.58 mg/mg/day, K_s=0.83 mg/L, K_I=3 mg/L
- Y determined from yield experiment
  - RESULTS: Y=0.8 mg/mg
- b chosen from literature values
  - RESULTS: B=0.1 1/day

2. *Isobutane Parameters*

- K_{max} fixed at 2.58 mg/mg/day (from Monod Curve)
- K_s determined from rapid, low concentration, pure culture test
  - RESULTS: K_S=0.05 mg/L

3. *Biomass Parameters*

- Y and b determined from simultaneous optimization to fit biomass data from short-term pure culture experiment (fixed parameters: K_{max}=2.58 mg/mg/day, K_s=0.05 mg/L)
  - RESULTS: Y=0.8 mg/mg, b=0 1/day
- b determined from optimization to fit isobutane data from long-term bioaugmented microcosm experiment (fixed parameters: Y=0.8 mg/mg, K_{max}=2.58 mg/mg/day, K_s=0.05 mg/L)
  - RESULTS: b=0.03 1/day
- Y re-optimized to fit biomass data from short-term pure culture experiment with updated b (fixed parameters: b=0.03 1/day, K_{max}=2.58 mg/mg/day, K_s=0.05 mg/L)
  - RESULTS: Y=0.885 mg/mg

4. *Isobutane Parameters (second iteration)*

- K_s doubled after adjustments to Y and b worsened fit
  - RESULTS: K_s=0.1 mg/L
- X_o increased by 30% to improve fit to first isobutane addition
  - RESULTS: X_o=3.6 mg/L

~final Isobutane and Biomass parameters fixed for determination of 1,4-dioxane parameters~

K_{max}=2.58 mg/mg/day, K_s=0.1 mg/L, Y=0.885 mg/mg, b=0.03 1/day, X_o=3.6 mg/L

5. *1,4-dioxane Parameters*

- K_{max} and K_s optimized simultaneously to fit rapid pure culture resting cell test
  - RESULTS: inconclusive; indicated first-order degradation
- First order rate constant, K_{FO}, determined by nonlinear regression to fit rapid pure culture resting cell test
  - RESULTS: K_{FO}=0.20 L/mg/day
- K_s determined as K_{max}/K_{FO} (K_{max}=0.87 mg/mg/day from Monod curve)
  - RESULTS: K_s=4.35 mg/L
- K_I optimized to fit 1,4-dioxane data from short-term pure culture experiment
  - RESULTS: K_I=0.13 mg/L (fixed parameters: K_{max}=0.87 mg/mg/day, K_s=4.35 mg/L)

~final 1,4-dioxane parameters~

K_{max}=0.87 mg/mg/day, K_s=4.35 mg/L, K_I=0.13 mg/L

Figure 20. Parameter Determination Summary

Table 8. Values for model input parameters and corresponding figures for each simulation in the fitting process

Simulation #	Related Figures	$K_{max, IB}$ (mg/mg biomass/day)	$K_{s, IB}$ (mg/L)	Y (mg biomass/mg isobutane)	b (1/day)	$K_{max, 14D}$ (mg/mg biomass/day)	$K_{s, 14D}$ (mg/L)	K_I (mg isobutane/L)	X_o (mg biomass/L)	K_{FO} (L/mg 1,4-dioxane/day)
1	Figure 13	2.58	0.83	0.8	0.1	0.87	31	3	2.78	NA
2	Figure 22	2.58	0.2	0.8	0.1	0.87	31	3	2.78	NA
3	Figure 23, Figure 24	2.58	0.05	0.8	0.1	0.87	31	3	2.78	NA
4	NA	2.58	0.05	0.8	0	0.87	31	3	2.78	NA
5	NA	2.58	0.05	0.8	0.03	0.87	31	3	2.78	NA
6	NA	2.58	0.05	1.08	0.04	0.87	31	3	2.78	NA
7	Figure 25	2.58	0.05	0.885	0.03	0.87	31	3	2.78	NA
8	Figure 26	2.58	0.1	0.885	0.03	0.87	31	3	3.6	NA
9	NA	2.58	0.1	0.885	0.03	NA	NA	NA	3.6	0.204
10	NA	2.58	0.1	0.885	0.03	NA	NA	NA	3.6	0.249
11	Figure 28	2.58	0.1	0.885	0.03	0.87	4.35	3	3.6	NA
12	Figure 29	2.58	0.1	0.885	0.03	0.87	4.35	0.13	3.6	NA

Table 9. Nash-Sutcliffe efficiencies to quantify goodness of fit to isobutane, biomass, and 1,4-dioxane data sets for each simulation

Simulation #	Isobutane n=21	Biomass n=5	1,4-dioxane n=25
1	-1.073	0.120	-0.741
2	0.318	0.759	-0.342
3	0.664	0.753	-0.247
4	0.625	0.957	-0.047
5	0.645	0.932	-0.109
6	0.575	0.873	0.136
7	0.627	0.955	-0.022
8	0.658	0.942	-0.007
9	0.658	0.942	0.623
10	0.658	0.942	0.467
11	0.658	0.942	0.707
12	0.658	0.942	0.929

As shown in Equations 11 and 13, the equations for isobutane and biomass are independent of 1,4-dioxane when the model does not consider transformation capacity. Therefore, fitting these data sets was the first step in adjusting the model. Relative to K_s, K_{max} is easy to determine correctly using a Monod curve developed as previously described, so the K_{max} value of 2.58 mg/mg/day was used in further model development. By constrast, K_s, especially when it is low, is potentially more difficult to estimate by constructing a Monod curve. Monod curves are constructed from initial linear rates of transformation, which come from the region of the degradation curve more influenced by K_{max}. Therefore, if K_s is low, it may not captured by these rate measurements. In order to obtain a better estimate of the $K_{s,IB}$ value, nonlinear regression was used to fit $K_{max,IB}$ and $K_{s,IB}$ to complete, low concentration degradation curves, as shown in Figure 21. The initial liquid concentration of isobutane for these curves ranged from 0.12 mg/L to 1.9 mg/L, which spans the $K_{s,IB}$ value determined from the Monod curve of 0.83 mg/L and the initial starting concentration of 0.3 mg/L for each addition in the microcosms and Pure Culture reactors.

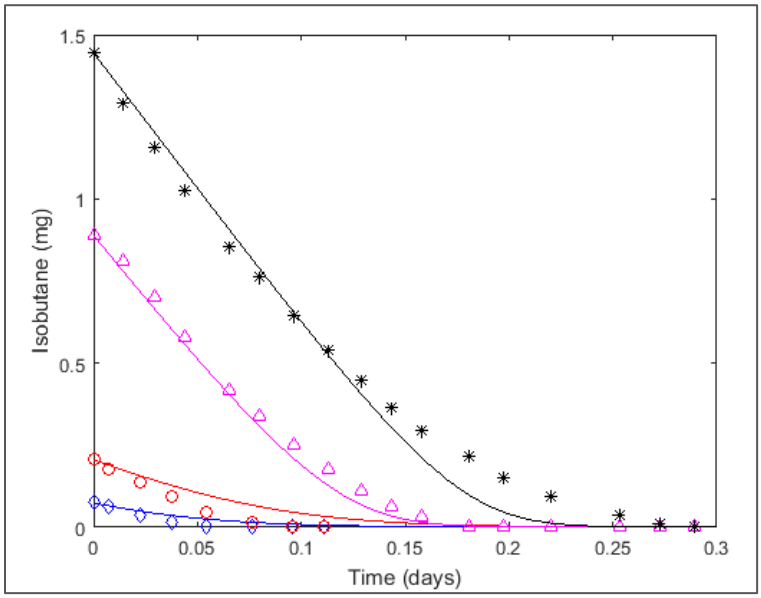

Figure 21. Isobutane transformation of low masses by pure culture 21198 for fitting $K_{s,IB}$. Model run with parameters simultaneoulsy fit to four curves.

$K_{max,IB}$ and $K_{s,IB}$ were simultaneously optimized for the four curves using the iterative search method to minimize the sum of the squared error. The range for $K_{max,IB}$ was 1 to 3 mg/mg/day with a step size of 0.1, and the range for $K_{s,IB}$ was 0 to 1.5 mg/L with a step size of 0.01. (b and Y were both set to zero in this optimization because the experiments occurred over a short time scale.) The optimum values were 1.4 mg/mg/d for K_{max} and 0.2 mg/L for $K_{s,IB}$ (the $K_{s,IB}$ value changed to 0.26 mg/L when the optimization was run with b=0.1 and Y=0.8). When 0.2 mg/L was used for $K_{s,IB}$ to model the multiple addition pure culture data (Simulation 2), the fit for the isobutane data improved to E=0.318. (The values of $K_{max,IB}$ determined from these optimizations to low concentration data was not representative of the system, so the value of 2.58 mg/mg/day determined from the Monod curve was used in the model, as shown in Table 8.) While the fit was significantly improved with this adjustment of $K_{s,IB}$, Figure 22 showed the model was still a relatively poor fit at the lowest concentrations. With the assumption that $K_{max,IB}$ was correct, this indicated $K_{s,IB}$ was too large.

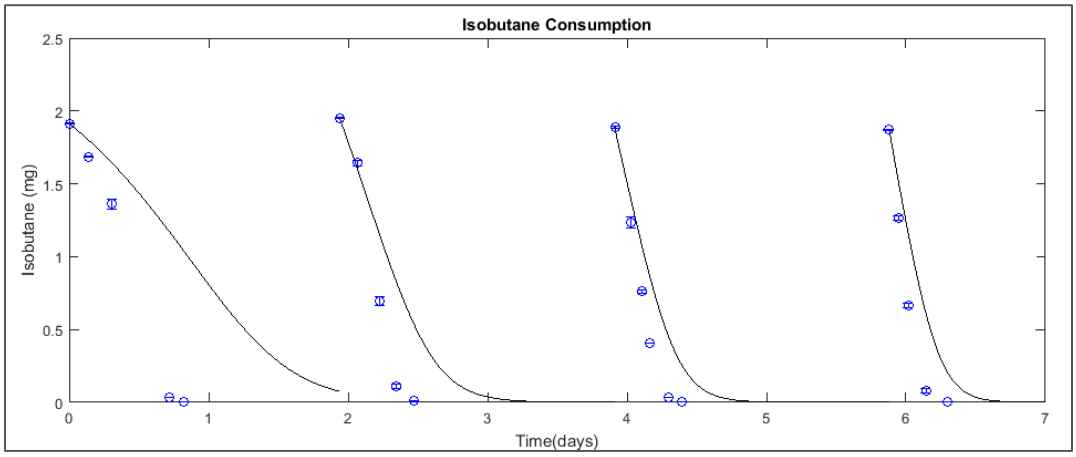

Figure 22. Model fit to isobutane data from the short-term Pure Culture experiment after $K_{s,IB}$ was lowered from 0.83 mg/L to 0.2 mg/L. $K_{max,IB}$, b, and Y fixed at 2.58 mg/mg/day, 0.1 1/day, and 0.8 mg/mg, respectively. (Simulation 2)

When $K_{s,IB}$ was determined using only the curve with the same initial liquid concentration of isobutane as the multiple addition experiment—0.3 mg/L (red circles in Figure 21)—the optimal $K_{s,IB}$ was 0.05 mg/L. This is approximately one order of magnitidue lower than literature values for butane and methane oxidizing microorganisms [60,104], however it further improved the fit to the data, as illustrated in Figure 23 and by the increase of E to 0.664 (Simulation 3).

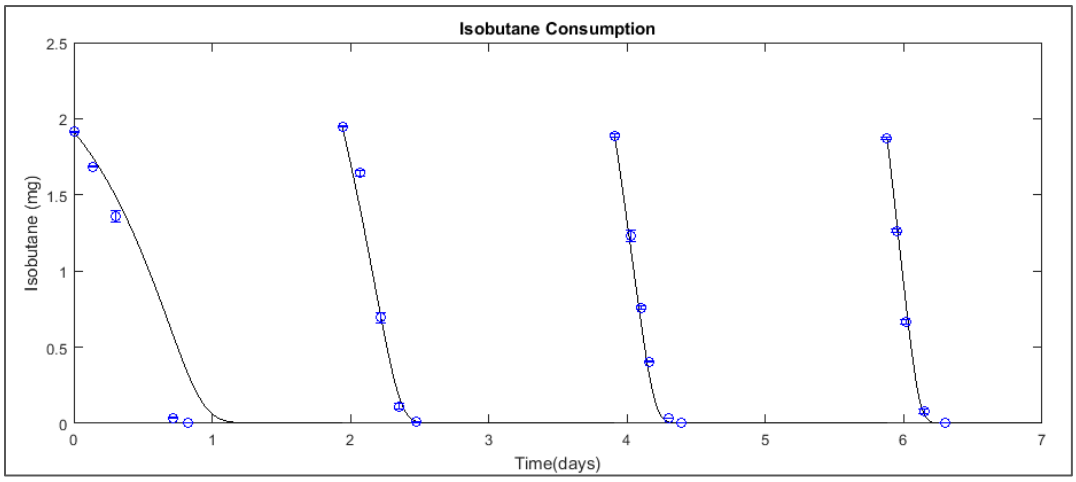

Figure 23. Model fit to isobutane data from the short-term Pure Culture experiment after $K_{s,IB}$ was lowered from 0.2 mg/L to 0.05 mg/L as determined from rapid degradation experiment with the same initial liquid isobutane concentration. $K_{max,IB}$, b, and Y fixed at 2.58 mg/mg/day, 0.1 1/day, and 0.8 mg/mg, respectively. (Simulation 3)

Adjusting the value of $K_{s,IB}$ for isobutane consumption also improved the fit of the biomass model, increasing the E value from 0.114 to 0.753. However, this test statistic was likely skewed high because there were only five data points in the biomass data set, and a visual assessment of the model fit in Figure 24 showed a poor fit to biomass data after the third and fourth additions. (The model simulation shown in Figure 24 was generated with parameter values from Simulation 3.)

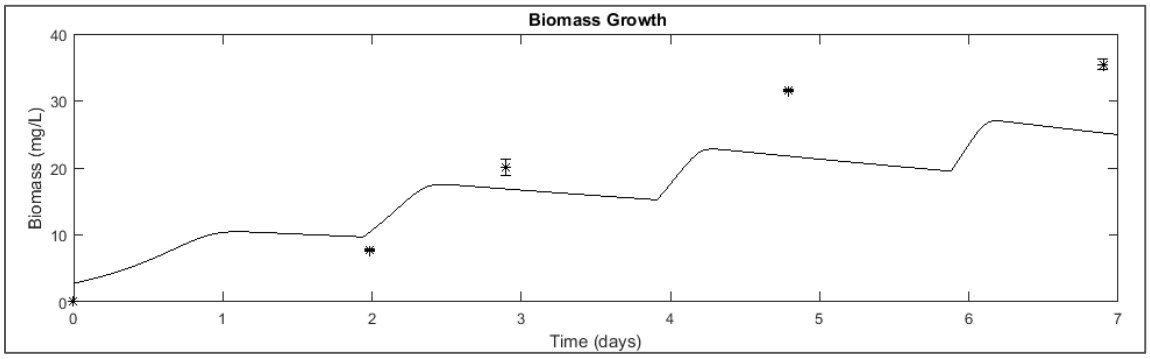

Figure 24. Model fit to biomass data from the short-term Pure Culture experiment with parameter values from Simulation 3, which give a good fit to isobutane data. $K_{max,IB}$, $K_{s,IB}$, b, and Y fixed at 2.58 mg/mg/day, 0.05 mg/L, 0.1 1/day, and 0.8 mg/mg, respectively (Simulation 3).

In order to improve the model fit, the parameters specific to biomass growth—yield from growth on isobutane, Y, and the endogenous decay coefficient, b—were also optimized using the iterative search method. With a range of 0 to 1.5 mg/mg and step size of 0.01 for Y and a range of 0 to 0.15 1/day and step size of 0.001 for b (with $K_{max,IB}$ and $K_{s,IB}$ fixed at 2.58 mg/mg/day and 0.05 mg/L, respectively), the optimum values were determined to be 0.8 mg/mg for Y and 0 1/day for b. These values increased the E value for biomass to 0.957 (Simulation 4, not shown). A yield of 0.8 was also calculated in a previous growth experiment, indicating this parameter optimization method gave a reasonable value for Y. However, a value of 0 1/day for b was not realistic because endogenous decay is a reality of microbial growth[106]. The endogenous decay coefficient is notoriously difficult to estimate, especially using relatively short-term experiments such as this approximately seven-day experiment. In addition, only having five data points for the optimization algorithm to use is not sufficient to capture the influence of b over this time scale.

Therefore, to determine a reasonable value for b, the optimization was performed to fit the isobutane data from the long-term bioaugmented microcosm experiment with Y, $K_{max,IB}$, and $K_{s,IB}$ fixed at 0.8 mg/mg, 2.58 mg/mg/day, and 0.05 mg/L, respectively. Data from only the first four additions were used because nutrient limitation appeared to impact rates beginning in the fifth addition. The optimum value for b over a range of 0 to 0.12 with step size of 0.005 was 0.03 1/day. When b and Y were optimized simultaneously using the isobutane data from the long-term microcosm experiment (range of 0 to 0.08 and step size 0.005 for b; range of 0.7 to 0.2 mg/mg and step size 0.01 for Y; $K_{max,IB}$ and $K_{s,IB}$ again fixed at 2.58 mg/mg/day and 0.05 mg/L) the optimal values were 0.040 1/day and 1.08 mg/mg, respectively.

When the updated values of b and Y were used in the model for the short-term pure culture experiment, Y=0.8 mg/mg and b=0.03 1/day (Simulation 5, not shown) resulted in a slight decrease in the E value for the model fit to the biomass data (0.960 to 0.932) but a slight increase in the E value for the model fit to the isobutane data (0.625 to 0.645). Y=1.08 mg/mg and b=0.04 1/day decreased the E values for the fits to both the isobutane and biomass data, to 0.575 and 0.873, respectively (Simulation 6, not shown). In addition to providing a better fit as determined by the E values, the short-term pure culture experiment was likely a better predictor of the yield. Therefore, the values of Y=0.8 mg/mg and b=0.03 1/day were used for further analysis.

Literature values for b ranged from 0.016 1/day to 0.15 1/day for methanotrophic and butane-utilizing cultures[60,104]. Because the b value of 0.03 1/day was determined from the first four additions to the long-term microcosm experiment, it was likely influenced the approximately month-long resting period between each addition. Microcosms were opened to the atmosphere immediately before each addition, meaning the resting period may have been oxygen limited and less microbial decay likely occurred[104]. Therefore, the b value of 0.03 1/day likely captured the dynamics of the long-term experiments but might under predict microbial decay in the short-term experiments. The paucity of biomass data points and the time scale of the short-term pure culture experiment prevented estimation of b (likely higher than 0.03

1/day) through the optimization procedures described previously. However, the short time scale of this experiment reduced the influence of b on model fit.

The yield of 0.8 mg/mg likely underestimated the true yield, which can be difficult to measure because endogenous decay does influence short-term experiments (though its impact is less readily visible). Therefore, Y was optimized using the iterative search method while b was set at 0.03 1/day ($K_{max,IB}$ and $K_{s,IB}$ still fixed at 2.58 mg/mg/day and 0.05 mg/L, respectively). A range of 0 to 1.5 mg/mg with step size of 0.001 produced an optimal Y of 0.885 mg/mg. When used in the model—Simulation 7—this yield value increased E to 0.955 for the biomass data. A visual assessment of Figure 25 confirms the good fit to the biomass data when Y=0.885 mg/mg and b=0.03 1/day.

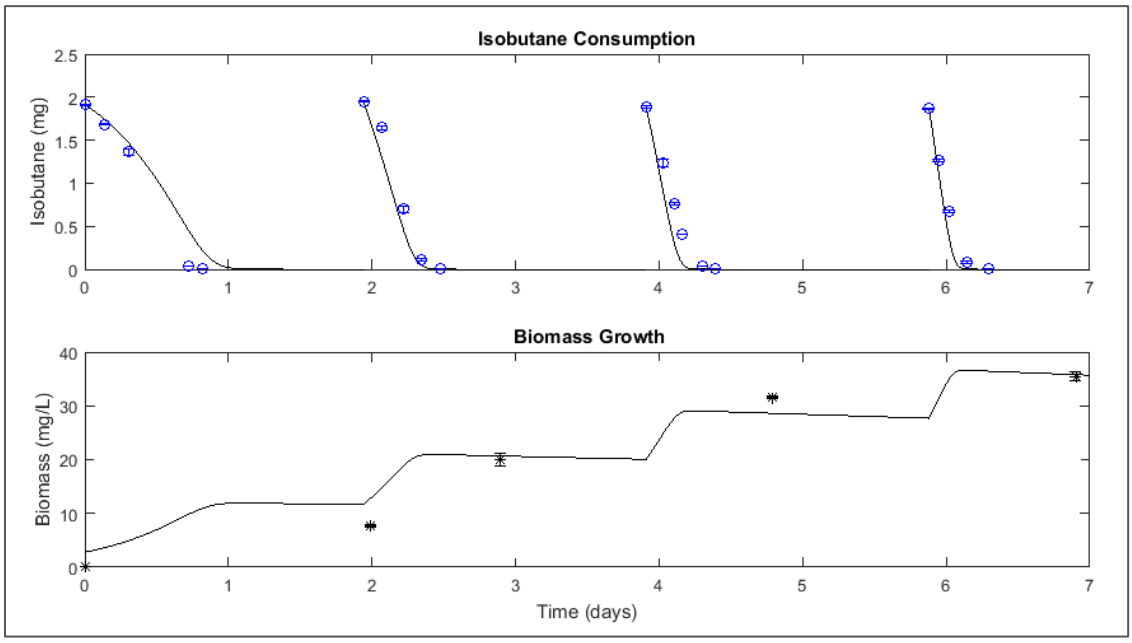

Figure 25. Model simulation showing over prediction of isobutane utilization after the optimization of Y and b in the short-term Pure Culture experiment. $K_{max,IB}$, $K_{s,IB}$, b, and Y fixed at 2.58 mg/mg/day, 0.05 mg/L, 0.03 1/day, and 0.885 mg/mg, respectively. (Simulation 7)

The interconnected nature of the isobutane degradation and biomass growth equations meant that increasing Y and decreasing b to fit the biomass data also affected the fit to the isobutane data. While the E value remained high, it did drop from 0.664 to 0.627, and a visual examination of Figure 25 showed the model shifted to over-prediction of isobutane utilization after the first addition. A source of this error was likely the $K_{s,IB}$ value, which, as previously

noted, was low relative to literature values. However, the model also under-predicted degradation in the first addition, an error that would be exacerbated by increasing the $K_{s,IB}$ value. These errors were addressed simultaneously by changing two parameters: increasing $K_{s,IB}$ to reduce the degradation rate at low concentrations, and increasing the initial biomass concentration, X_o, to increase the overall rate of degradation in the first addition. (The initial biomass was a measured value determined through TSS analysis of the inoculum solution.) As shown in Figure 26 (Simulation 8), increasing the initial biomass by 30% to 3.6 mg/L and doubling $K_{s,IB}$ to 0.1 mg/L (with $K_{max,IB}$, b, and Y fixed at 2.58 mg/mg/day, 0.03 1/day and 0.885 mg/mg, respectively) improved the fit to the isobutane data for later additions. The model still under predicted isobutane utilization in the first addition, however increasing the initial biomass prevented the fit from worsening by only increasing the $K_{s,IB}$ value. Based on the E value, these adjustments slightly worsened the fit to the biomass data (E dropped from 0.955 to 0.942). Another iteration of optimization and adjustments to b and Y could further improve this fit, however, changes would be small enough they were likely not outside the realm of errors from analytics and optimization with only five available points in the biomass data set.

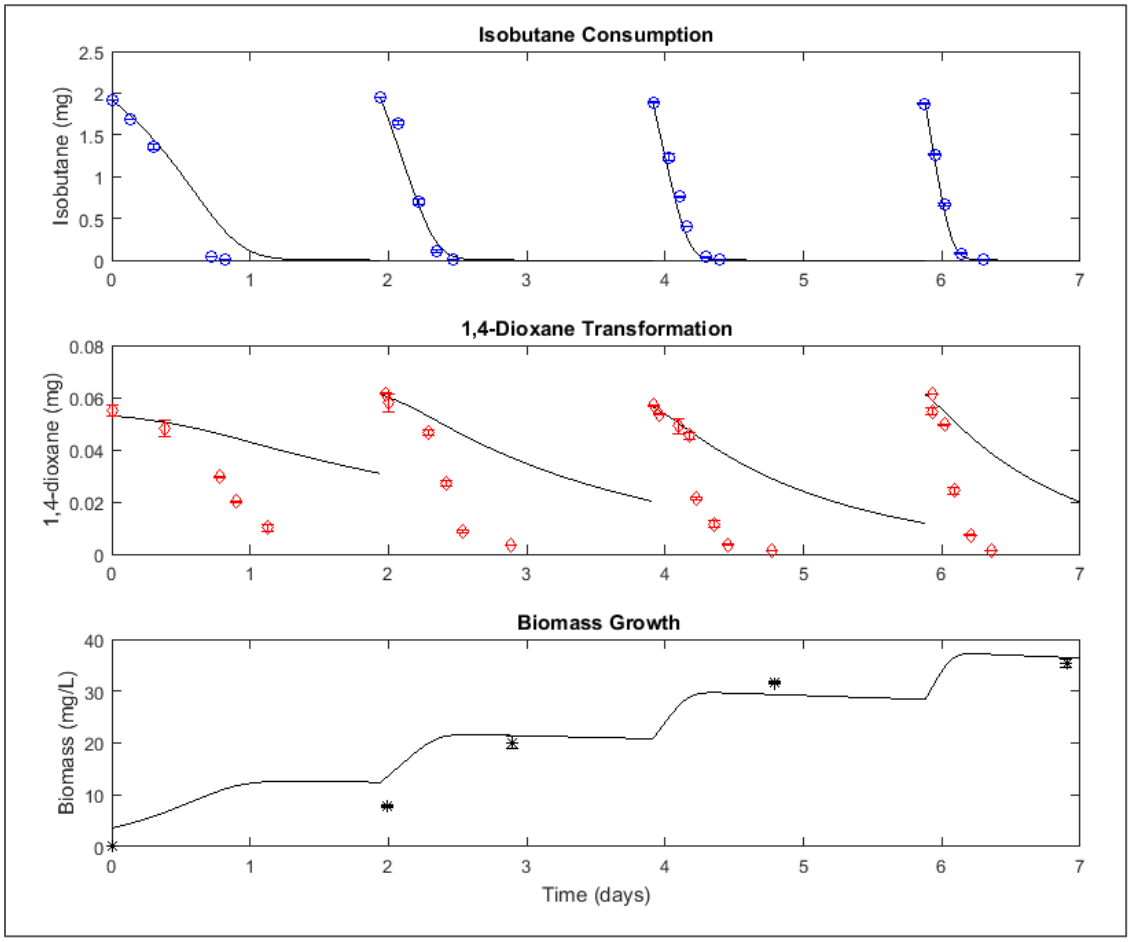

Figure 26. Model fit to isobutane, 1,4-dioxane, and biomass data from the short-term Pure Culture experiment after $K_{s,IB}$ was increased from 0.05 mg/L to 0.1 mg/L and initial biomass increased from 2.78 mg/L to 3.60 mg/L. $K_{max,IB}$, b, and Y fixed at 2.58 mg/mg/day, 0.03 1/day, and 0.885 mg/mg, respectively. (Simulation 8)

As observed by a comparison between Figure 19 and Figure 26, the updated parameters used to achieve good fits for the isobutane and biomass data in Simulation 8 also improved the model fit for 1,4-dioxane data. The E value increased from -0.741 with the original set of parameters in Simulation 1 to -0.007. However, an E value of less than zero is still a poor fit, as illustrated in Figure 26. Further improvement was made using similar fitting techniques as for the isobutane and biomass data. Because transformation capacity was not included in the model, changes to the 1,4-dioxane parameters did not impact the fit to the isobutane and biomass data. All model simulations used to improve the fit to the 1,4-dioxane data were run with the optimized isobutane and biomass parameters used in Simulation 8: $K_{max,IB}$=2.58 mg/mg/day, $K_{s,IB}$=0.1 mg/L, Y=0.885 mg/mg, b=0.03 1/day, and X_o=3.6 mg/L.

Given the low concentrations of 1,4-dioxane tested in the microcosm and multiple addition pure culture studies and the under prediction of the model shown in Figure 26, it was again assumed that the K_s value determined from the Monod curve was too high. Therefore, the iterative search method was used to simultaneously optimize $K_{max,14D}$ and $K_{s,14D}$ for data from a rapid, pure culture, resting-cell degradation test for a starting 1,4-dioxane concentration of 100 µg/L. Because isobutane was not present in this experiment, the competitive inhibition term in the denominator of Equation 12 did not influence the optimization. Different ranges and step sizes for $K_{max,14D}$ and $K_{s,14D}$ in the optimization resulted in significantly different "optimum" values for the parameters, indicating that the Michaelis-Menten equation was not a good representation of the data set.

The initial concentration of 1,4-dioxane in each addition was two orders of magnitude lower than the $K_{s,14D}$ value determined from the Monod curve. This made the 1,4-dioxane concentration a negligible component of the denominator in Equation 12, letting $K_{max,14D}/K_{s,14D}$ act as a first order constant, K_{FO}, as shown in Equation 20.

$$\frac{dM_{14D}}{dt} = -K_{FO} * X * V_l * \frac{M_{14D}}{V_l + V_g * H_{cc,14D}} \quad (20)$$

Two methods were used to determine the value of the first order rate constant. The first was a nonlinear regression of the low concentration 1,4-dioxane degradation curve using the "nlinfit" command in MATLAB to solve for K_{FO} in Equation 21, the integrated form of Equation 20.

$$M_{14D} = \frac{M_{14D,0}}{V_l + V_g * H_{cc,14D}} * V_l * e^{-K_{FO} * X * t} \quad (21)$$

$M_{14D,0}$ is the initial mass of 1,4-dioxane in the reactor. The second method was a linear regression of the natural log of the 1,4-dioxane data vs time using the MATLAB command "polyfit" (with a first order specification). The resulting coefficient was equal to K_{FO}*X. The fit of

each model to the experimental data is shown in Figure 27, the nonlinear regression on the left and the linear regression on the right. The nonlinear regression returned a value for the first order constant of 0.204 L/mg 21198/day, and a value of 0.249 L/mg 21198/day from the linear fit to the natural log of the data. The blue line in each plot shows the model when the first order rate constant was 0.028 L/mg 21198/day, equal to the ratio of $K_{max,14D}$ and $K_{s,14D}$ determined from the Monod curve (Figure 17). As illustrated in Figure 27, the first order constant determined from the Monod curve values did not fit the low concentration data, and it was an order of magnitude smaller than the first order constant determined from the regressions. This indicated the $K_{s,14D}$ value of 31.0 mg/L determined from the Monod curve was too large and underestimated the rate when combined with $K_{max,14D}$.

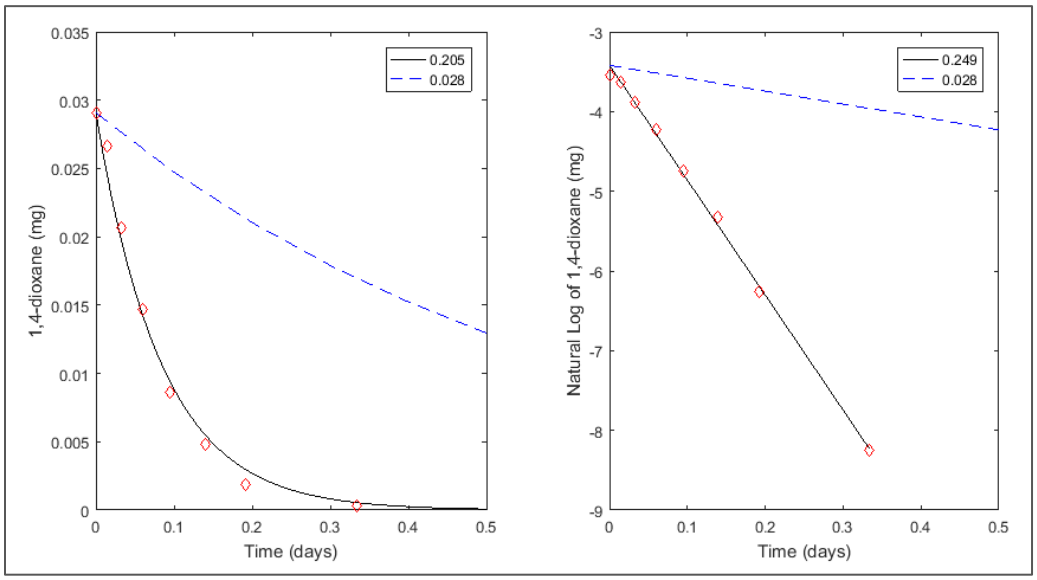

Figure 27. 1,4-dioxane degradation in a rapid, low concentration, pure culture resting cell test. Model fits using a first order rate constant determined by regression to the data (solid) and by the ratio of $K_{max,14D}$ to $K_{s,14D}$ values determined from the Monod curve (dashed). The left plot shows nonlinear regression and the right plot shows linear regression. The legends show values of first order rate constants (L/mg 21198/day).

When the model was run using Equation 20 and each of the first order rate constants determined from the regressions of the resting cell degradation data, the model fit was most improved by using the value of the first order constant determined from the nonlinear regression. K_{FO}=0.205 L/mg 21198/day (Simulation 9, not shown) improved the fit to an E value of 0.623, whereas K_{FO}=0.249 L/mg 21198/day yielded a fit of E=0.467 (Simulation 10, not

shown). Therefore, the value 0.205 L/mg 21198/day was used for further calculations. $K_{s,14D}$ was estimated by assuming the $K_{max,14D}$ value determined from the Monod curve was correct, and then dividing that value by the value of the first order rate constant, 0.205 L/mg 21198/day. The resulting $K_{s,14D}$ value of 4.35 mg/L was still an order of magnitude greater than the initial 1,4-dioxane concentration. This made the 1,4-dioxane concentration a negligible component of the denominator of Equation 12 and supported the hypothesis that 1,4-dioxane degradation occurred according to first order kinetics. According Figure 2, degradation of 1,4-dioxane would likely be first order throughout the plume at Fort Carson. The highest concentration contour (the source zone) is ">300 µg/L," which is an order of magnitude less than $K_{s,14D}$ value determined here. The median maximal concentration of 194 1,4-dioxane plumes in California was 365 µg/L^2, suggesting that 1,4-dioxane cometabolism would generally occur at first order rates.

When the new value of $K_{s,14D}$ was used in the competitive inhibition model (Equation 12) for the multiple addition experiment (Simulation 11), the E value further increased to 0.703, indicating a good fit. However, as shown in Figure 28, the model simulated more rapid transformation of 1,4-dioxane than occurred in the experiment. The model did not capture the initial lag in 1,4-dioxane transformation of each addition when the mass of isobutane was greater than approximately 1 mg (0.15 mg/L in liquid), which indicated the need to increase the influence of the competitive inhibition term by changing the value of the inhibition constant, K_I.

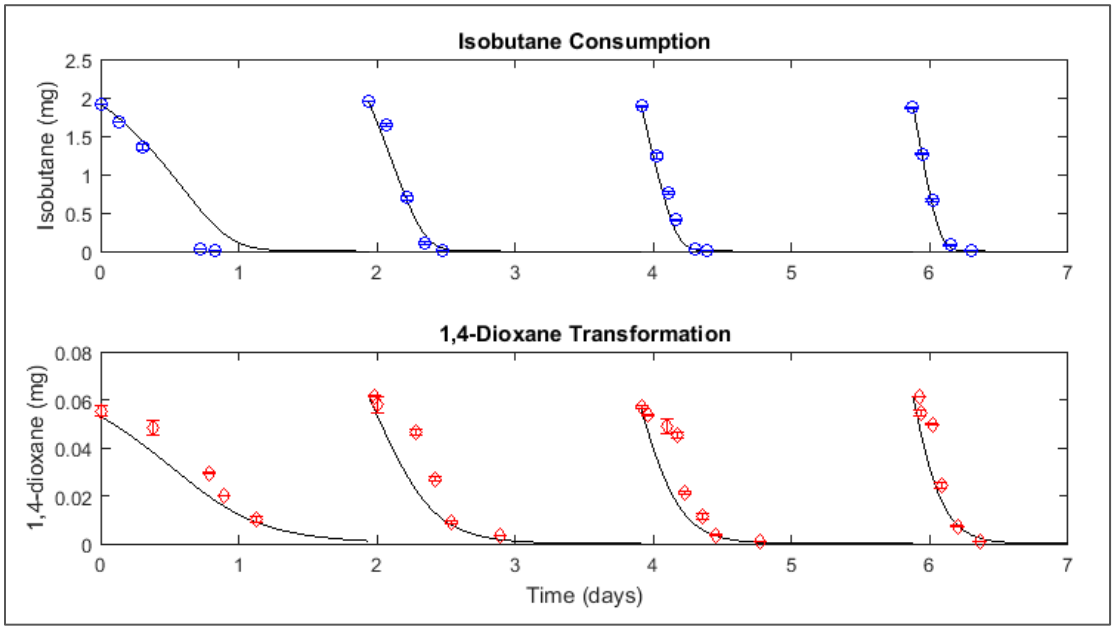

Figure 28. Model fit to isobutane and 1,4-dioxane data from the short-term Pure Culture experiment after decreasing $K_{s,14D}$ from 31 mg/L to 4.35 mg/L. $K_{max,1IB}$, $K_{s,IB}$, $K_{max,14D}$, K_I, b, Y and X_o fixed at 2.58 mg/mg/day, 0.1 mg/L, 0.87 mg/mg/day, 3mg/L, 0.03 1/day, 0.885 mg/mg, and 3.6 mg/L, respectively. (Simulation 11)

In order to capture the competitive inhibition illustrated in the data, K_I in Equation 12 was optimized to fit the multiple addition 1,4-dioxane data using an iterative search method with a range of 0 to 3 mg/L and step size of 0.01 ($K_{max,14D}$ and $K_{s,14D}$ were fixed at 0.87 mg/mg/day and 4.35 mg/L, respectively). The optimal value was 0.13 mg/L, which, as shown in Figure 29 (Simulation 12), captured the isobutane inhibition in the data and increased the E value to 0.929 for the fit to 1,4-dioxane data.

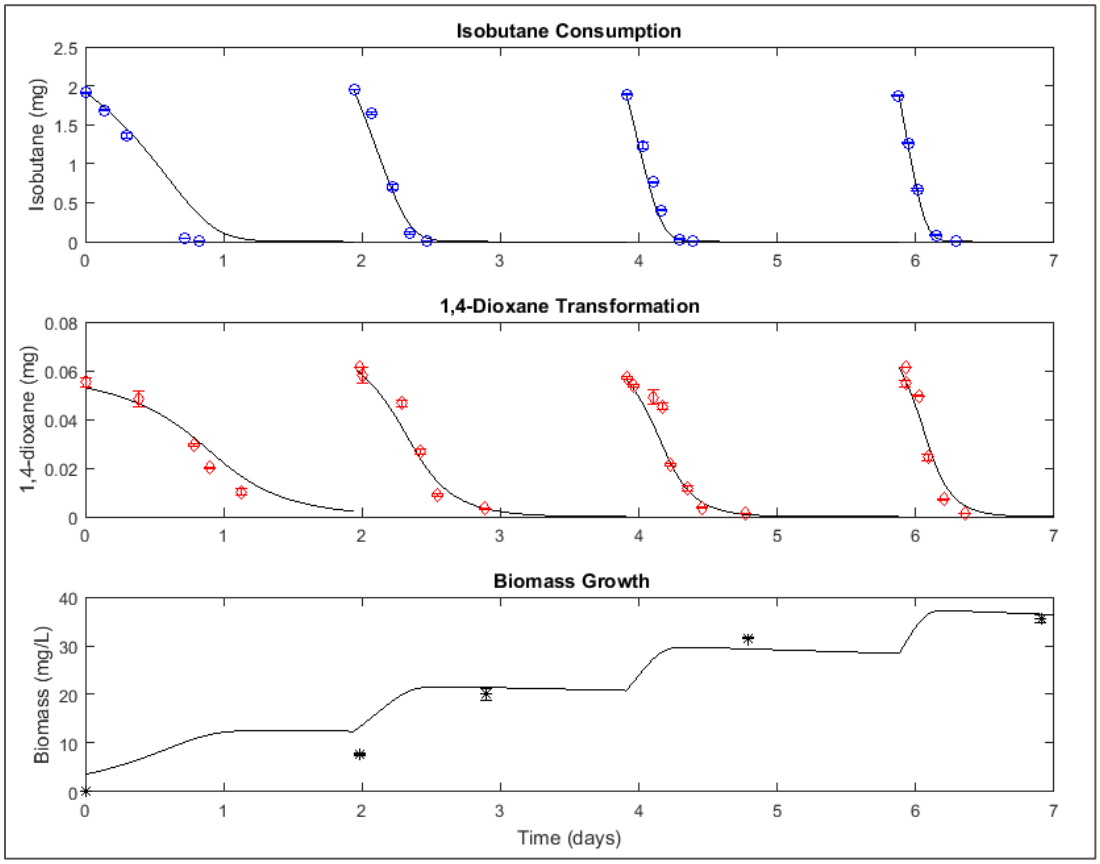

Figure 29. Model fit to isobutane, 1,4-dioxane, and biomass data from the short-term Pure Culture experiment after final adjustments to all parameters (Simulation 12). Final parameter values used for the simulation: $K_{max,1IB}$=2.58 mg/mg/day, $K_{s,IB}$=0.1 mg/L, $K_{max,14D}$,=0.87 mg/mg/day, $K_{s,14D}$=4.35 mg/L, K_I=0.13 mg/L, b=0.03 1/day, Y=0.885 mg/mg, and X_o=3.6 mg/L.

Figure 29 shows the model simulation for isobutane, 1,4-dioxane, and biomass after the adjustment of all parameters. The final parameter values were $K_{max,1IB}$=2.58 mg/mg/day, $K_{s,IB}$=0.1 mg/L, $K_{max,14D}$,=0.87 mg/mg/day, $K_{s,14D}$=4.35 mg/L, K_I=0.13 mg/L, b=0.03 1/day, Y=0.885 mg/mg, and X_o=3.6 mg/L. These values highlight the difference between direct metabolism and cometabolism. The values of K_{max}, K_s, and Y for CB1190, the most well-studied direct 1,4-dioxane metabolizer, are 66 mg 1,4-dioxane/mg TSS/day, 160 mg/L, and 0.036 mg TSS/mg 1,4-dioxane, respectively[13]. Direct metabolism by CB1190 occurs at a faster rate, however biomass yield is an order of magnitude lower than 21198 growth on isobutane. In addition, CB1190's K_s value is higher than 21198's, indicating CB1190's dioxane-monooxygenase enzyme has less affinity for 1,4-dioxane than 21198's isobutane monooxygenase. Low biomass yield and low

affinity for 1,4-dioxane in CB1190 and other direct metabolizers could contribute to the occurrence of natural attenuation of 1,4-dioxane at only approximately 20% of sites in the California GeoTracker database with a half-life of two to five years[50]. These parameter values also suggest that direct metabolizers may not be effective as bioaugmentation cultures over time and in low concentration plumes.

The final E values for the model fit to the isobutane, 1,4-dioxane, and biomass data were 0.658, 0.929, and 0.942, respectively. Each value is relatively close to one, indicating a good fit. The lowest E value was for the isobutane fit, which is surprising because visual assessment of the models in Figure 29 suggests that the isobutane model was actually the best fitting of the three. The relatively low E value was likely because the isobutane data set contains a high number of data points and they have larger absolute values than the 1,4-dioxane data points. This highlights the limitations of using the Nash-Sutcliffe Efficiency as a method for quantifying goodness of fit and making comparisons between data sets, however it was a useful test statistic for quantifying the fit of each data set individually. As shown in the list of E values in Table 9, the most significant improvements to model fits corresponded to simulations in which K_s values were lowered from the initial Monod curve estimates, which illustrates the importance of determining kinetic parameters that reflect low concentrations.

The sensitivity of each model parameter was tested individually. The model was run with an increase or decrease of a single parameter from the final value used in Simulation 12, and the change in the Nash-Sutcliffe Efficiency, E, was noted. Table 10 lists the percent difference in E for the fits to the isobutane, biomass, and 1,4-dioxane data sets with the alteration of each parameter. A list of the alternate parameter values and resulting E values is located in Appendix 0. As highlighted in Table 10, the model fits to the biomass and 1,4-dioxane data sets were most sensitive to a 30% increase in the microbial yield, Y. The model fit to the isobutane data was also highly sensitive to an increase in Y, though it was most sensitive to a 30% decrease in the value of $K_{max,IB}$. The most notable changes to the kinetic parameters in the fitting process were to the K_s values, which was necessary for the model to fit the low concentrations in the system. However, the sensitivity analysis shows that—after obtaining

parameters that achieve a good fit—the model is actually most sensitive to changes to the value of Y, and more sensitive to changes to K_{max} than K_s (with the exception of the 1,4-dioxane fit to the 30% decrease in $K_{s,14D}$).

Table 10. Sensitivity test: percent change in Nash-Sutcliffe Efficiency for the fit to isobutane, biomass, and 1,4-dioxane data sets when model parameters were individually increased or decreased by 30%

	% DIFFERENCE IN NASH-SUTCLIFFE EFFICIENCY					
	parameter 30% greater			parameter 30% less		
PARAMETER	Isobutane fit	Biomass fit	1,4-Dioxane fit	Isobutane fit	Biomass fit	1,4-Dioxane fit
$K_{MAX, IB}$	6.85	0.36	2.35	24.80	0.35	5.07
$K_{S, IB}$	3.18	0.07	0.69	0.52	0.11	0.34
Y	21.39	140.10	32.23	8.21	19.04	10.10
B	0.32	0.03	0.15	0.43	0.57	0.27
$K_{MAX, 14D}$	0.00	0.00	4.48	0.00	0.00	5.93
$K_{S, 14D}$	0.00	0.00	2.86	0.00	0.00	7.45
K_I	0.00	0.00	1.41	0.00	0.00	0.26
X_O	2.45	2.90	0.19	9.50	1.77	3.41

Figure 30 shows the model run with ±30% changes to Y, the parameter to which the model fit to the biomass and 1,4-dioxane data sets are most sensitive. The change in biomass concentrations were consistent with the 30% increase and decrease in Y. Equation 13 is linear with respect to Y, so the divergence in the biomass model should compound over multiple additions with altered Y values. However, Equations 11 and 12 are not linear with respect to Y, so, as shown in Figure 30, divergence from the original isobutane and 1,4-dioxane models does not compound in repeated additions.

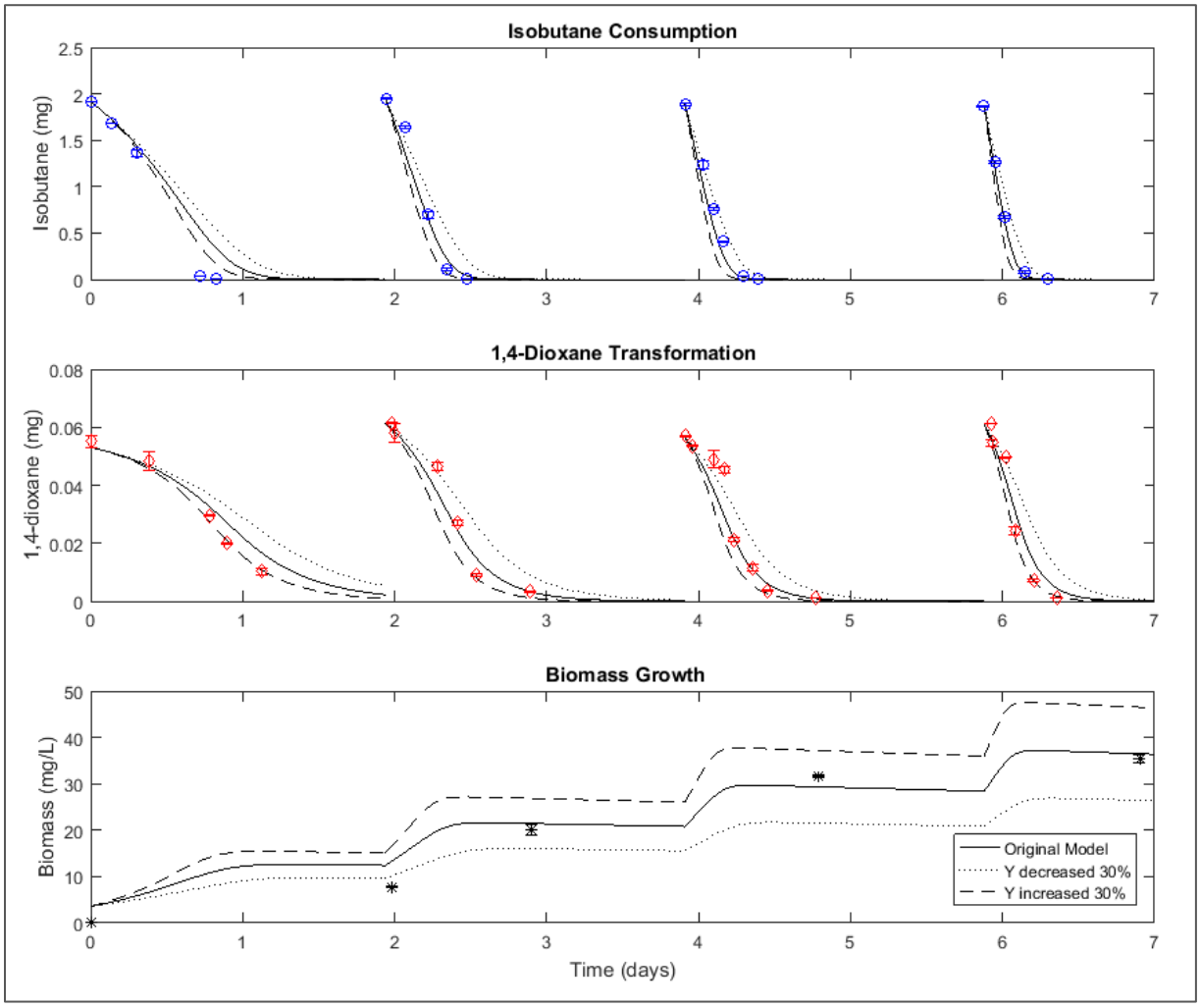

Figure 30. Isobutane, 1,4-dioxane, and biomass data from the short-term Pure Culture experiment with model run with final Y (0.885 mg/mg) and 30% increase (Y=1.151 mg/mg) and 30% decrease (Y=0.620 mg/mg).

Figure 31 shows the model run with ±30% changes to $K_{max,IB}$, the parameter to which the model fit to the isobutane data set is most sensitive. As illustrated by the figure, altering $K_{max,IB}$ causes the model to diverge most significantly from isobutane and 1,4-dioxane data sets in the first two additions, and the effect is muted by the fourth addition. In early additions biomass, X, is small, making $K_{max,IB}$ a more influential variable in Equation 11 and therefore more deviation from the original model. In later additions the impact was reduced by larger biomass values. The 30% increase in $K_{max,IB}$ results in a better fit to this data for the first addition, without appearing to significantly worsen the fit for later additions. This calls into question the decision to fix $K_{max,IB}$ as the value from the Monod curve without further iteration in the parameter

fitting process. It appears that an increased $K_{max,IB}$ could improve model fit (likely also resulting in a higher $K_{s,IB}$ value). Determination of a higher $K_{max,IB}$ value could be incorporated into the iterative parameter fitting process described here, or by fitting to high concentration isobutane transformation curves. (Simultaneous optimization of K_{max} and K_s to fit low concentration isobutane transformation curves shown in Figure 21 resulted in a low $K_{max,IB}$ value of 1.4 mg/mg/day because the small mass of isobutane transformed did not allow the rate to reach the Kmax value.)

As expected, altering $K_{max,IB}$ does not significantly impact the biomass model because it does not change the total biomass generated in the system. However, similar to the model fits to the isobutane and 1,4-dioxane data sets, it has the greatest effect on the shape of the biomass model for the first two additions.

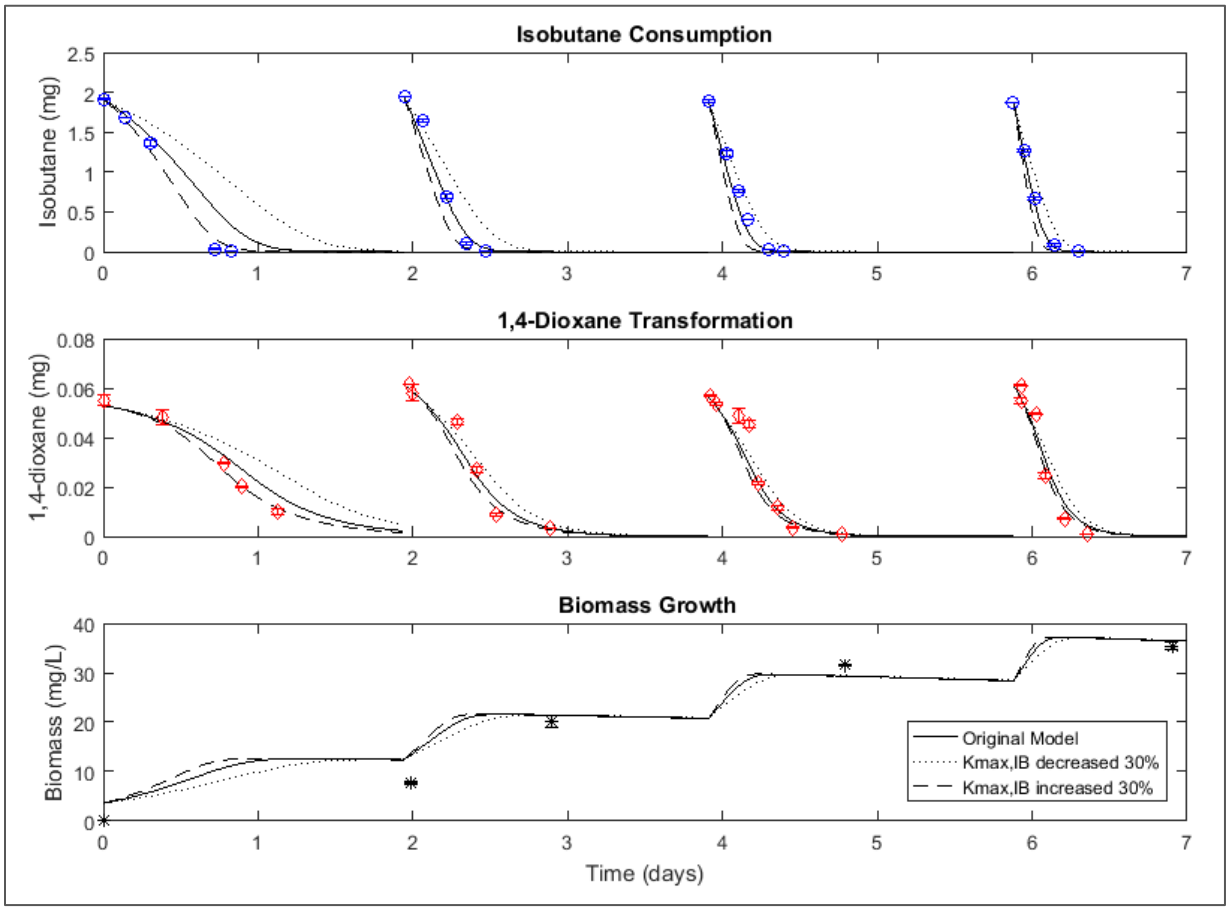

Figure 31. Isobutane, 1,4-dioxane, and biomass data from the short-term Pure Culture experiment with model run with final $K_{max,IB}$ (2.58 mg/mg/day) and 30% increase ($K_{max,IB}$=3.354 mg/mg/day) and 30% decrease ($K_{max,IB}$ =1.806 mg/mg/day).

2. Model fit to various microcosm data sets

After the parameters were set by analysis of the short-term Pure Culture experiment (except b, which was optimized from the long-term microcosm experiment), the model was run with the short and long-term microcosm experiments. The biomass shown in the figures is theoretical as optical density measurements were not possible due to the aquifer solids. Only initial biomass concentrations in the bioaugmented microcosms (the bioaugmentation inoculum) were measured values. As shown in a comparison between Figure 32 and Figure 18, after adjusting the parameters the model provides a better fit for the short-term bioaugmented microcosm data ("Bioaug Uw") than with the original values. The E values improved from -1.05 to 0.403 for the isobutane fit and from -0.128 to -0.094 for the 1,4-dioxane fit. While improved, the negative E value for the fit to the 1,4-dioxane indicates the mean of the data is a better representation than the model. Visual analysis of Figure 32 suggests that competitive inhibition by the presence of isobutane is not well replicated by the model. It appears that the quality of the 1,4-dioxane data could have also contributed to the poor fit. The initial 1,4-dioxane measurement for the second (and potentially the fourth) addition was lower than the second measurement, and was therefore a poor initial value for the model run. However, when the mass of the second measurement was used as the initial values for the second and fourth addition model runs, the model still provided a poor fit. The E value increased negligibly to -0.074, indicating further parameter adjustment was necessary.

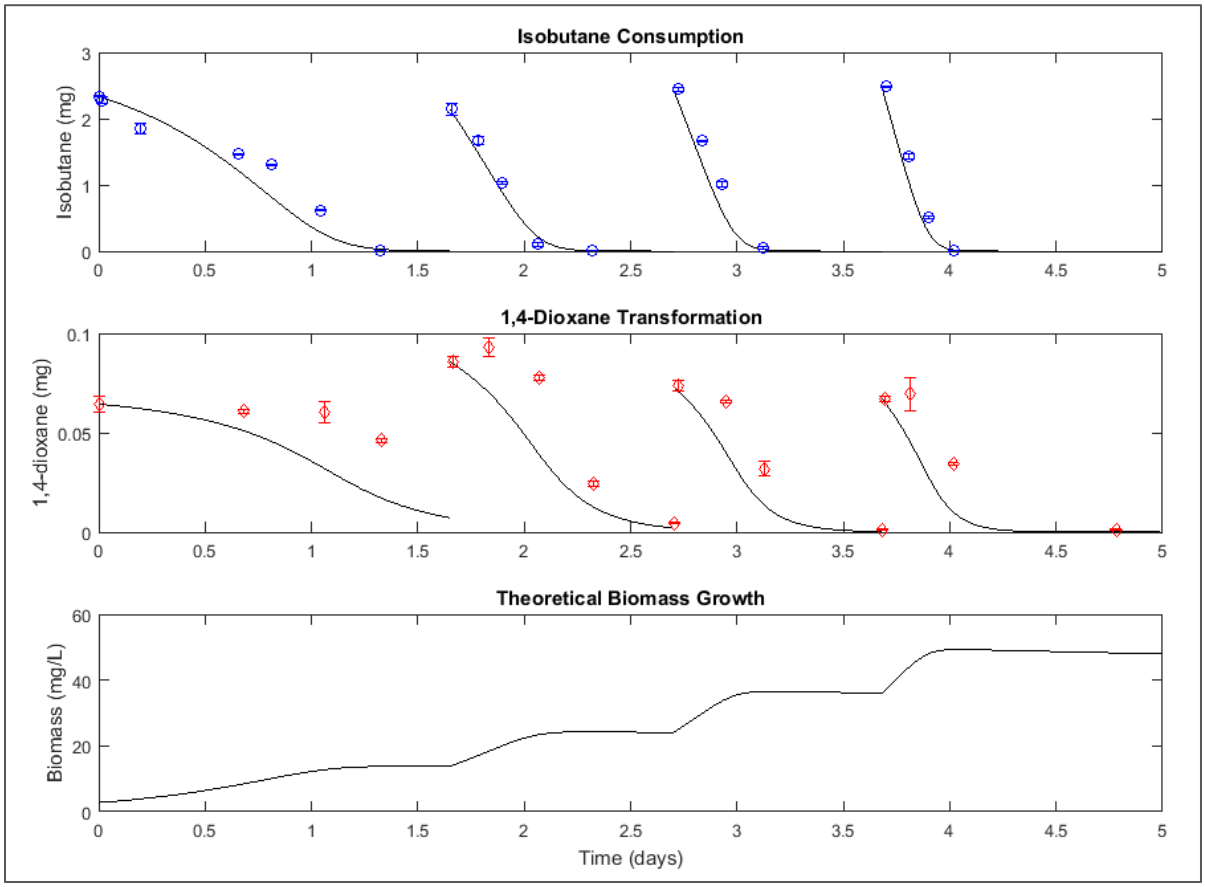

Figure 32. Model fit to isobutane, 1,4-dioxane, and theoretical biomass data from the short-term bioaugmented microcosms not experiencing nutrient limitation ("Bioaug Uw") using parameter values from Simulation 12. $K_{max,1IB}$=2.58 mg/mg/day, $K_{s,IB}$=0.1 mg/L, $K_{max,14D}$,=0.87 mg/mg/day, $K_{s,14D}$=4.35 mg/L, K_I=0.13 mg/L, b=0.03 1/day, and Y=0.885 mg/mg. X_o=2.78 mg/L.

When the inhibition coefficient, K_I, was fit to the 1,4-dioxane data from the "Bioaug Uw" microcosms using the iterative search method with a range of 0 to 0.1 mg/L and step size of 0.001, the optimum value was 0.009 mg/L. This parameter value increased the E value to 0.316, and, as shown in Figure 33, captured the primary substrate inhibition. The value of K_I optimized for the "Bioaug Uw" data set is 93% less than the value optimized to the Pure Culture experiment used for parameter fitting (0.13 mg/L). The sensitivity analysis indicated the model was relatively insensitive to changes to K_I (1.4% and 0.26% difference in E values for the 1,4-dioxane fit with a 30% increase and decrease to the parameter value, respectively). Therefore, a change of approximately one order of magnitude was required to shift the model. The

decrease from 0.13 mg/L to 0.009 mg/L is a large change in the value of K_I, which is discussed below in relation to model fits to other sets of microcosms.

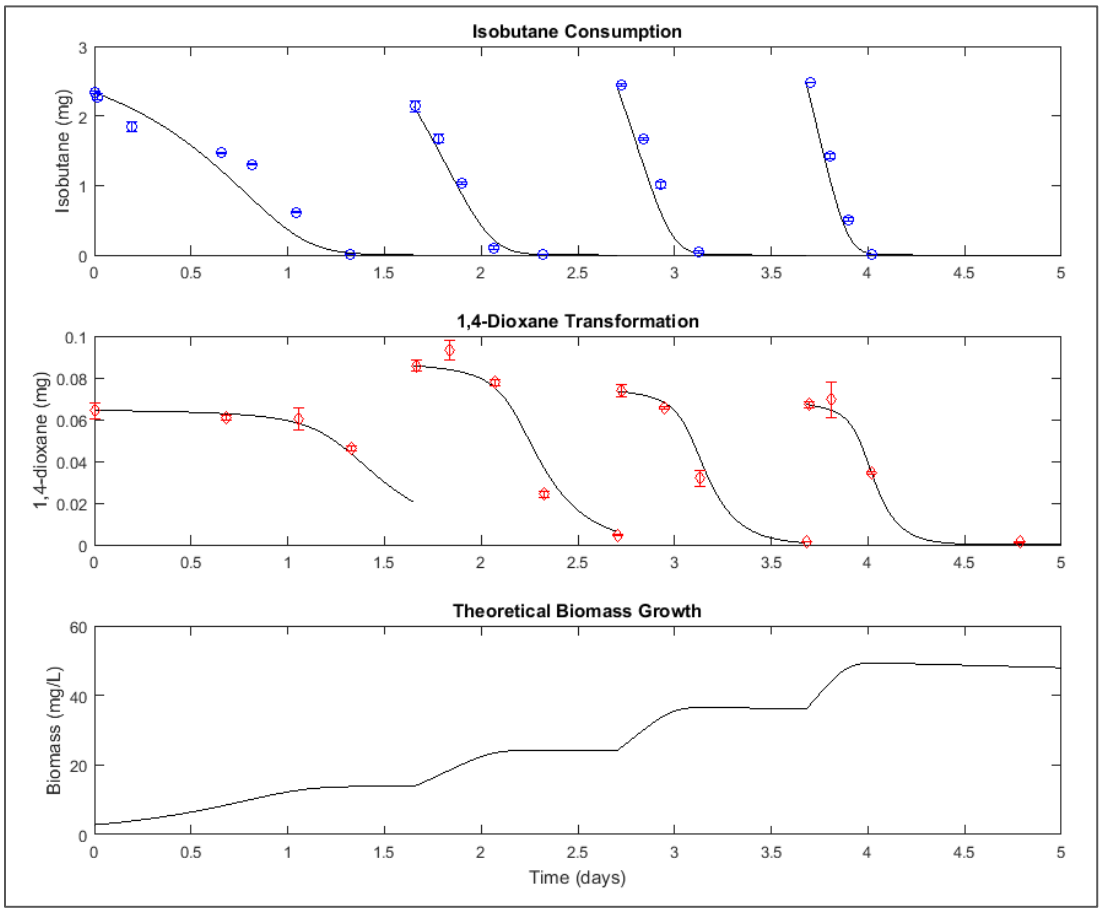

Figure 33. Model fit after optimization of K_I to isobutane, 1,4-dioxane, and theoretical biomass data from the short-term bioaugmented microcosms not experiencing nutrient limitation ("Bioaug Uw"). K_I=0.009 mg/L. Other parameter values from Simulation 12. $K_{max,1IB}$=2.58 mg/mg/day, $K_{s,IB}$=0.1 mg/L, $K_{max,14D}$,=0.87 mg/mg/day, $K_{s,14D}$=4.35 mg/L, b=0.03 1/day, and Y=0.885 mg/mg.

The parameters determined from fitting to the Pure Culture experiment (Simulation 12) resulted in good model fits to the isobutane and 1,4-dioxane data sets for the first six of seven additions in the long-term bioaugmented experiment, as shown in Figure 34. Each column of subplots shows the isobutane, 1,4-dioxane, and theoretical biomass for each of the seven additions, with the time between additions removed (typically one month). The full experiment lasted over 300 days, with good model fits to the first six additions spanning 280 days. E values for the isobutane and 1,4-dioxane fits for the full experiment were 0.462 and 0.227,

respectively, and increased to 0.593 and 0.578 when the data from the seventh addition was removed from the calculation.

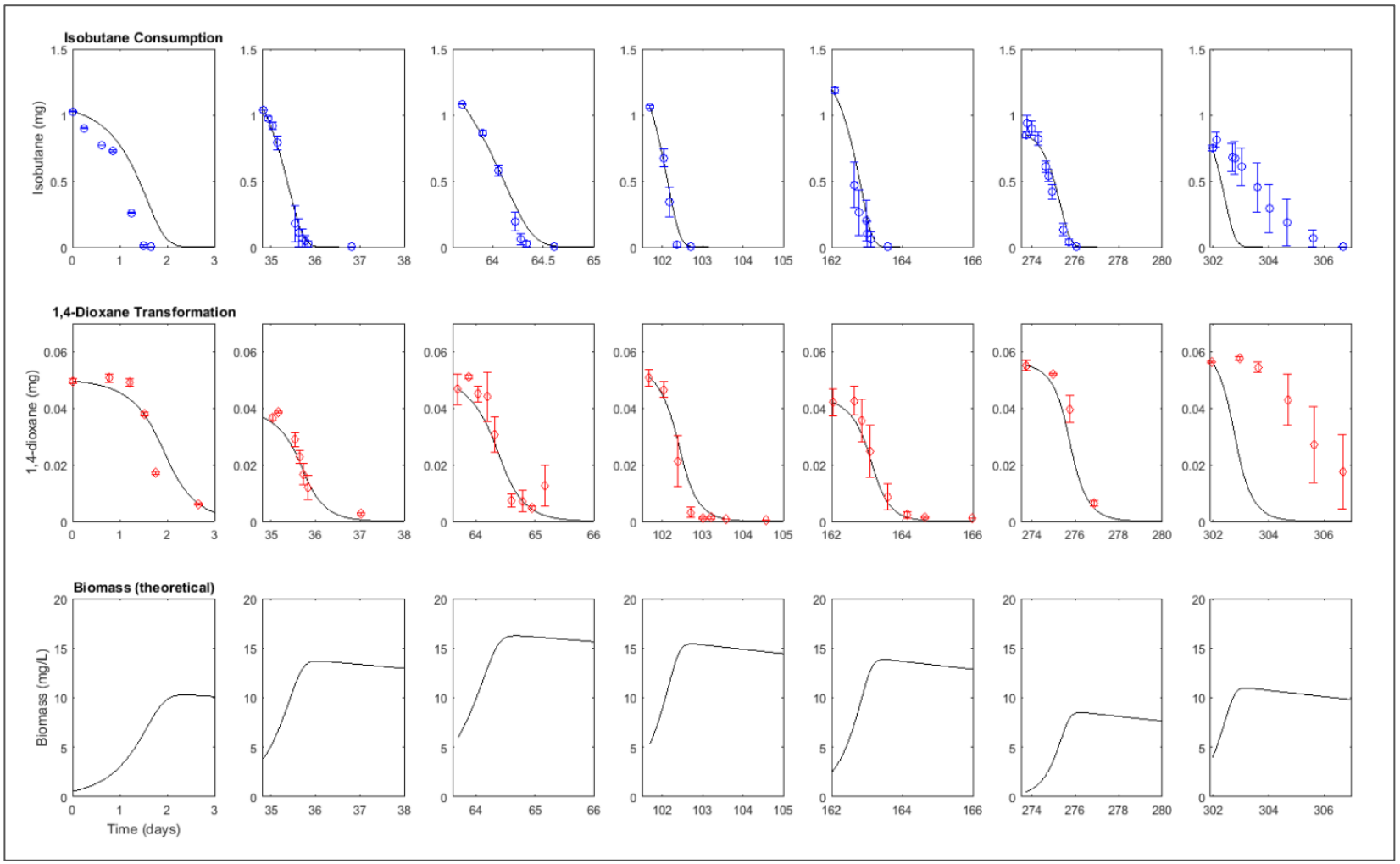

Figure 34. Model fit to isobutane, 1,4-dioxane, and theoretical biomass data from the long-term bioaugmented microcosms using parameter values from Simulation 12. $K_{max,1IB}$=2.58 mg/mg/day, $K_{s,IB}$=0.1 mg/L, $K_{max,14D}$,=0.87 mg/mg/day, $K_{s,14D}$=4.35 mg/L, K_I=0.13 mg/L, b=0.03 1/day, and Y=0.885 mg/mg. X_o=0.56 mg/L.

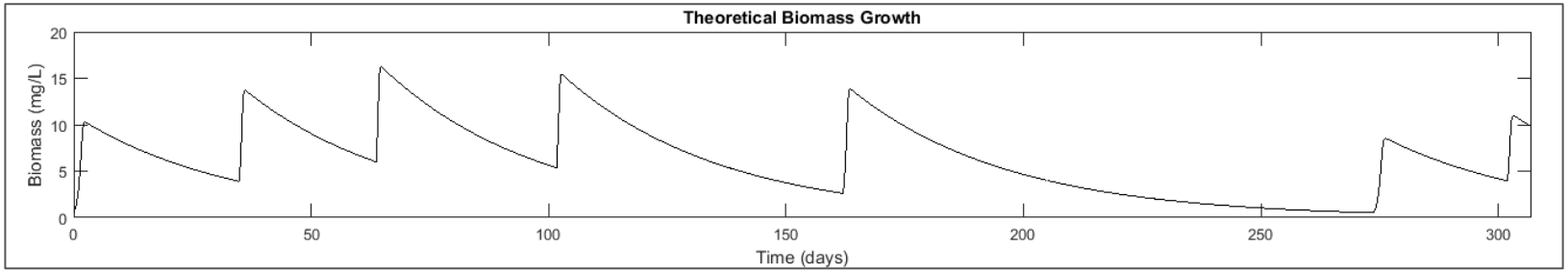

Figure 35. Theoretical biomass growth in long-term bioaugmented microcosms with model generated from parameters in Simulation 12 shown on a continuous time scale.

Initial zero order rates of isobutane and 1,4-dioxane transformation for each addition in the long-term bioaugmented microcosms (presented in Figure 8) showed slowing in the fifth, sixth, and sevenths additions, which potentially suggested inorganic nutrient limitation. However, good model fit through the sixth addition suggests biomass decay was likely partially responsible for the rate decrease. The time between the fourth and fifth additions was approximately two months, and approximately 3.5 months passed between additions passed between the fifth and sixth additions. This allowed for more biomass decay between additions, as shown by the snapshots for each addition in Figure 34 and the theoretical biomass growth presented continuously in Figure 35. Good model fits after these long resting periods confirmed the accuracy of the value of b determined from only the first four additions, which experienced more standard lag periods of one month. The seventh addition, however, occurred one month after the sixth, resulting in less biomass decay and higher modeled rates. However, the model over predicted the transformation of both isobutane and 1,4-dioxane illustrated by the data, which suggested that nutrient limitation affected transformation in the seventh addition.

Use of the K_I value of 0.009 mg/L obtained from the optimization of the short-term bioaugmented microcosms in place of 0.13 mg/L from the fit to the pure culture data worsened the fit to the long-term bioaugmented microcosms. The E value for the 1,4-dioxane fit when the model was run with K_I=0.009 mg/L decreased to 0.385 when calculated for the first six additions and to 0.145 when calculated for all seven additions. This indicated the K_I value optimized for the short-term bioaugmented microcosms (“Bioaug Uw”) was not a better fit for all microcosm environments.

The poor model fit to data in nutrient limited systems is illustrated in Figure 36, which shows the model run for short-term microcosms that were bioaugmented with washed 21198 and received 200 µL growth media as inorganic nutrient amendment (“Bioaug W+N”). The model provides a relatively good fit for the first and second additions, but a poor fit for the third and fourth additions for both isobutane and 1,4-dioxane data. When the model is run with parameters from Simulation 12, E values for the isobutane fit decrease from 0.283 when calculated for the first two additions to -0.178 when calculated for all four additions. E values

for the 1,4-dioxane fit decrease from 0.5179 to when calculated for the first two additions to -1.442 when calculated for all four additions. Zero order rate calculations indicated slowing and potentially nutrient limitation in the fourth addition, however the poor model fit to the third addition suggests nutrient limitation may have occurred earlier in the experiment.

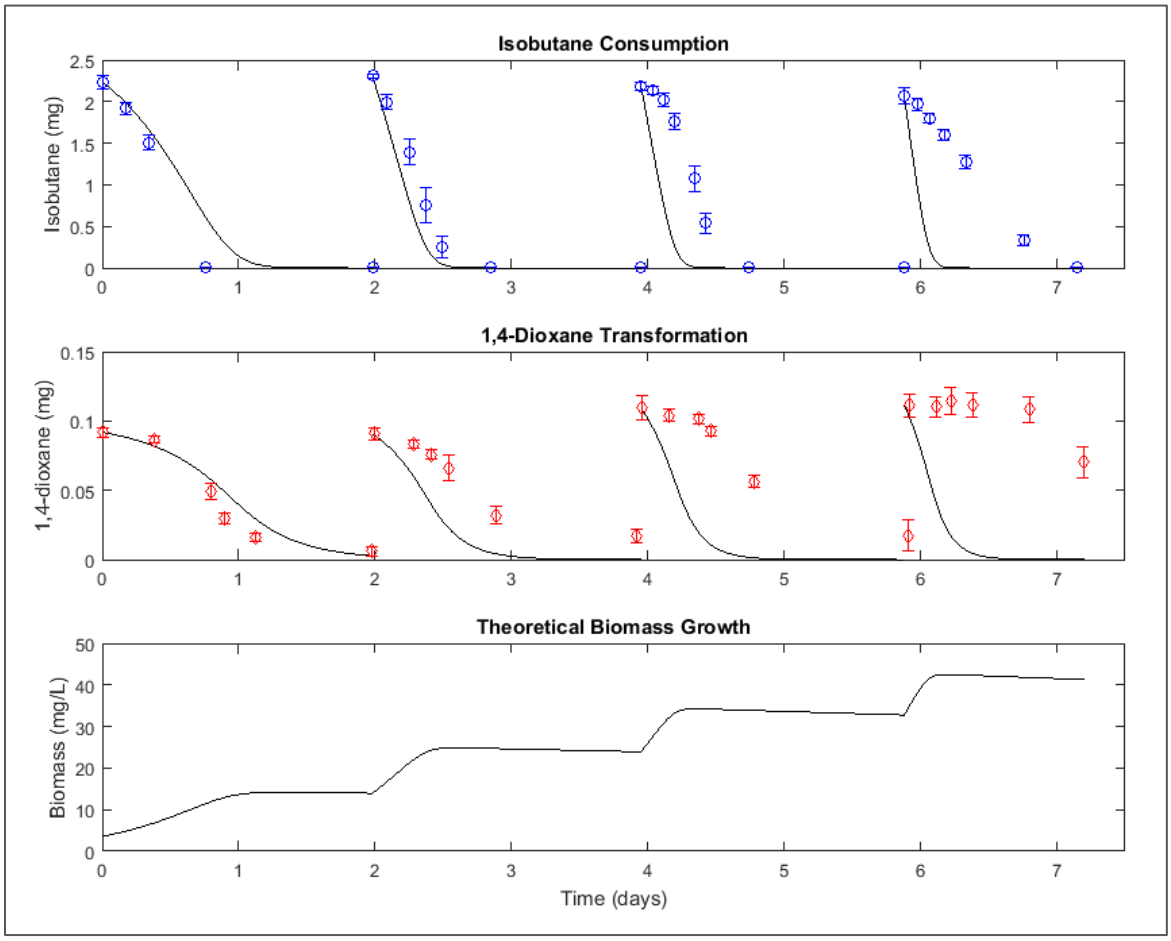

Figure 36. Model fit to isobutane, 1,4-dioxane, and theoretical biomass data from short-term microcosms bioaugmented with washed 21198 and given growth media as inorganic nutrient amendment ("Bioaug W+N"). Model run with parameter values from Simulation 12. $K_{max,1IB}$=2.58 mg/mg/day, $K_{s,IB}$=0.1 mg/L, $K_{max,14D}$,=0.87 mg/mg/day, $K_{s,14D}$=4.35 mg/L, K_I=0.13 mg/L, b=0.03 1/day, and Y=0.885 mg/mg. X_o=3.6 mg/L.

While the model fit to the 1,4-dioxane data in Figure 36 appears to under predict primary substrate inhibition, this is primarily due to the model's over prediction of both isobutane and 1,4-dioxane transformation. The model fit as quantified by E was not improved by using K_I=0.009 mg/L in place of 0.13 mg/L.

Using the model for native microcosms was complicated because the initial biomass concentration, X_o, was not known. An estimate of the value was determined by adjusting X_o so that the model provided a good fit to isobutane utilization in the first addition. For the three sets of native microcosms, the X_o values were $6x10^{-7}$ mg/L for short-term native microcosms with 200 µL growth media ("Native+N"), $3x10^{-4}$ mg/L for the short-term native microcosms without inorganic nutrient amendment ("Native no N") , and $2x10^{-4}$ mg/L for the long-term native microcosms (also without inorganic nutrient amendment). Assuming a single cell mass of 1 pg[107], these concentrations suggest the initial number of isobutane-utilizing cells in each microcosms were approximately $1.08x10^2$, $5.4x10^4$, and $1.9x10^4$, respectively. As expected, these low cell counts indicate microorganisms capable of utilizing isobutane are limited in microbial communities native to the subsurface. The initial biomass concentrations needed to get a good fit was similar between the two sets of microcosms with the same nutrient condition, the long-term microcosms and the short-term microcosms without nutrient amendment. These sets of microcosms also each had biostimulation lags of approximately six days, whereas "Native+N" had a lag of approximately 10 days.

Nutrient limitation was also likely a major factor in the model fit to native microcosms as zero order rate analysis suggested that all sets of native microcosms were nutrient limited. The model fit to the short-term "Native+N" microcosms using parameters from Simulation 12 is shown in Figure 37. While the adjustment of X_o enabled a good fit to isobutane transformation in the first addition (E=0.976), the model over predicts isobutane utilization rates in all later additions. E decreases to -0.062 when calculated from all four additions. Figure 37 shows the model fit to the 1,4-dioxane data is poor for all additions. Use of the lower inhibition constant value of 0.009 mg/L resulted in good model fit for the first addition (E=0.913), however rates in later additions were likely strongly impacted by nutrient limitation and the reduction in K_I was insufficient to develop a good fit (E=-1.830 when calculated from all four additions). Similar to the fit to the "Bioaug W+N" microcosms, the poor model fit beginning in the second addition suggests nutrient limitation may have occurred earlier than suggested by the analysis of the zero order rates.

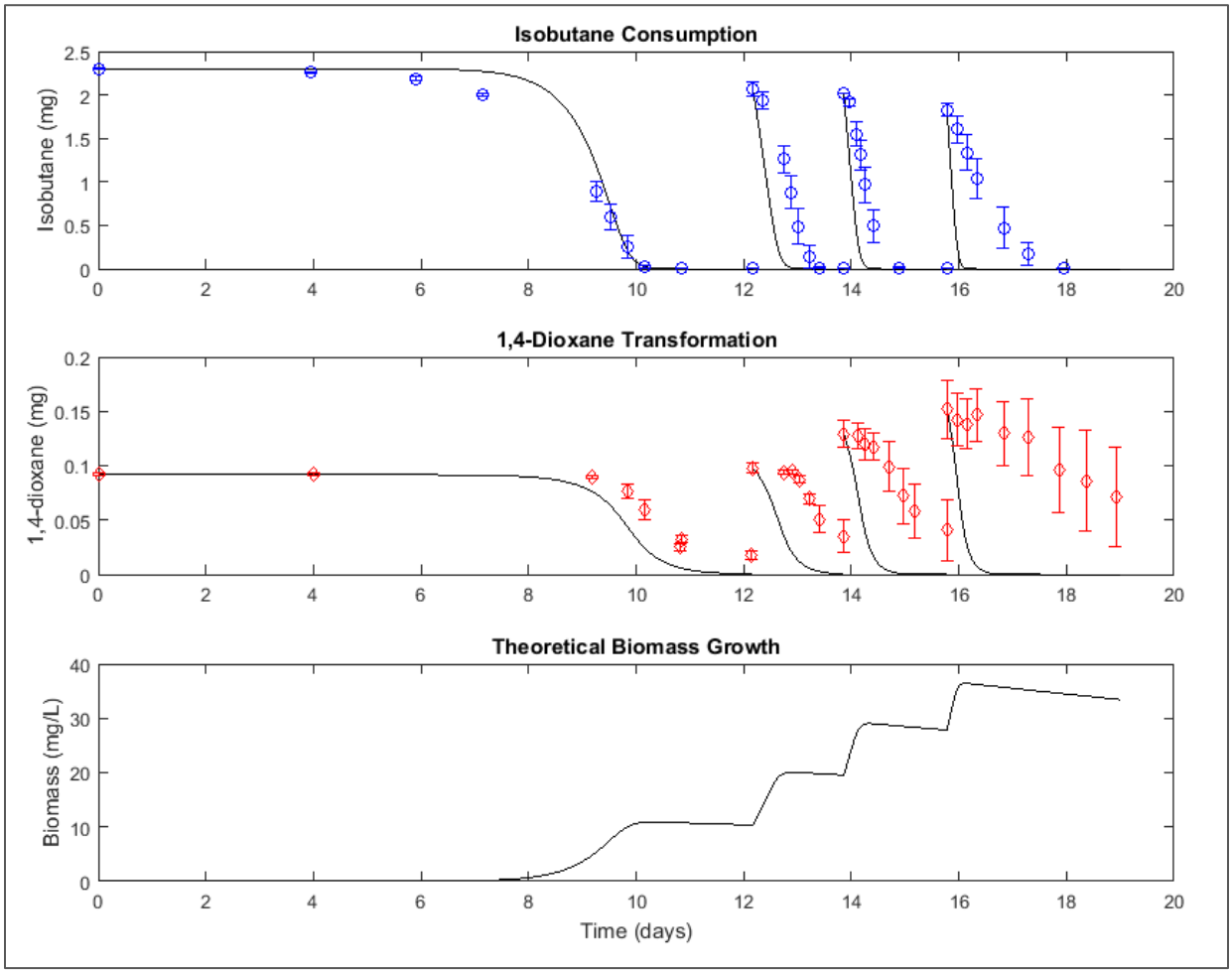

Figure 37. "Native+N" with model fit to isobutane, 1,4-dioxane, and theoretical biomass data (short-term native microcosms with inorganic nutrient amendment). Model run with parameter values from Simulation 12. $K_{max,1IB}$=2.58 mg/mg/day, $K_{s,IB}$=0.1 mg/L, $K_{max,14D}$,=0.87 mg/mg/day, $K_{s,14D}$=4.35 mg/L, K_I=0.13 mg/L, b=0.03 1/day, and Y=0.885 mg/mg. X_o=6x10^{-7}.

The model resulted in similarly poor fits to the most nutrient limited short-term microcosms ("Native no N"), as shown in Figure 38 (run with parameters from Simulation 12). Again, poor model fits to early additions suggested that nutrient limitation may have occurred earlier than suggested by decreases in zero order rates.

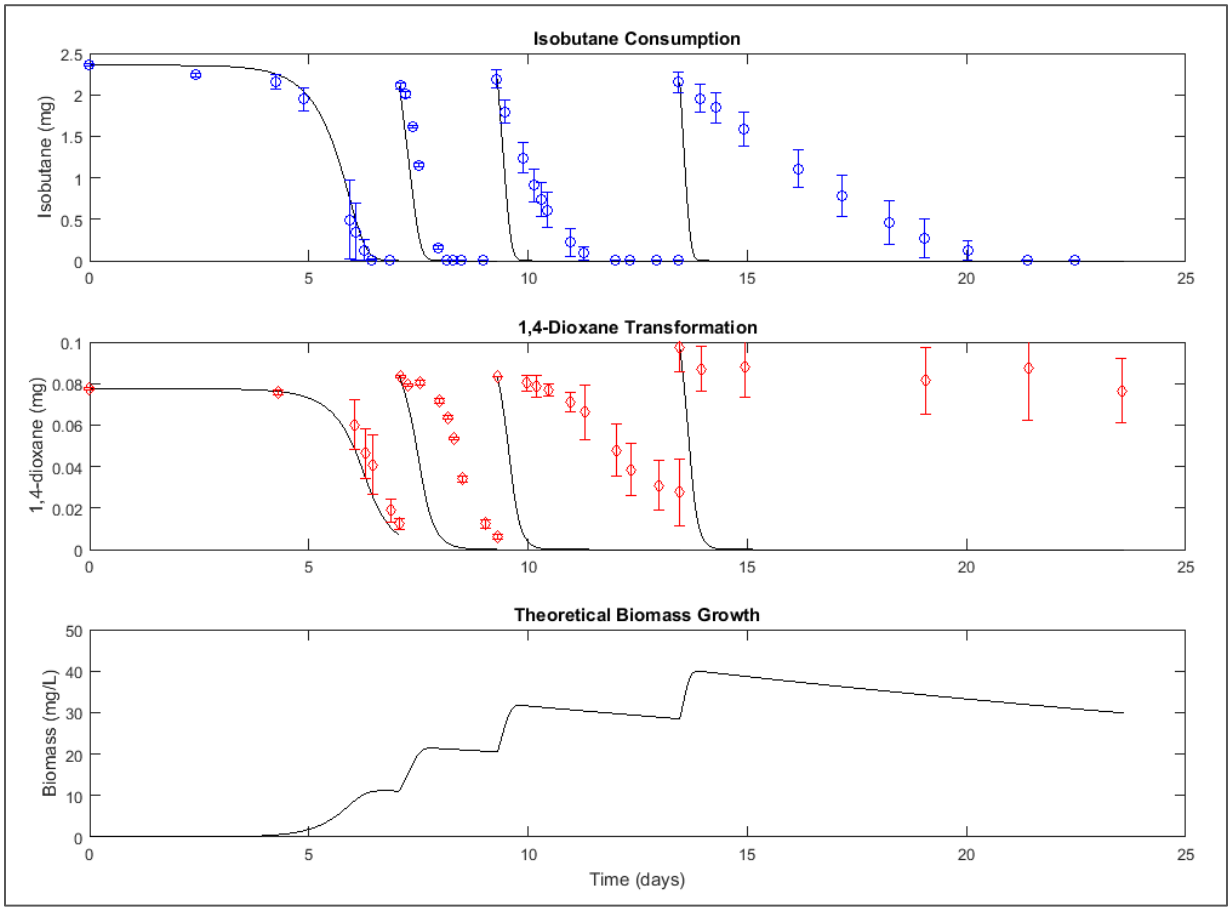

Figure 38. "Native no N" with model fit to isobutane, 1,4-dioxane, and theoretical biomass data (short-term native microcosms without inorganic nutrient amendment). Model run with parameter values from Simulation 12. $K_{max,1IB}$=2.58 mg/mg/day, $K_{s,IB}$=0.1 mg/L, $K_{max,14D}$,=0.87 mg/mg/day, $K_{s,14D}$=4.35 mg/L, K_I=0.13 mg/L, b=0.03 1/day, and Y=0.885 mg/mg. X_o=3x10^{-4}.

After adjusting the initial biomass concentration to achieve a good model fit for the first addition in the long-term native microcosms, the model provided a poor fit for the second through fifth additions, as shown in Figure 39. Again, this likely illustrated the influence of inorganic nutrient limitation. However, after two of the three microcosms received nutrient augmentation in the sixth addition, the model provided a good fit to the increased rates of transformation of both isobutane and 1,4-dioxane, as shown in Figure 39. Rates decreased again in the seventh addition, which, as shown in the figure, worsened the fit of the model to the data. As discussed previously, the reduction of rates in the seventh addition indicated the nutrient augmentation in the sixth addition was not enough to provide an excess and allow for continued high rates of transformation. Therefore these slower rates would not be replicated

by the model. However, the good fit for the sixth addition potentially indicated that the model is able to simulate transformation in the native microcosms just as well as in the bioaugmented microcosms when the system is not nutrient limited. This result also suggested the method of estimating the initial biomass concentration by fitting the model to the first isobutane transformation curve is accurate enough to allow for good fits to transformation in later additions. However, a comparison of the continuous biomass growth and decay curves for the long-term native and bioaugmented microcosms in Figure 35 and Figure 40 showed they are almost identical in shape after the biostimulation lag in the first addition, meaning a the initial biomass concentration is not an influential parameter for long-term modeling.

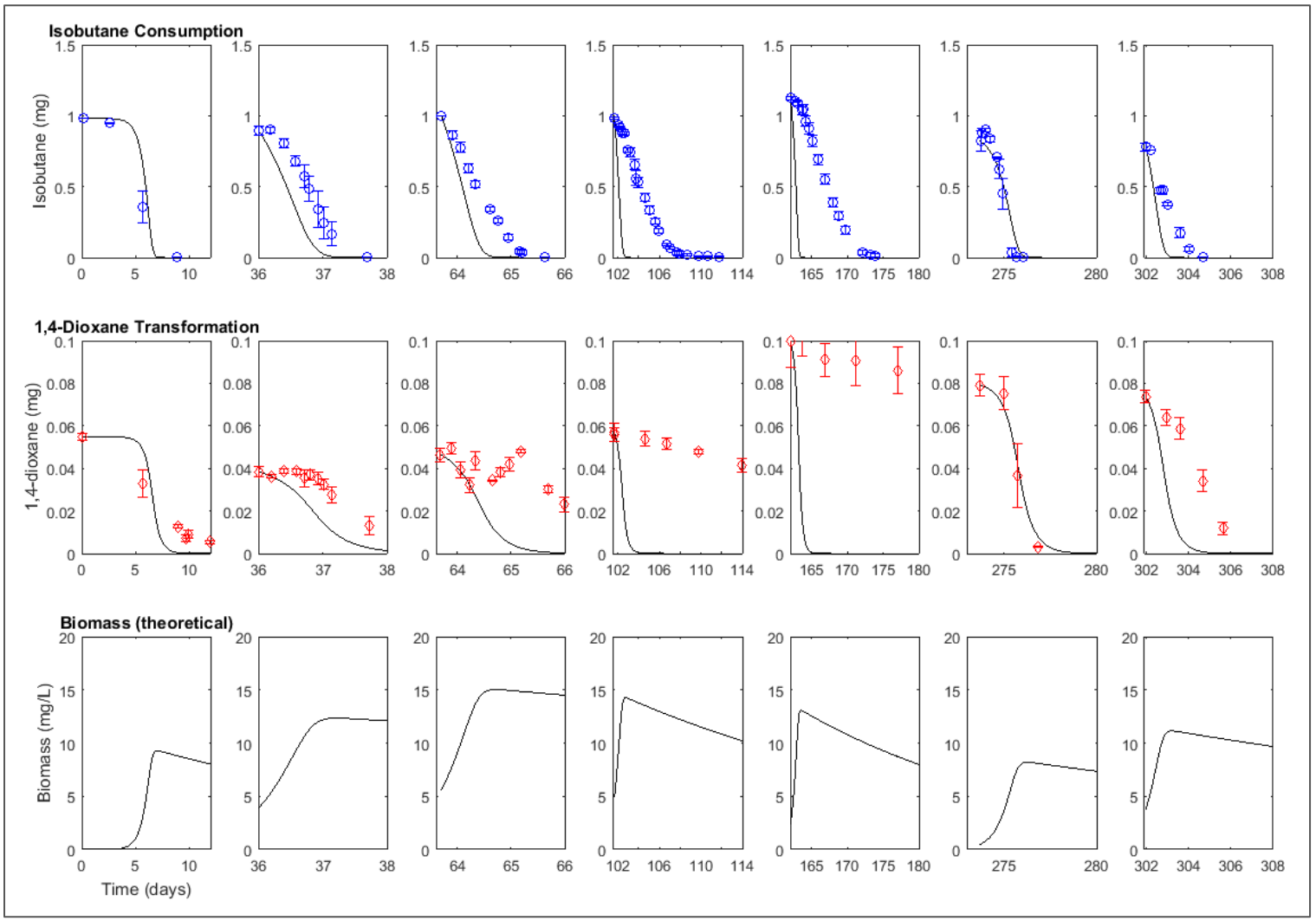

Figure 39. Long-term native microcosms with model. Model fit to isobutane, 1,4-dioxane, and theoretical biomass data from long-term native microcosms. Model run with parameter values from Simulation 12. $K_{max,1IB}$=2.58 mg/mg/day, $K_{s,IB}$=0.1 mg/L, $K_{max,14D}$,=0.87 mg/mg/day, $K_{s,14D}$=4.35 mg/L, K_I=0.13 mg/L, b=0.03 1/day, and Y=0.885 mg/mg. X_o=2x10^{-4}.

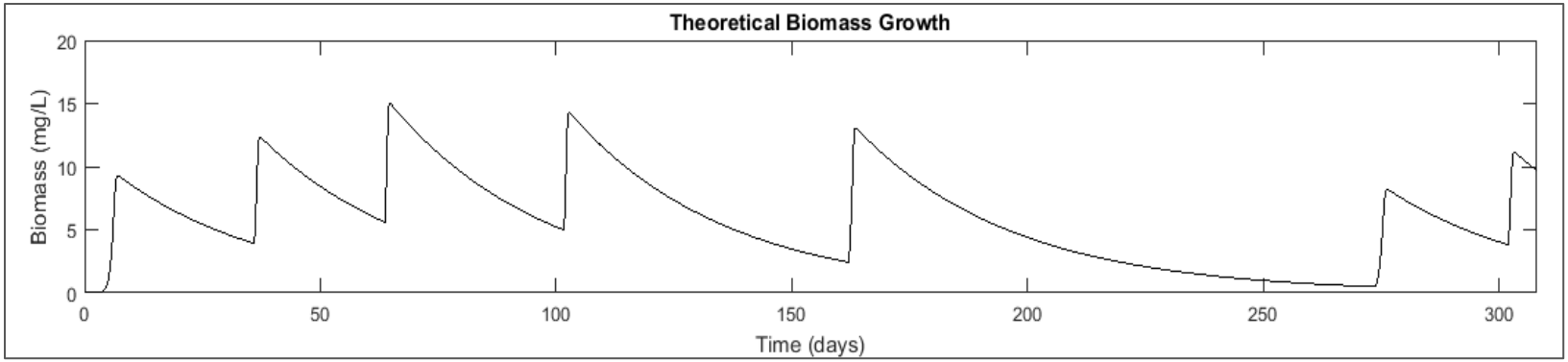

Figure 40. Theoretical biomass growth in long-term native microcosms with model generated from parameters in Simulation 12 shown on a continuous time scale.

V. CONCLUSION

Microcosms constructed with aquifer solids from Fort Carson, Colorado were used to assess aerobic cometabolism of 1,4-dioxane via bioaugmentation with 21198, biostimulation with isobutane as a primary substrate, the effect of TCE as a co-contaminant, and the influence of inorganic nutrients. Simultaneous utilization of isobutane, transformation of 1,4-dioxane, and growth of biomass were modeled according to Michaelis-Menten and Monod kinetics. Results of the study showed:

- Isobutane effectively biostimulated 1,4-dioxane-degrading microorganisms from the Fort Carson aquifer solids after a lag period of approximately one week, indicating isobutane would potentially be an effective primary substrate to induce cometabolism of 1,4-dioxane in the field.
- Microcosms bioaugmented with 21198 showed immediate degradation of 1,4-dioxane after isobutane was consumed below 0.15 mg/L. This indicated 21198 survived inoculation in the microcosm environment and would potentially be viable for use as a bioaugmentation culture in the field. Primary substrate inhibition of 1,4-dioxane transformation was also observed.
- Relative to 1,4-dioxane, TCE was not readily cometabolized in bioaugmented or native microcosms, however at a concentration of 200 μg/L it did not inhibit isobutane utilization or 1,4-dioxane transformation.
- The availability of inorganic nutrients was an important limiting factor in isobutane utilization and 1,4-dioxane transformation in both native and bioaugmented microcosms. After the initial biostimulation lag period, differences in the performance of bioaugmented and native microcosms were not significant when enough inorganic nutrients were also present in each system. When the bioaugmentation inoculum was delivered in spent growth media (that included additional nutrients), bioaugmented microcosms sustained higher degradation rates for repeated additions of 1,4-dioxane. Artificial groundwater alone was not a sufficient source of inorganic nutrients to sustain transformation.

- Modeling showed that 1,4-dioxane was transformed in the microcosms according to first order kinetics. The K_s value fit to the data was an order of magnitude higher than the median maximum 1,4-dioxane of plumes in the field, indicating cometabolism of 1,4-dioxane would typically occur at first order rates. Modeling highlighted the importance of the K_s value in simulating transformation of low concentrations of both isobutane and 1,4-dioxane. However, after parameter values were set to fit experimental data, the model was most sensitive to changes in the values of Y and $K_{max,IB}$. The model was able to predict isobutane utilization and 1,4-dioxane degradation for approximately 300 days in bioaugmented microcosms in which there were sufficient inorganic nutrients. Modeling illustrated the influence of inorganic nutrients on the rates of isobutane and 1,4-dioxane transformation through increased divergence between the model and experimental data as microcosms became more nutrient limited.
- The model development process highlighted the limitations of Monod curves for parameter estimation, especially for low concentrations of primary and cometabolic substrates. The iterative process of fitting a single parameter or two parameters simultaneously to a variety of pure culture data sets yielded a model that accurately represented experimental data in microcosms that were not nutrient limited. The iterative search method used to fit most of the parameters was a simple, inelegant approach, however it worked well given the complexity of the model equations and size of data sets addressed in this thesis. (It would potentially be unusable if fitting more than two parameters simultaneously or for using more computationally expensive model equations.) The Nash-Sutcliffe Efficiency (Equation 15) was a useful test statistic for assessing the goodness of fit of the model to each data set (isobutane consumption, 1,4-dioxane degradation, and biomass growth). However, comparisons of goodness of fit between data sets were not possible using this test statistic because it was skewed by the relative magnitude and number of the data points in each data set.

In summary, the success of isobutane as a biostimulant for 1,4-dioxane-degrading cultures and 21198 as a bioaugmentation culture in aquifer microcosms merits further investigation for use at the field scale. The microcosm studies presented in this thesis highlighted several factors that would be relevant for scale up to the field: primary substrate inhibition of 1,4-dioxane degradation would likely necessitate pulsed delivery of isobutane to the subsurface; inorganic nutrient augmentation would likely be necessary for sustained 1,4-dioxane degradation; and while bioaugmentation could potentially result in rapid, initial degradation, it does not appear to have a substantial long-term benefit over biostimulation (with nutrient augmentation) alone. Expansion of the model to include reactive transport processes would also inform field scale applications.

VI. FUTURE WORK

The work presented in this thesis could be expanded in numerous directions. Molecular methods could be used to compare the microbial composition of native (biostimulated) and bioaugmented microcosms. This would facilitate better understanding of long and short-term effects of bioaugmentation. Further exploration of the individual inorganic nutrient(s) limiting microbial activity would also be beneficial for scaling this process up to the field. Additional assessment of isobutane as a primary substrate and 21198 as a model microorganism could continue in order to determine intermediate and final transformation products of 1,4-dioxane cometabolism using 1,4-[^{13}C]dioxane. Packed column studies could be performed to assess aerobic cometabolism in a transport scenario. Single well push-pull tests could be used to evaluate biostimulation with isobutane and bioaugmentation with 21198 in the field. Finally, the kinetic model could be updated to account for inorganic nutrient limitation and expanded into a reactive transport model to simulate the column and field tests.

VII. REFERENCES

1. Mohr, T. K. G., Stickney, J. A. & DiGuiseppi, W. H. *Environmental Investigation and Remediation: 1,4-Dioxane and other Solvent Stabilizers*. (CRC Press, 2010).
2. Adamson, D. T. *et al.* A Multisite Survey To Identify the Scale of the 1,4-Dioxane Problem at Contaminated Groundwater Sites. *Environ. Sci. Technol. Lett.* **1,** 254–258 (2014).
3. Anderson, R. H., Anderson, J. K. & Bower, P. A. Co-occurrence of 1,4-dioxane with trichloroethylene in chlorinated solvent groundwater plumes at US Air Force installations: Fact or fiction. *Integr. Environ. Assess. Manag.* **8,** 731–737 (2012).
4. Zenker, M. J., Borden, R. C. & Barlaz, M. A. Occurrence and Treatment of 1,4-Dioxane in Aqueous Environments. *Environ. Eng. Sci.* **20,** 423–432 (2003).
5. DiGuiseppi, W., Walecka-Hutchison, C. & Hatton, J. 1,4-Dioxane Treatment Technologies: 1,4-Dioxane Treatment Technologies. *Remediat. J.* **27,** 71–92 (2016).
6. Chiang, S.-Y. (Dora), Anderson, R. (Hunter), Wilken, M. & Walecka-Hutchison, C. Practical Perspectives of 1,4-Dioxane Investigation and Remediation. *Remediat. J.* **27,** 7–27 (2016).
7. Favara, P., Tunks, J., Hatton, J. & DiGuiseppi, W. Sustainable Remediation Considerations for Treatment of 1,4-Dioxane in Groundwater: Sustainable Remediation for Treatment of 1,4-Dioxane in Groundwater. *Remediat. J.* **27,** 133–158 (2016).
8. Li, M., Fiorenza, S., Chatham, J. R., Mahendra, S. & Alvarez, P. J. J. 1,4-Dioxane biodegradation at low temperatures in Arctic groundwater samples. *Water Res.* **44,** 2894–2900 (2010).
9. Inoue, D. *et al.* 1,4-Dioxane degradation potential of members of the genera Pseudonocardia and Rhodococcus. *Biodegradation* 1–10 (2016). doi:10.1007/s10532-016-9772-7
10. Sei, K. *et al.* Isolation and characterization of bacterial strains that have high ability to degrade 1,4-dioxane as a sole carbon and energy source. *Biodegradation* **24,** 665–674 (2012).
11. Chen, D.-Z. *et al.* Intermediates and substrate interaction of 1,4-dioxane degradation by the effective metabolizer Xanthobacter flavus DT8. *Int. Biodeterior. Biodegrad.* **106,** 133–140 (2016).
12. Li, M. *et al.* Hindrance of 1,4-dioxane biodegradation in microcosms biostimulated with inducing or non-inducing auxiliary substrates. *Water Res.* **112,** 217–225 (2017).
13. Mahendra, S. & Alvarez-Cohen, L. Kinetics of 1,4-Dioxane Biodegradation by Monooxygenase-Expressing Bacteria. *Environ. Sci. Technol.* **40,** 5435–5442 (2006).
14. Pugazhendi, A., Banu, J. R., Dhavamani, J. & Yeom, I. T. Biodegradation of 1,4-dioxane by Rhodanobacter AYS5 and the role of additional substrates. *Ann. Microbiol.* **65,** 2201–2208 (2015).
15. Vainberg, S. *et al.* Biodegradation of Ether Pollutants by Pseudonocardia sp. Strain ENV478. *Appl. Environ. Microbiol.* **72,** 5218–5224 (2006).
16. Zenker, M. J., Borden, R. C. & Barlaz, M. A. Mineralization of 1, 4-dioxane in the presence of a structural analog. *Biodegradation* **11,** 239–246 (2000).

17. Lippincott, D. *et al.* Bioaugmentation and Propane Biosparging for In Situ Biodegradation of 1, 4-Dioxane. *Groundw. Monit. Remediat.* **35,** 81–92 (2015).
18. Hand, S., Wang, B. & Chu, K.-H. Biodegradation of 1,4-dioxane: Effects of enzyme inducers and trichloroethylene. *Sci. Total Environ.* **520,** 154–159 (2015).
19. Kelley, S. L., Aitchison, E. W., Deshpande, M., Schnoor, J. L. & Alvarez, P. J. J. Biodegradation of 1,4-dioxane in planted and unplanted soil: effect of bioaugmentation with amycolata sp. CB1190. *Water Res.* **35,** 3791–3800 (2001).
20. Arulazhagan, P., Rajesh Banu J, Yeom I.T., Sivaraman C & Srikanth M. Role of nutrients on biodegradation of 1, 4 dioxane by a bacterial consortium enriched from industrial sludge. *Adv. Environ. Biol.* **7,** (2013).
21. Teaf, C. M. & Garber, M. M. TOXICOLOGY AND ENVIRONMENTAL REGULATION OF 1, 4-DIOXANE. *Contam. Soils Sediments Water Energy* **20,** 67–78 (2015).
22. Patricia A. Buffler, Susan M. Wood, Lucina Suarez & Duane J. Kilian. Mortality Follow-up of Workers Exposed to 1,4-Dioxane. : Journal of Occupational and Environmental Medicine. *J. Occup. Med.* **20,** 255–259 (1978).
23. US Environmental Protection Agency. The Third Unregulated Contaminant Monitoring Rule (UCMR 3): Data Summary, July 2016. (2016).
24. Bell, C., Quinnan, J. & Trigger, G. Innovations in the Management of 1,4-Dioxane. (2016).
25. US EPA, O. National Primary Drinking Water Regulations. *US EPA* (2015). Available at: https://www.epa.gov/ground-water-and-drinking-water/national-primary-drinking-water-regulations. (Accessed: 15th July 2017)
26. Mazurkiewicz, J. & Tomasik, P. Why 1,4-dioxane is a water-structure breaker. *J. Mol. Liq.* **126,** 111–116 (2006).
27. Nishimura, T., Iizuka, S., Kibune, N. & Ando, M. Study of 1,4-Dioxane Intake in the Total Diet Using the Market-Basket Method. *J. Health Sci.* **50,** 101–107 (2004).
28. Simonich, S. M. *et al.* Probabilistic analysis of risks to us drinking water intakes from 1,4-dioxane in domestic wastewater treatment plant effluents. *Integr. Environ. Assess. Manag.* **9,** 554–559 (2013).
29. Stepien, D. K., Diehl, P., Helm, J., Thoms, A. & Püttmann, W. Fate of 1,4-dioxane in the aquatic environment: From sewage to drinking water. *Water Res.* **48,** 406–419 (2014).
30. Adamson, D. T., de Blanc, P. C., Farhat, S. K. & Newell, C. J. Implications of matrix diffusion on 1,4-dioxane persistence at contaminated groundwater sites. *Sci. Total Environ.* **562,** 98–107 (2016).
31. Crownover, E. & Schroder, D. L. Remediation of 1,4-Dioxane via Electrical Resistance Heating. (2016).
32. Burris, D., Hinchee, R., Dahlen, P. & Johnson, P. 1,4-Dioxane Vadose Remediation by Enhanced Soil Vapor Extraction. (2016).
33. Aitchison, E. W., Kelley, S. L., Alvarez, P. J. & Schnoor, J. L. Phytoremediation of 1, 4-dioxane by hybrid poplar trees. *Water Environ. Res.* **72,** 313–321 (2000).
34. Mandelbaum, R. T., Shati, M. R. & Ronen, D. In situ microcosms in aquifer bioremediation studies. *FEMS Microbiol. Rev.* **20,** 489–502 (1997).

35. Frascari, D., Zanaroli, G. & Danko, A. S. In situ aerobic cometabolism of chlorinated solvents: A review. *J. Hazard. Mater.* **283,** 382–399 (2015).
36. Mahendra, S. & Alvarez-Cohen, L. Pseudonocardia dioxanivorans sp. nov., a novel actinomycete that grows on 1,4-dioxane. *Int. J. Syst. Evol. Microbiol.* **55,** 593–598 (2005).
37. Parales, R. E., Adamus, J. E., White, N. & May, H. D. Degradation of 1,4-dioxane by an actinomycete in pure culture. *Appl. Environ. Microbiol.* **60,** 4527–4530 (1994).
38. Kim, Y.-M., Jeon, J.-R., Murugesan, K., Kim, E.-J. & Chang, Y.-S. Biodegradation of 1,4-dioxane and transformation of related cyclic compounds by a newly isolated Mycobacterium sp. PH-06. *Biodegradation* **20,** 511 (2009).
39. Bernhardt, D. & Diekmann, H. Degradation of dioxane, tetrahydrofuran and other cyclic ethers by an environmental Rhodococcus strain. *Appl. Microbiol. Biotechnol.* **36,** 120–123 (1991).
40. Sales, C. M., Grostern, A., Parales, J. V., Parales, R. E. & Alvarez-Cohen, L. Oxidation of the Cyclic Ethers 1,4-Dioxane and Tetrahydrofuran by a Monooxygenase in Two Pseudonocardia Species. *Appl. Environ. Microbiol.* **79,** 7702–7708 (2013).
41. Rodriguez, F. J. B. Evaluation of 1, 4-dioxane biodegradation under aerobic and anaerobic conditions. (Clemson University, 2016).
42. Steffan, R. J. *Biodegradation of 1, 4-Dioxane*. (DTIC Document, 2007).
43. Shen, W., Chen, H. & Pan, S. Anaerobic biodegradation of 1,4-dioxane by sludge enriched with iron-reducing microorganisms. *Bioresour. Technol.* **99,** 2483–2487 (2008).
44. Bell, C., McDonough, J., Houston, K. S. & Gerber, K. Stable Isotope Probing to Confirm Field-Scale Co-Metabolic Biodegradation of 1,4-Dioxane. *Remediat. J.* **27,** 47–59 (2016).
45. Li, M. *et al.* Bench-scale biodegradation tests to assess natural attenuation potential of 1,4-dioxane at three sites in California. *Biodegradation* **26,** 39–50 (2015).
46. Sei, K. *et al.* Evaluation of the biodegradation potential of 1,4-dioxane in river, soil and activated sludge samples. *Biodegradation* **21,** 585–591 (2010).
47. Gedalanga, P. *et al.* A Multiple Lines of Evidence Framework to Evaluate Intrinsic Biodegradation of 1,4-Dioxane. *Remediat. J.* **27,** 93–114 (2016).
48. Gedalanga, P. B. *et al.* Identification of Biomarker Genes To Predict Biodegradation of 1,4-Dioxane. *Appl. Environ. Microbiol.* **80,** 3209–3218 (2014).
49. Li, M. *et al.* The Abundance of Tetrahydrofuran/Dioxane Monooxygenase Genes (thmA/dxmA) and 1,4-Dioxane Degradation Activity Are Significantly Correlated at Various Impacted Aquifers. *Environ. Sci. Technol. Lett.* **1,** 122–127 (2014).
50. Adamson, D. T., Anderson, R. H., Mahendra, S. & Newell, C. J. Evidence of 1,4-Dioxane Attenuation at Groundwater Sites Contaminated with Chlorinated Solvents and 1,4-Dioxane. *Environ. Sci. Technol.* **49,** 6510–6518 (2015).
51. Nakamiya, K., Hashimoto, S., Ito, H., Edmonds, J. S. & Morita, M. Degradation of 1,4-Dioxane and Cyclic Ethers by an Isolated Fungus. *Appl. Environ. Microbiol.* **71,** 1254–1258 (2005).
52. Mahendra, S., Petzold, C. J., Baidoo, E. E., Keasling, J. D. & Alvarez-Cohen, L. Identification of the Intermediates of in Vivo Oxidation of 1,4-Dioxane by Monooxygenase-Containing Bacteria. *Environ. Sci. Technol.* **41,** 7330–7336 (2007).

53. Hyman, M. R. & Wood, P. M. Suicidal inactivation and labelling of ammonia mono-oxygenase by acetylene. *Biochem. J.* **227,** 719–725 (1985).
54. Sales, C. M. *et al.* Genome Sequence of the 1,4-Dioxane-Degrading Pseudonocardia dioxanivoransStrain CB1190. *J. Bacteriol.* **193,** 4549–4550 (2011).
55. Zhang, S., Gedalanga, P. B. & Mahendra, S. Biodegradation Kinetics of 1,4-Dioxane in Chlorinated Solvent Mixtures. *Environ. Sci. Technol.* **50,** 9599–9607 (2016).
56. Michael L. Shuler & Fikret Kargi. *Bioprocess Engineering Basic Concepts*. (Prentice Hall, 1992).
57. Kim, Y., Arp, D. J. & Semprini, L. A combined method for determining inhibition type, kinetic parameters, and inhibition coefficients for aerobic cometabolism of 1,1,1-trichloroethane by a butane-grown mixed culture. *Biotechnol. Bioeng.* **77,** 564–576 (2002).
58. Criddle, C. S. (Michigan S. U. The Kinetics of Cometabolism. *Biotechnol. Bioeng. U. S.* **41:11,** (1993).
59. Chang, H.-L. & Alvarez-Cohen, L. Model for the Cometabolic Biodegradation of Chlorinated Organics. *Environ. Sci. Technol.* **29,** 2357–2367 (1995).
60. Semprini, L., Dolan, M. E., Mathias, M. A., Hopkins, G. D. & McCarty, P. L. Laboratory, field, and modeling studies of bioaugmentation of butane-utilizing microorganisms for the in situ cometabolic treatment of 1,1-dichloroethene, 1,1-dichloroethane, and 1,1,1-trichloroethane. *Adv. Water Resour.* **30,** 1528–1546 (2007).
61. Mahendra, S., Grostern, A. & Alvarez-Cohen, L. The impact of chlorinated solvent co-contaminants on the biodegradation kinetics of 1,4-dioxane. *Chemosphere* **91,** 88–92 (2013).
62. Pornwongthong, P., Mulchandani, A., Gedalanga, P. B. & Mahendra, S. Transition metals and organic ligands influence biodegradation of 1,4-dioxane. *Appl. Biochem. Biotechnol.* **173,** 291–306 (2014).
63. Zhou, Y., Huang, H. & Shen, D. Multi-substrate biodegradation interaction of 1, 4-dioxane and BTEX mixtures by Acinetobacter baumannii DD1. *Biodegradation* **27,** 37–46 (2016).
64. *BOSICON, 3rd International Conference on Contaminated Sites Remediation: 12 - 14 September 2012, Rome, Italy*. (AIDIC, 2012).
65. Carpenter, S. Microcosm Experiments have Limited Relevance for Community and Ecosystem Ecology. *Ecology* **77,** 677–6800 (1996).
66. ATCC 21198 Strain Browser - StrainInfo. Available at: http://www.straininfo.net/strains/101166/browser. (Accessed: 19th October 2016)
67. Biosafety in Microbiological and Biomedical Laboratories (BMBL) 5th Edition - CDC. Available at: http://www.cdc.gov/biosafety/publications/bmbl5/index.htm. (Accessed: 19th October 2016)
68. Shields-Menard, S. A. *et al.* Draft Genome Sequence of Rhodococcus rhodochrous Strain ATCC 21198. *Genome Announc.* **2,** (2014).
69. Vandergeize, R. & Dijkhuizen, L. Harnessing the catabolic diversity of rhodococci for environmental and biotechnological applications. *Curr. Opin. Microbiol.* **7,** 255–261 (2004).
70. Bell, K. S., Philp, J. C., Aw, D. W. J., Christofi, N. & others. The genus Rhodococcus. *J. Appl. Microbiol.* **85,** 195–210 (1998).

71. de Carvalho, C. C. C. R. & da Fonseca, M. M. R. The remarkable Rhodococcus erythropolis. *Appl. Microbiol. Biotechnol.* **67,** 715–726 (2005).
72. Martinkova, L., Uhnakova, B., Patek, M., Nesvera, J. & Kren, V. Biodegradation potential of the genus Rhodococcus. *Environ. Int.* **35,** 162–177 (2009).
73. Malachowsky, K. J., Phelps, T. J., Teboli, A. B., Minnikin, D. E. & White, D. C. Aerobic Mineralization of Trichloroethylene, Vinyl Chloride, and Aromatic Compounds by Rhodococcus Species. *Appl. Environ. Microbiol.* **60,** 542–548 (1994).
74. Kuntz, R. L., Brown, L. R., Zappi, M. E. & French, W. T. Isopropanol and acetone induces vinyl chloride degradation in Rhodococcus rhodochrous. *J. Ind. Microbiol. Biotechnol.* **30,** 651–655 (2003).
75. Sorkhoh, N. A., Ghannoum, M. A., Ibrahim, A. S., Stretton, R. J. & Radwan, S. S. Crude oil and hydrocarbon-degrading strains of Rhodococcus rhodochrous isolated from soil and marine environments in Kuwait. *Environ. Pollut.* **65,** 1–17 (1990).
76. Nalli, S., Cooper, D. G. & Nicell, J. A. Biodegradation of plasticizers by Rhodococcus rhodochrous. *Biodegradation* **13,** 343–352
77. Rylott, E. L. *et al.* An explosive-degrading cytochrome P450 activity and its targeted application for the phytoremediation of RDX. *Nat. Biotechnol.* **24,** 216–219 (2006).
78. Baxter, J. & Cummings, S. P. The current and future applications of microorganism in the bioremediation of cyanide contamination. *Antonie Van Leeuwenhoek* **90,** 1–17 (2006).
79. Bock, C., Kroppenstedt, R. M. & Diekmann, H. Degradation and bioconversion of aliphatic and aromatic hydrocarbons by Rhodococcus ruber 219. *Appl. Microbiol. Biotechnol.* **45,** 408–410 (1996).
80. Goltz, M. N., Bouwer, E. J. & Huang, J. Transport issues and bioremediation modeling for the in situ aerobic co-metabolism of chlorinated solvents. *Biodegradation* **12,** 127–140 (2001).
81. Zenker, M. J., Borden, R. C. & Barlaz, M. A. Modeling cometabolism of cyclic ethers. *Environ. Eng. Sci.* **19,** 215–228 (2002).
82. Liu, L., Binning, P. J. & Smets, B. F. Evaluating Alternate Biokinetic Models for Trace Pollutant Cometabolism. *Environ. Sci. Technol.* **49,** 2230–2236 (2015).
83. Alvarez-Cohen, L. & McCarty, P. L. A cometabolic biotransformation model for halogenated aliphatic compounds exhibiting product toxicity. *Environ. Sci. Technol.* **25,** 1381–1387 (1991).
84. Jenal-Wanner, U. & McCarty, P. L. Development and Evaluation of Semicontinuous Slurry Microcosms to Simulate in Situ Biodegradation of Trichloroethylene in Contaminated Aquifers. *Environ. Sci. Technol.* **31,** 2915–2922 (1997).
85. Bekins, B. A., Warren, E. & Godsy, E. M. A Comparison of Zero-Order, First-Order, and Monod Biotransformation Models. *Ground Water* **36,** 261–268 (1998).
86. Sun, M., Lopez-Velandia, C. & Knappe, D. R. U. Determination of 1,4-Dioxane in the Cape Fear River Watershed by Heated Purge-and-Trap Preconcentration and Gas Chromatography–Mass Spectrometry. *Environ. Sci. Technol.* **50,** 2246–2254 (2016).
87. Draper, W. M., Dhoot, J. S., Remoy, J. W. & Perera, S. K. Trace-level determination of 1,4-dioxane in water by isotopic dilution GC and GC-MS. *The Analyst* **125,** 1403–1408 (2000).

88. Sander, R. *Compilation of Henry's law constants for inorganic and organic species of potential importance in environmental chemistry*. (Max-Planck Institute of Chemistry, Air Chemistry Department Mainz, Germany, 1999).
89. Kottegoda, S., Waligora, E. & Hyman, M. Metabolism of 2-methylpropene (isobutylene) by the aerobic bacterium Mycobacterium sp. strain ELW1. *Appl. Environ. Microbiol.* **81,** 1966–1976 (2015).
90. Edelmann, P. *Effects of Irrigating with Wastewater on Ground-water Quality at Fort Carson Military Reservation Golf Course Near Colorado Springs, Colorado*. (United States Geological Survey, 1984).
91. Steven C.Chapra. *Applied Numerical Methods with MATLAB for engineers and scientists*. (McGraw Hill, 2012).
92. Krause, P., Boyle, D. P. & Bäse, F. Comparison of different efficiency criteria for hydrological model assessment. *Adv Geosci* **5,** 89–97 (2005).
93. Smith, L. H., McCarty, P. L. & Kitanidis, P. K. Spreadsheet method for evaluation of biochemical reaction rate coefficients and their uncertainties by weighted nonlinear least-squares analysis of the integrated Monod equation. *Appl. Environ. Microbiol.* **64,** 2044–2050 (1998).
94. Michael T. Madigan, John M. Martinko, David A. Stahl & David P. Clark. *Brock Biology of Microorganisms*. (Pearson, 2012).
95. Swindoll, C. M., Aelion, C. M. & Pfaender, F. K. Influence of inorganic and organic nutrients on aerobic biodegradation and on the adaptation response of subsurface microbial communities. *Appl. Environ. Microbiol.* **54,** 212–217 (1988).
96. Chu, K.-H. & Alvarez-Cohen, L. Evaluation of toxic effects of aeration and trichloroethylene oxidation on methanotrophic bacteria grown with different nitrogen sources. *Appl. Environ. Microbiol.* **65,** 766–772 (1999).
97. Kim, Y., Istok, J. D. & Semprini, L. Push-Pull Tests for Assessing In Situ Aerobic Cometabolism. *Ground Water* **42,** 329–337 (2004).
98. Pfiffner, S. M., Palumbo, A. V., Phelps, T. J. & Hazen, T. C. Effects of nutrient dosing on subsurface methanotrophic populations and trichloroethylene degradation. *J. Ind. Microbiol. Biotechnol.* **18,** 204–212 (1997).
99. Muter, O. *et al.* The role of nutrients in the biodegradation of 2,4,6-trinitrotoluene in liquid and soil. *J. Environ. Manage.* **98,** 51–55 (2012).
100. Carol Wiseman, Randy Pratt, Andrew Davidson & Clifford R. Lange. Cometabolic Bioremediation of 1,4-Dioxane. (2016).
101. Steffensen, W. S. & Alexander, M. Role of competition for inorganic nutrients in the biodegradation of mixtures of substrates. *Appl. Environ. Microbiol.* **61,** 2859–2862 (1995).
102. Cirino, P. C. & Arnold, F. H. Protein engineering of oxygenases for biocatalysis. *Curr. Opin. Chem. Biol.* **6,** 130–135 (2002).
103. Karigar, C. S. & Rao, S. S. Role of Microbial Enzymes in the Bioremediation of Pollutants: A Review. *Enzyme Res.* **2011,** e805187 (2011).

104. Semprini, L. & McCarty, P. L. Comparison Between Model Simulations and Field Results for In-Situ Biorestoration of Chlorinated Aliphatics: Part 1. Biostimulation of Methanotrophic Bacteria. *Ground Water* **29,** 365–374 (1991).
105. Mohammad Azizian & Suvadee Thankiatkul. Monod curves. (2016).
106. Pirt, S. J. The Maintenance Energy of Bacteria in Growing Cultures. *Proc. R. Soc. Lond. B Biol. Sci.* **163,** 224–231 (1965).
107. Philips, R. M. & R. » How big is an E. coli cell and what is its mass? Available at: http://book.bionumbers.org/how-big-is-an-e-coli-cell-and-what-is-its-mass/. (Accessed: 17th July 2017)

VIII. APPENDICES

A. Recipe for mineral salts media (growth media)

Table A-1. Mineral salts media trace element solution

Compound	Mass (g) added to 500 mL ultra-pure water
EDTA	25
$ZnSO_4 \cdot 7H_2O$	11
$CaCl_2$	2.27
$MnCl_2 \cdot 4H_2O$	2.53
$FeSO_4 \cdot 7H_2O$	2.5
$(NH_4)_6Mo_7O_{24} \cdot 4H_2O$	0.55
$CuSO_4 \cdot 5H_2O$	0.753
$CoCl_2 \cdot 6H_2O$	0.855

1. Adjust pH to 6.0 with KOH
2. Store in the refrigerator.

Solution 1 (concentrated by 10x)
To 1000mL of ultra-pure water, add: 20 g NH_4Cl, 0.75 g $MgCl_2 \cdot 6H_2O$, 1.0 g $(NH_4)_2SO_4$, and 2.0 mL trace element solution

Solution 2 (concentrated by 100x)
To 1000mL of ultra-pure water, add: 155 g K_2HPO_4 and 85 g NaH_2PO_4

Autoclave Solution 1 and Solution 2 separately. Mix 1X concentration by dilution with autoclaved DI water.

B. Heterotrophic and Minimal Media Plates

Heterotrophic growth plates

Plate Count Agar can be purchased premixed (Difco 247940) or by mixing 3 g tryptic soy, 10 g glucose, and 15 g agar in 1000mL ultra-pure water. Autoclave.

Store at 4C prior to use. After streaking, wrap in parafilm and incubate at room temperature.

Minimal media plates

21198 is maintained on 1x minimal media plates grown in desiccators with 2-3% isobutane overpressure. These plates are prepared by adding 15g of agar to 890mL ultra-pure water and autoclaving. When the agar mixture is cool to the touch, add 100mL of mineral salts media Solution 1 (10x) and 10mL of Solution 2 (100x).

C. Artificial Groundwater Recipe

4 solutions prepared separately at different strengths and diluted accordingly to obtain a 1x concentration. To make 1L 1x artificial groundwater, add 50 mL Solution 1 and 1 mL of each Solution 2,3, and 5 to 947 mL autoclaved DI water.

Table C-1. Artificial groundwater recipe

Solution 1	MW (g/mol)	mass (g) added to 1L DI for 1X soln	mass (g) added to 1L DI for 20X soln	mass (g) added to 500 mL DI for 20X soln	Ion	1X conc. (mg/L)	20X conc. (mg/L)	
CaSO4	136.14	0.475	9.5	4.75	Mg	100.9	2018.3	*add 50 ml to make 1 L solution*
MgSO4	120.4	0.5	10	5	Na	352.4	7048.3	
Na2SO4	142.04	0.75	15	7.5	Ca	190.5	3809.8	
NaHCO3	84	0.4	8	4	SO4	1240.5	24810.4	
CaCl2	111	0.14	2.8	1.4	Cl	89.55	1791.0	
					CO3	285.71	5714.3	
Solution 2	MW (g/mol)	mass (mg) added to 1L DI for 1X soln	mass (g) added to 1L DI for 1000X soln	mass (g) added to 500 mL DI for 1000X soln	Ion	1X conc. (mg/L)	1000X conc. (mg/L)	
KCl	74.55	6.00	6.00	3	K	3.147	3146.9	*add 1 ml to make 1 L soln*
NaF	42	1.75	1.75	0.875	Na	1.292	1291.7	
NaNO2	69	1.00	1.00	0.5	Mn	0.182	181.9	
MnSO4.H2O	169	0.56	0.56	0.28	NH4	0.675	674.7	
NH4NO3	80.04	3.00	3.00	1.5	NO3	2.324	2323.8	
					F	0.792	791.7	
					NO2	0.667	666.7	
					SO4	0.318	318.1	
					Cl	2.857	2857.1	
trace elements 1	MW (g/mol)	mass (mg) added to 1L DI for 1X soln	mass (g) added to 1L DI for 1,000,000X soln	mass (g) added to 100 mL DI for 1,000,000X soln	Ion	1X conc. (mg/L)	Conc. (mg/L) in 100 mL of 1,000,000X solution	*add 100 uL of 1,000,000X solution to 100 mL for 1000X solution. Then 1mL of 1000X solution for 1L 1X solution.*
CrCl3.6H2O	266.36	0.013	13	1.3	Cr	0.00254	2537.9	
CdCl2	183.32	0.005	5	0.5	Cd	0.00307	3065.7	
					Cl	0.00713	7134.4	
trace elements 2	MW (g/mol)	mass (mg) added to 1L DI for 1X soln	mass (g) added to 1L DI for 100,000X soln	mass (g) added to 100 mL DI for 100,000X soln	ion	1x conc. (mg/L)	conc. (mg/L) of 100,000X soln	*add 1 mL of 100,000X soln to 100 mL for 1000X soln. Then add 1 mL of 1000X soln for 1L of 1X soln.*
NaH2PO4.H2O	138	0.200	20	2	Na	0.033	3333.3	
FeCl2.4H2O	198.75	0.300	30	3	P	0.045	4492.8	
					Fe	0.084	8422.6	
					Cl	0.107	10717.0	

D. Long-term Microcosm Experiment

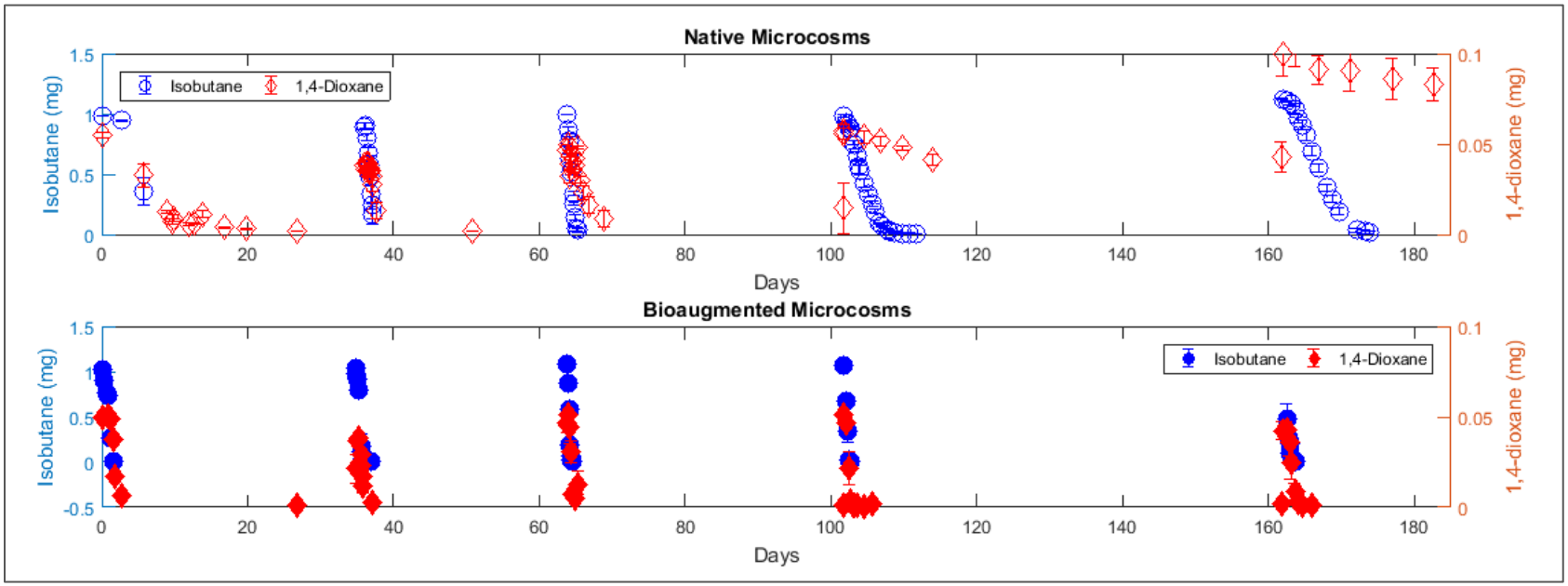

Figure D-1.Isobutane and 1,4-dioxane transformation in native and bioaugmented microcosms on a continuous time scale during the long-term experiment.

E. Zero-order rate calculations for long-term microcosm experiment

Individual isobutane and 1,4-dioxane degradation curves from which initial, zero order linear rates were calculated in the long-term microcosm experiment. Each row of subplots corresponds to one addition. The first three columns in each subplot are bioaugmented microcosms, the last three are native microcosms. The blue line shows the linear regression, and the corresponding R^2 value is given in the legend of each subplot.

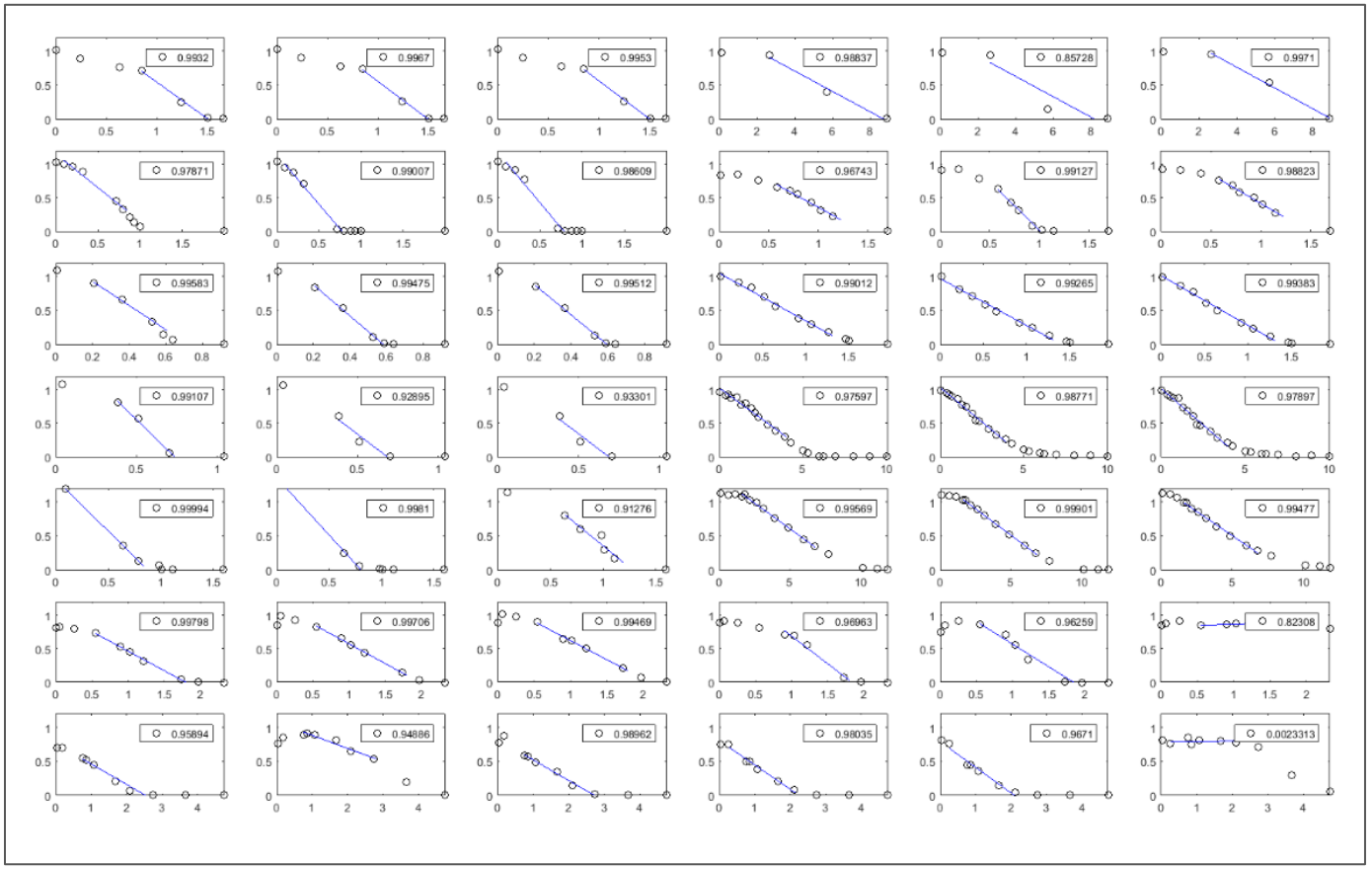

Figure E-1. Initial linear rates for isobutane transformation in the long term experiment without TCE present. Averaged rates shown and referenced in Figure 8, Figure 9, and Figure 12.

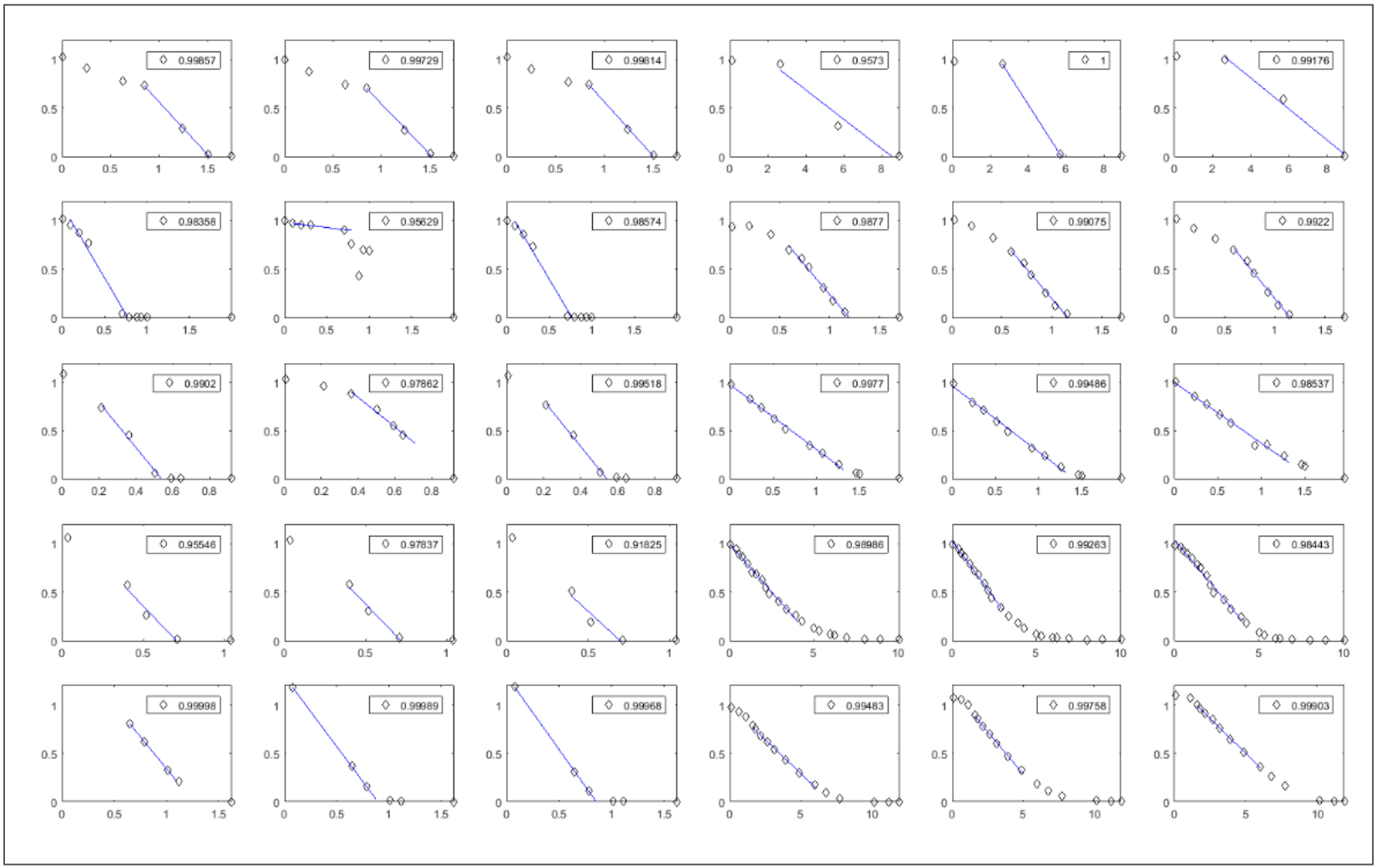

Figure E-2.Initial linear rates for isobutane transformation in the long term experiment with TCE present. Averaged rates shown and referenced in Figure 12.

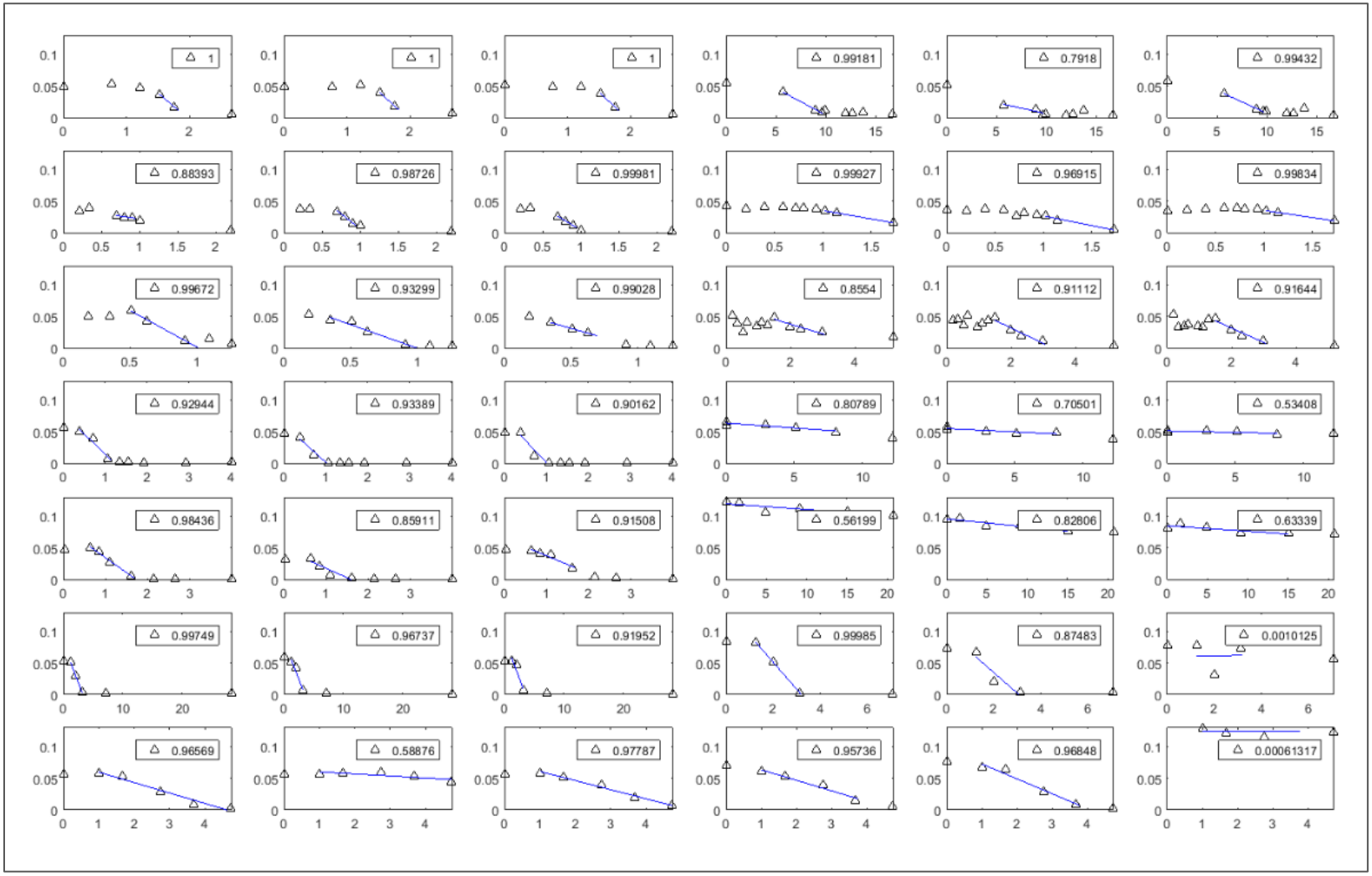

Figure E-3. Initial linear rates for 1,4-dioxane transformation in the long term experiment without TCE present. Averaged rates shown and referenced in Figure 8, Figure 9, and Figure 12

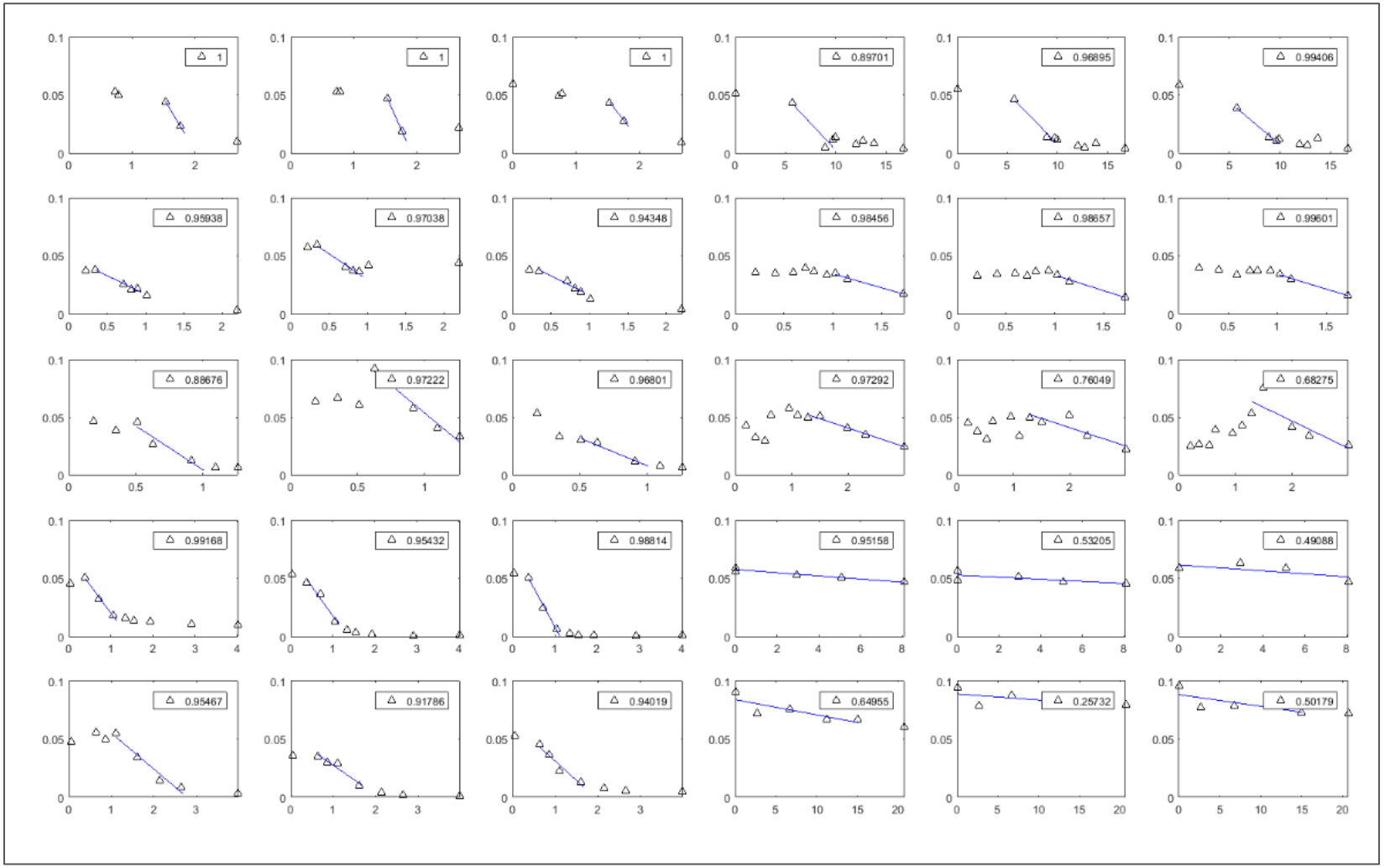

Figure E-4. .Initial linear rates for 1,4-dioxane transformation in the long term experiment with TCE present. Averaged rates shown and referenced in Figure 12.

F. Short-term microcosms

Isobutane and 1,4-dioxane transformation in microcosms and pure culture reactors on continuous time scales during the short-term experiment.

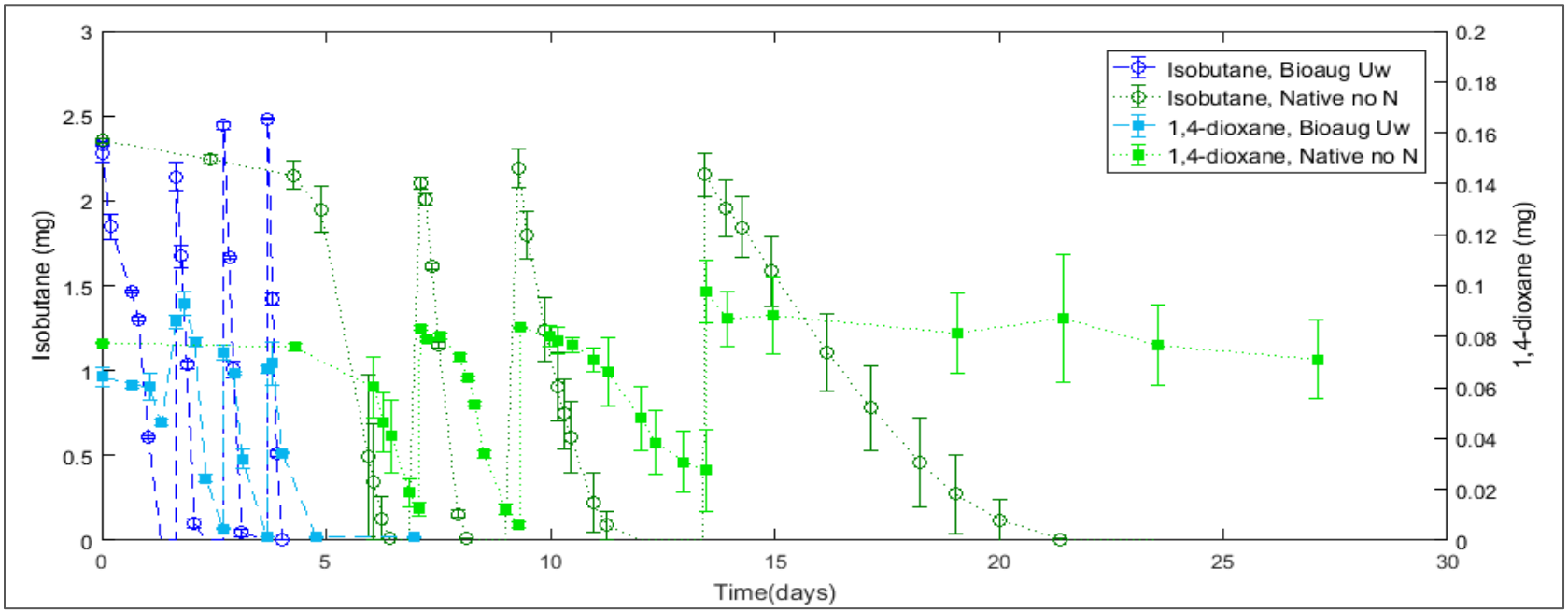

Figure F-1. Isobutane and 1,4-dioxane transformation in short term microcosms with unequal inorganic nutrient conditions on a continuous time scale.

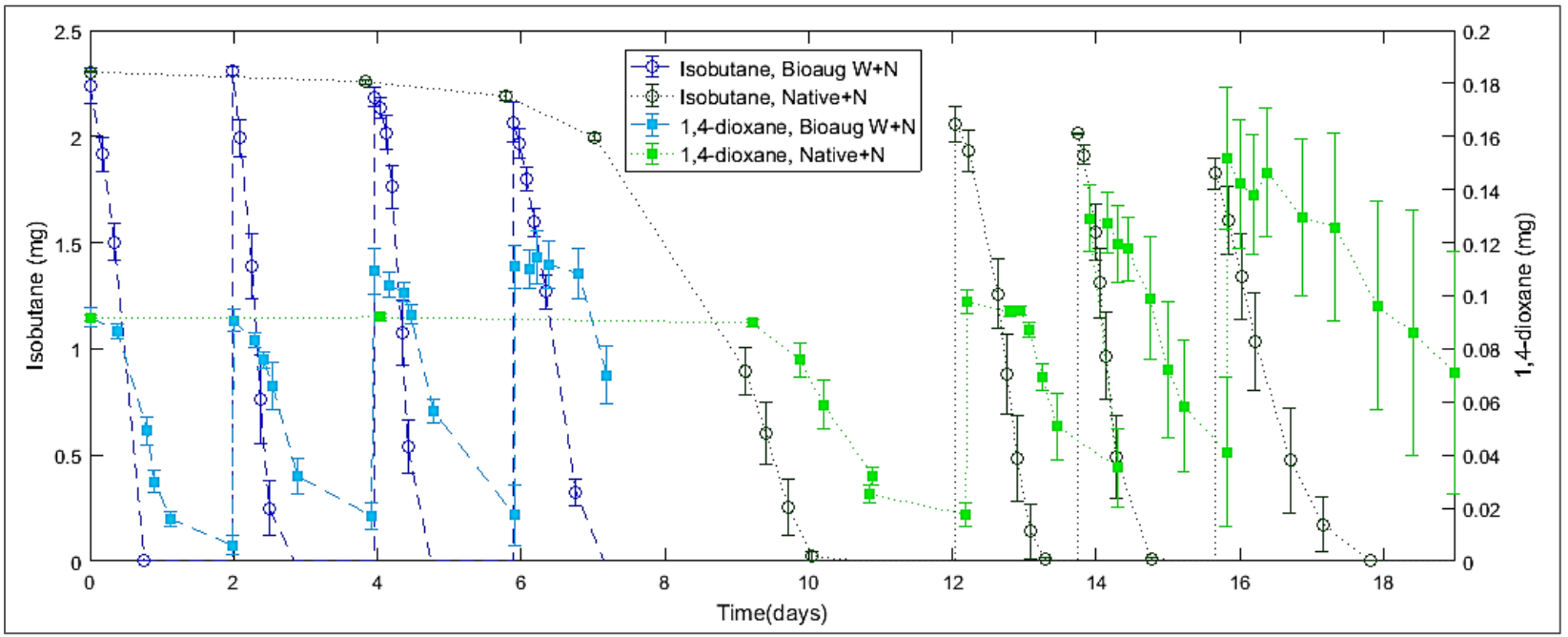

Figure F-2. Isobutane and 1,4-dioxane transformation in short term microcosms with equal inorganic nutrient conditions on a continuous time scale.

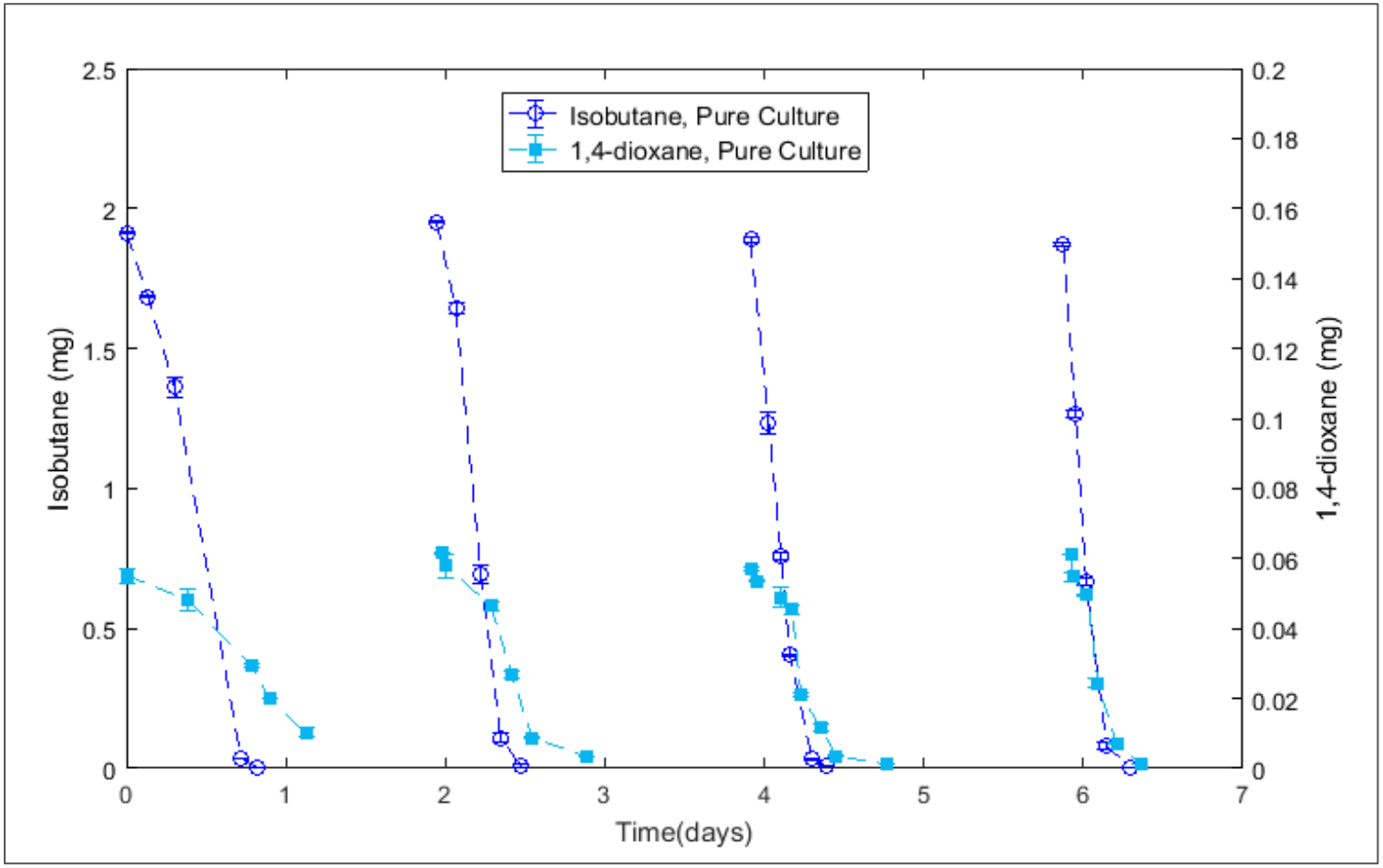

Figure F-3. Isobutane and 1,4-dioxane transformation in short term pure culture reactors on a continuous time scale.

G. Linear rate calculations: short-term microcosms

Individual isobutane and 1,4-dioxane degradation curves from which initial, zero order linear rates were calculated in the short-term microcosm experiment. Each row of subplots corresponds to one addition. The first two to three columns in each subplot are bioaugmented microcosms, the last two to three are native microcosms. The blue line shows the linear regression, and the corresponding R^2 value is given in the legend of each subplot.

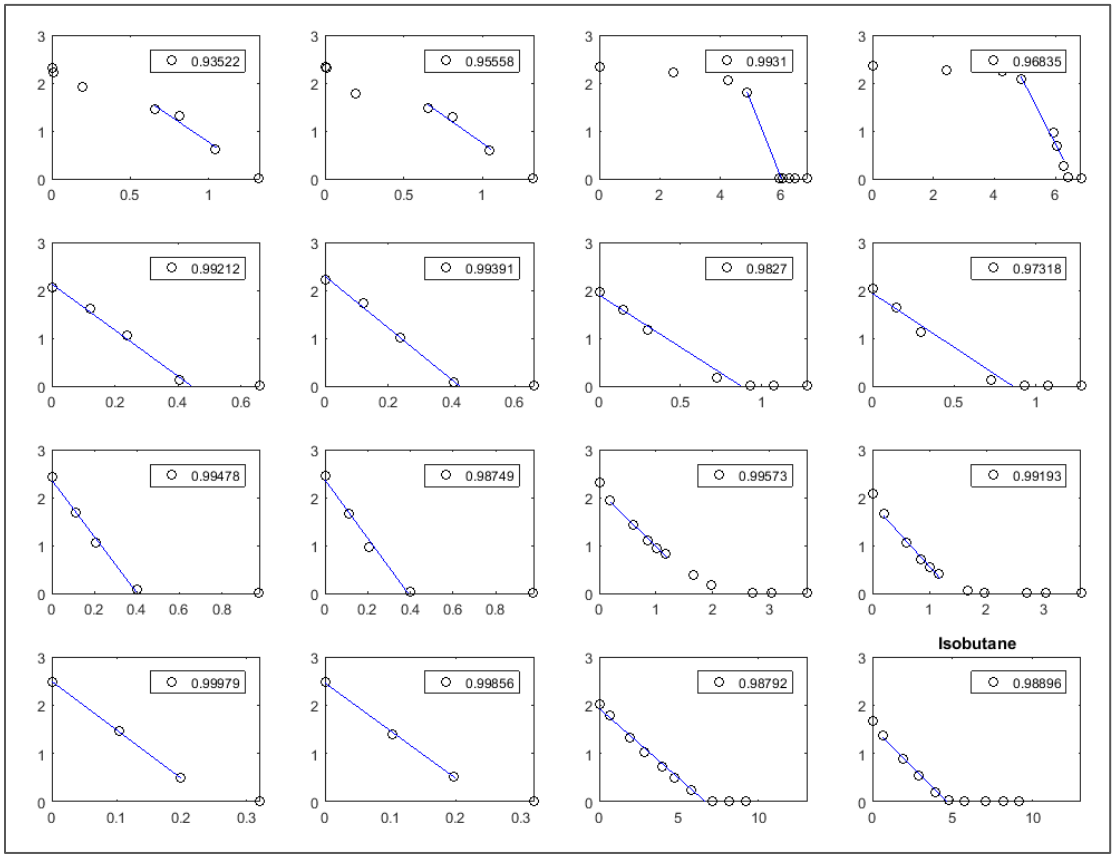

Figure G-1. Initial linear rates for isobutane transformation in the short-term experiment for "Bioaug Uw" and "Native no N". Averaged rates shown and referenced in Figure 14.

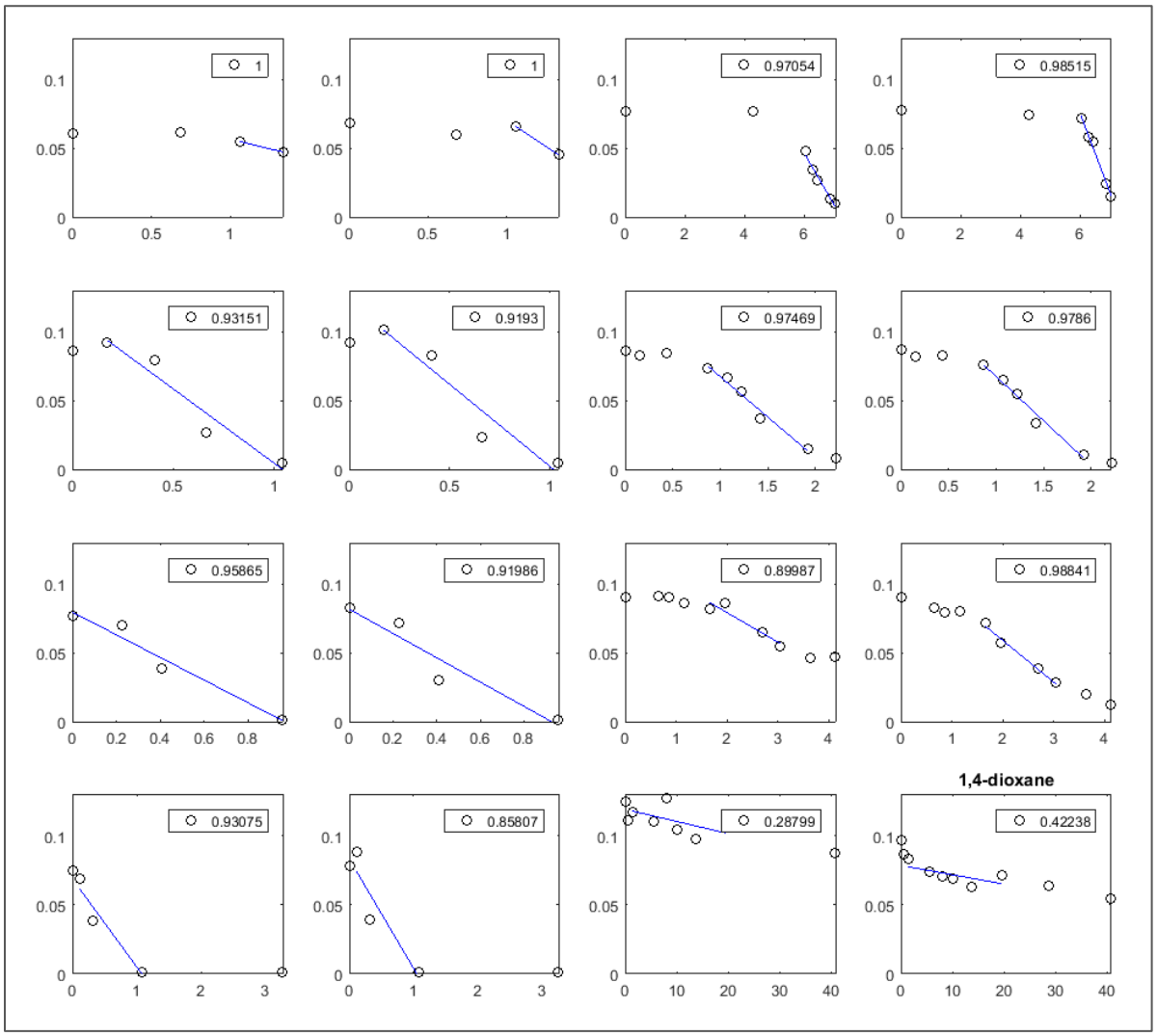

Figure G-2. Initial linear rates for 1,4-dioxane transformation in the short-term experiment for "Bioaug Uw" and "Native no N". Averaged rates shown and referenced in Figure 14.

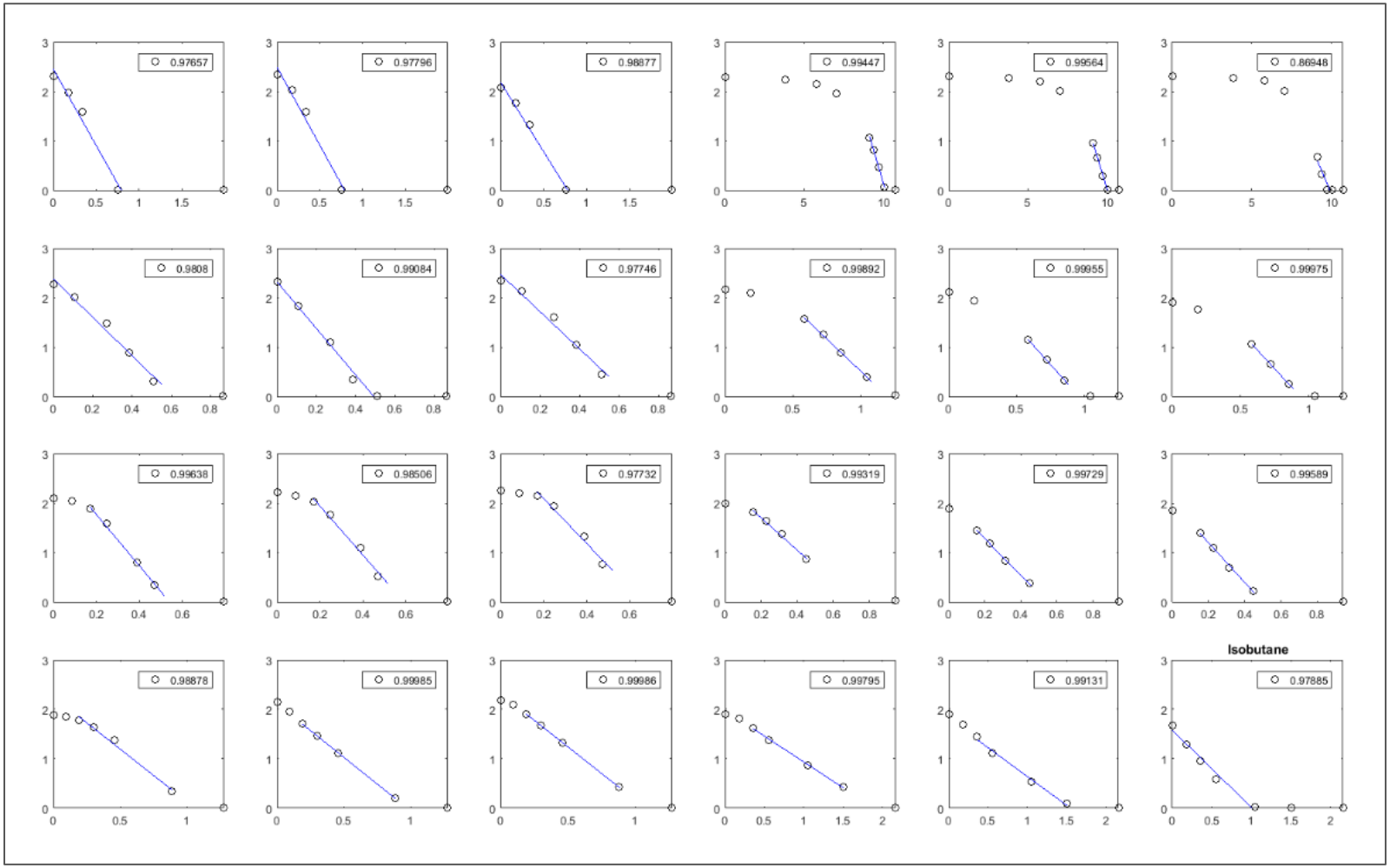

Figure G-3. Initial linear rates for isobutane transformation in the short-term experiment for "Bioaug W+N" and "Native+N". Averaged rates shown and referenced in Figure 14.

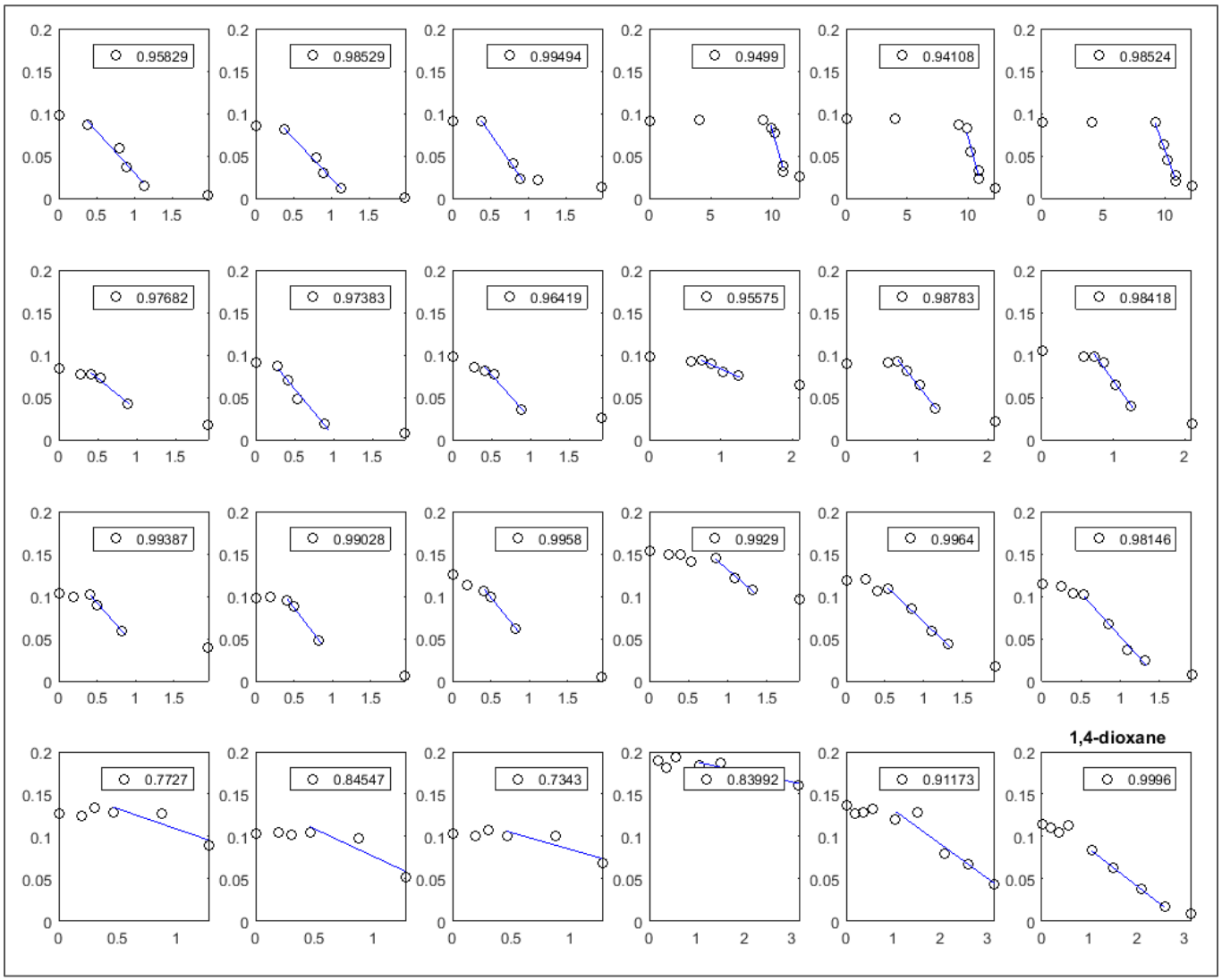

Figure G-4. Initial linear rates for 1,4-dioxane transformation in the short-term experiment for "Bioaug W+N" and "Native+N". Averaged rates shown and referenced in Figure 14.

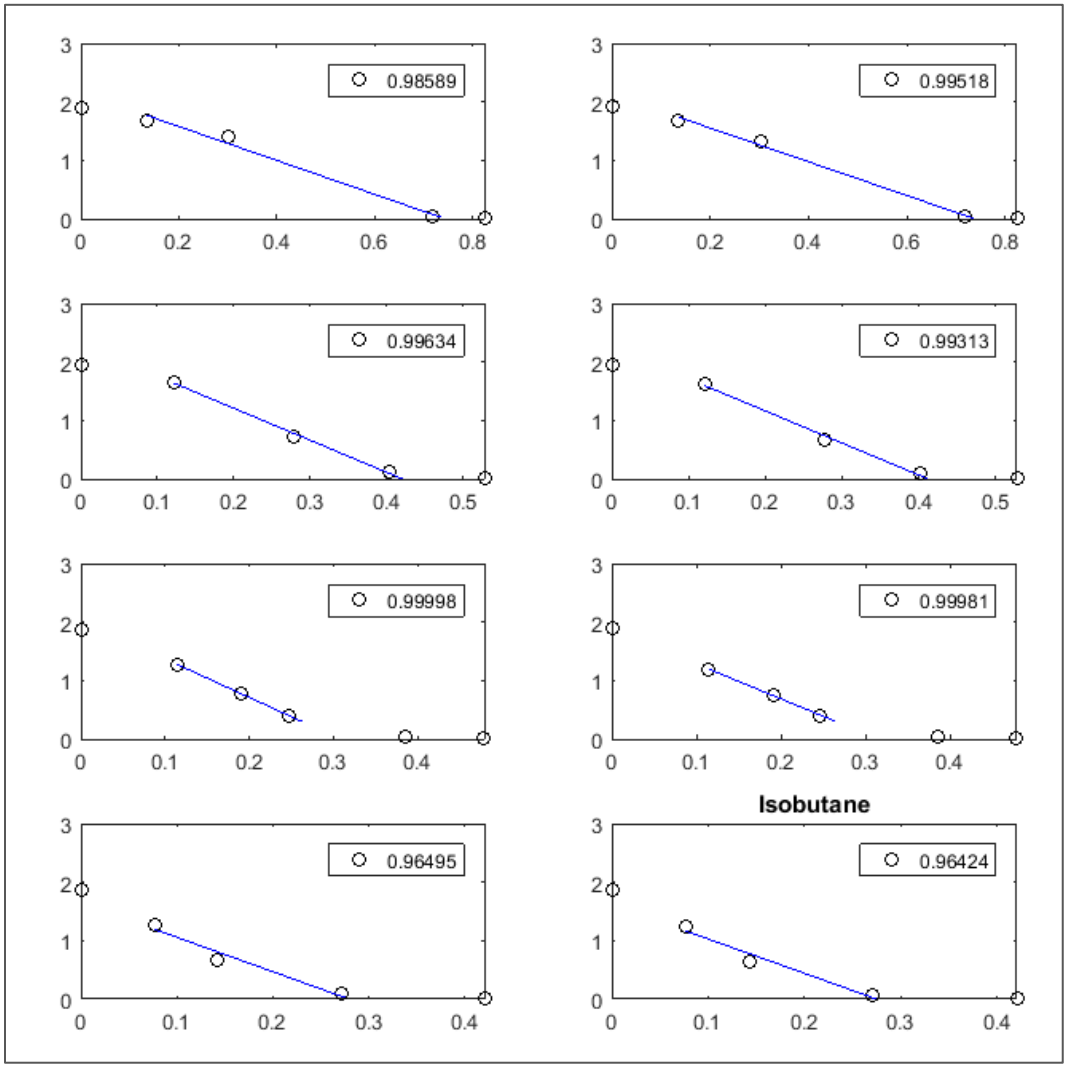

Figure G-5. Initial linear rates for isobutane transformation in the short-term experiment for pure culture reactors. Averaged rates shown and referenced in Figure 14.

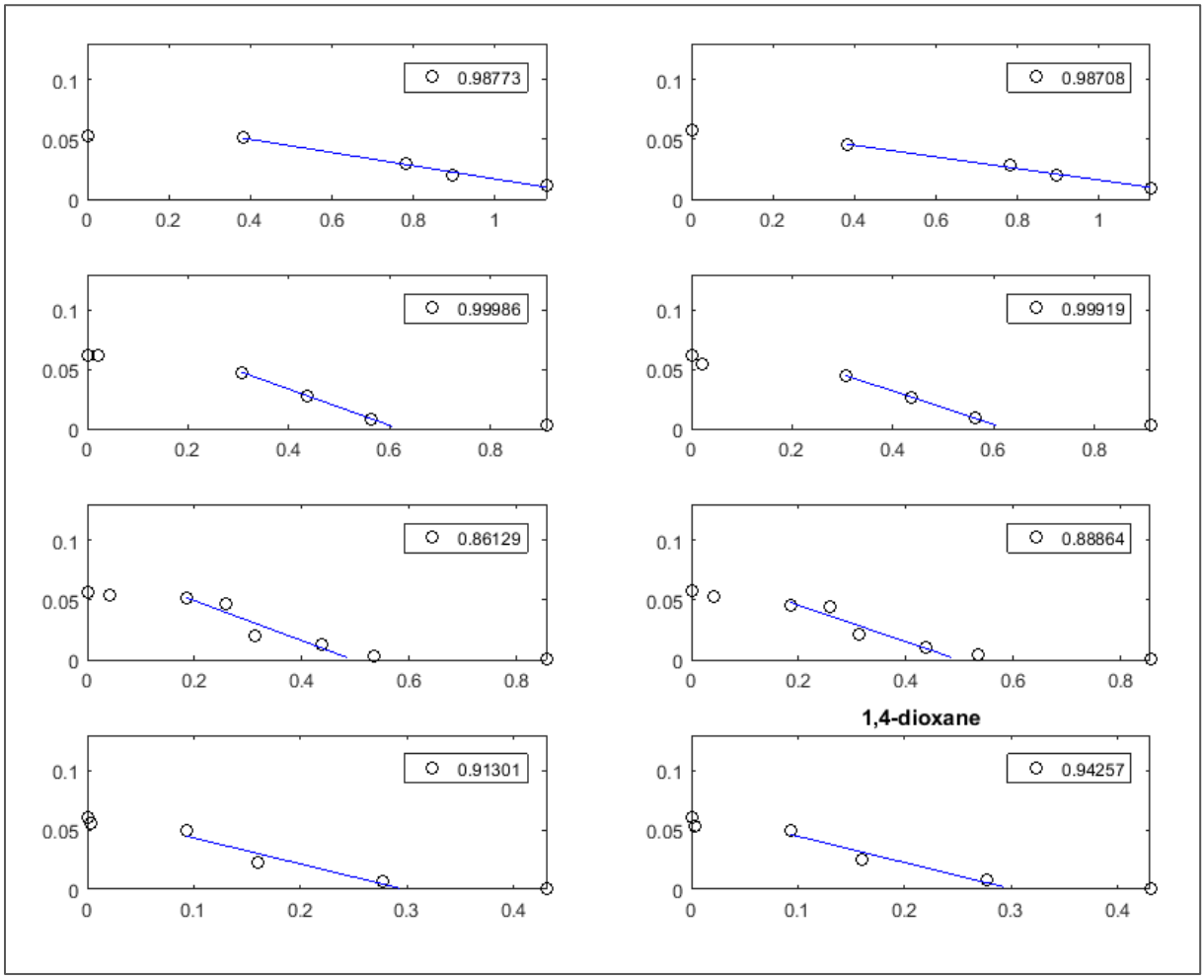

Figure G-6. Initial linear rates for 1,4-dioxane transformation in the short-term experiment for pure culture reactors. Averaged rates shown and referenced in Figure 14.

H. Sensitivity test data: alternate parameter values and resulting E values

Table H-1. Altered parameter values used in sensitivity analysis and resulting E values.

				E values, 30% greater			E values, 30% less		
Parameter	Optimized Value	30% greater	30% less	IB	X	14D	IB	X	14D
Kmax, IB	2.58	3.354	1.806	0.613	0.939	0.9072	0.4949	0.9457	0.8819
Ks, IB	0.1	0.130	0.070	0.6372	0.9431	0.9226	0.6547	0.9414	0.9258
Y	0.885	1.151	0.620	0.5173	-0.3779	0.6296	0.6041	0.763	0.8352
b	0.03	0.039	0.021	0.6602	0.9427	0.9304	0.6553	0.937	0.9265
Kmax, 14D	0.87	1.131	0.609	0.6581	0.9424	0.8874	0.6581	0.9424	0.8739
Ks, 14D	4.35	5.655	3.045	0.6581	0.9424	0.9024	0.6581	0.9424	0.8598
KI	0.13	0.169	0.091	0.6581	0.9424	0.9159	0.6581	0.9424	0.9314
X0	3.6	4.680	2.520	0.6742	0.9151	0.9272	0.5956	0.9591	0.8973